1980-06

An experimental study of solid propellant deflagration using high speed motion pictures and postfire residue analysis

DiLoreto, Vincent Daniel

NAVAL POSTGRADUATE SCHOOL
Monterey, California

THESIS

AN EXPERIMENTAL STUDY OF SOLID PROPELLANT DEFLAGRATION USING HIGH SPEED MOTION PICTURES AND POSTFIRE RESIDUE ANALYSIS

by

Vincent Daniel DiLoreto

June 1980

Thesis Advisor: D. W. Netzer

Approved for public release; distribution unlimited

SECURITY CLASSIFICATION OF THIS PAGE (When Data Entered)

REPORT DOCUMENTATION PAGE

READ INSTRUCTIONS BEFORE COMPLETING FORM

1. REPORT NUMBER	2. GOVT ACCESSION NO. / 3. RECIPIENT'S CATALOG NUMBER
4. TITLE (and Subtitle): AN EXPERIMENTAL STUDY OF SOLID PROPELLANT DEFLAGRATION USING HIGH SPEED MOTION PICTURES AND POSTFIRE RESIDUE ANALYSIS	5. TYPE OF REPORT & PERIOD COVERED: Engineer's thesis; June 1980
	6. PERFORMING ORG. REPORT NUMBER
7. AUTHOR(s): Vincent Daniel DiLoreto	8. CONTRACT OR GRANT NUMBER(s)
9. PERFORMING ORGANIZATION NAME AND ADDRESS: Naval Postgraduate School, Monterey, California 93940	10. PROGRAM ELEMENT, PROJECT, TASK AREA & WORK UNIT NUMBERS: 61152N:RR000-01-10, N0001480WR00054
11. CONTROLLING OFFICE NAME AND ADDRESS: Naval Postgraduate School, Monterey, California 93940	12. REPORT DATE: June 1980 / 13. NUMBER OF PAGES: 120
14. MONITORING AGENCY NAME & ADDRESS (if different from Controlling Office): Naval Postgraduate School, Monterey, California 93940	15. SECURITY CLASS. (of this report): Unclassified / 15a. DECLASSIFICATION/DOWNGRADING SCHEDULE

16. DISTRIBUTION STATEMENT (of this Report)

Approved for public release; distribution unlimited

17. DISTRIBUTION STATEMENT (of the abstract entered in Block 20, if different from Report)

18. SUPPLEMENTARY NOTES

19. KEY WORDS (Continue on reverse side if necessary and identify by block number)

solid propellants, motion pictures, residue

20. ABSTRACT (Continue on reverse side if necessary and identify by block number)

Six aluminized propellants were investigated through strand burning in a windowed combustion bomb at 500 psi and 1000 psi. Postfire particle residues were analyzed with a scanning electron microscope and found to have bi-modal size distributions. The mean diameter of the fine particle distribution was approximately 10 μm in all cases while the mean diameter of the coarse particles was approximately the same size as the initial aluminum cast in

DD FORM 1 JAN 73 1473 EDITION OF 1 NOV 65 IS OBSOLETE
S/N 0102-014-6601

SECURITY CLASSIFICATION OF THIS PAGE (When Data Entered)

20. (continued)
the propellant. Measurements taken from the high speed motion pictures included resolution, propellant burning rate, the diameter of the burning particles ejected from the surface, and vertical velocity of burning particles. The diameters of the burning particles were approximately 7 to 12 times the diameter of the initial aluminum cast in the propellant. Aluminum size had only small effects on burning rate. The smallest particle that could be accurately resolved with the motion pictures was approximately 60 μm.

Approved for public release; distribution unlimited

An Experimental Study of Solid Propellant Deflagration Using High Speed Motion Pictures and Postfire Residue Analysis

by

Vincent Daniel DiLoreto
Major, United States Marine Corps
B.S., Pennsylvania State University, 1971

Submitted in partial fulfillment of the
requirements for the degrees of

MASTER OF SCIENCE IN AERONAUTICAL ENGINEERING

and

AERONAUTICAL ENGINEER

from the

NAVAL POSTGRADUATE SCHOOL
June 1980

ABSTRACT

Six aluminized propellants were investigated through strand burning in a windowed combustion bomb at 500 psi and 1000 psi. Postfire particle residues were analyzed with a scanning electron microscope and found to have bi-modal size distributions. The mean diameter of the fine particle distribution was approximately 10 μm in all cases while the mean diameter of the coarse particles was approximately the same size as the initial aluminum cast in the propellant. Measurements taken from the high speed motion pictures included resolution, propellant burning rate, the diameter of burning particles ejected from the surface, and vertical velocity of burning particles. The diameters of the burning particles were approximately 7 to 12 times the diameter of the initial aluminum cast in the propellant. Aluminum size had only small effects on burning rate. The smallest particle that could be accurately resolved with the motion pictures was approximately 60 μm.

TABLE OF CONTENTS

LIST OF TABLES

LIST OF FIGURES

ACKNOWLEDGEMENT

In addition to my appreciation for the patience and understanding shown by my wife and daughter during this study, I would like to acknowledge the advice and assistance provided by Professor D. W. Netzer. Appreciation is also expressed to Mr. E. Dubrov for his general assistance throughout the project and to Mr. C. Patton of the Hopkins Marine Institute for his instruction in SEM microscopy.

I. INTRODUCTION

Practically all tactical missiles and many strategic missiles employ solid propellants for missile propulsion. Solid propellants are primarily of two types: double base and composite. Double base propellants normally consist of a mixture of monopropellant molecules, such as nitrocellulose and nitroglycerine. Composite propellants normally consist of a mixture of oxidizer particles, such as ammonium perchlorate (AP), imbedded in a fuel/binder, such as polybutadiene-acrylic-acid (PBAA). In addition, most solid propellants contain metal additives. The most common metal additive is aluminum in a fine powder form. The purpose of the aluminum is twofold: first, to increase the energy content and thus the specific impulse; second, to suppress pressure oscillations in the flow field by means of two phase flow interactions between the chamber gas and the aluminum/aluminum oxide (Al/Al_2O_3) particles which are injected into the chamber flow as the propellant burns.

The burning propellant may produce agglomerates of Al/Al_2O_3 which can contain thousands of the original aluminum particles added to the propellant. The agglomerate size is a function of many factors such as propellant type, original aluminum size, chamber pressure, burning rate, and aluminum concentration. Two phase flow in the rocket motor can result

in large losses in delivered impulse. These losses result from thermal and velocity lag of agglomerates in the flow field. In addition, unburned aluminum can also cause performance losses. Two phase flow processes in the nozzle produce the breakup of sufficiently large agglomerates and thereby permit reasonable combustion efficiencies to be attained. In general, smaller agglomerate masses lead to higher combustion efficiencies and lower two phase flow losses as the combustion products are accelerated through the rocket nozzle. However, the frequencies of the undesired acoustic instabilities dictate the required range of agglomerate mass and size to defeat the pressure oscillations.

The competing chemical, thermodynamic, aerodynamic, and physical processes are very complex and it is difficult to quantitatively identify the magnitude of the various specific impulse losses. Optimization and prediction of rocket motor performance through measurement and theoretical techniques are hindered by uncertainties. The introduction of aluminum into the propellant further complicates these problems by introducing two phase combustion, two phase heat transfer, and two phase flow phenomena.

Numerous investigations have been conducted to examine the aspects of aluminum combustion in solid propellants and solid propellant rocket motors. Studies of burning aluminized propellants and propellant ingredients in quiescent atmospheres have revealed some of the details of the processes taking

place on the surface [1, 2, 3]. Models have also been proposed to account for the agglomeration and ignition mechanism of aluminum particles in solid propellants [4]. Detailed size analyses of propellant constituents and combustion products have been used extensively [5]. The combustion and agglomeration processes of aluminum particles emitted from the surface of a propellant burning under cross flow conditions have also been investigated [6]. In addition, experiments have been conducted on the breakup of Al/Al_2O_3 agglomerates in accelerating flow fields [7].

Detailed analysis of actual motor firings has provided some information on the relationship between solid propellant formulation variables and motor performance [8]. Considerable information about the behavior of aluminized propellants in solid rocket motors has also been compiled and reported [9]. Results have been correlated on three aspects of aluminum combustion in solid propellants and solid propellant rocket motors: formation of Al/Al_2O_3 agglomerates during propellant combustion, the influence of cross flow on agglomerate formation, and agglomerate breakup under shear flow conditions [10].

Most of the individual investigations discussed above have utilized only one, or perhaps two, principal diagnostic techniques to study a particular aspect of solid propellant combustion. Little has been done to relate the results obtained from the various methods. It would be desirable to be able to relate the principal information that is obtained from the

most widely used experimental techniques. This could be done by applying the various methods to a specially formulated series of metallized propellants burned under a parametric series of operating environments. This approach should result in a better understanding of the effects of design variables and propellant properties on two phase flow phenomena and should provide valuable new information for validating/improving analytical models.

In order to address this problem, a research effort has been initiated at the Naval Postgraduate School. This effort was begun under the sponsorship of the Naval Postgraduate School Foundation Research Program and subsequently expanded through sponsorship of the Air Force Rocket Propulsion Laboratory (AFRPL), Edwards, California. The propellants to be employed have been provided by the Aerojet Solid Propulsion Company and by the Naval Weapons Center, China Lake, California. The investigation consists of three interrelated and concurrent phases: (a) high speed motion picture and residue analysis from propellant strands burned in a windowed combustion bomb, (b) mean particle size determination from 2-D and 3-D rocket motors using light scattering methods, and (c) holographic studies of the combustion process in a windowed 2-D motor.

A series of combustion bomb tests were conducted in which propellant strands were burned in an inert gas environment at various pressures. The windowed combustion bomb permitted high speed motion picture analysis of the burning

propellant strand from which burning rate and the velocity and diameter of burning agglomerates can be obtained. Postfire residue can also be collected and prepared for examination under an optical or electron microscope to determine the size distribution and composition of particles in the residue. The major advantages of the combustion bomb technique are: (a) the entire duration of the burning of the propellant strand can be recorded to observe the time varying characteristics of the event, (b) collection of postfire residue can be carefully controlled, (c) combustion pressure can be independently varied, and (d) tests are easily conducted and inexpensive.

The major disadvantage of the combustion bomb technique relates to the different burning environment that exists in comparison to the rocket motor propellant grain, for example: (a) there is no cross flow over the burning surface, (b) the particle laden flow does not accelerate through a nozzle, (c) burning agglomerates are quenched in the cold inert gas used to pressurize the bomb, and (d) heat transfer to the burning surface and the related burning rate are often dependent upon the dimensions of the propellant strand and the combustion bomb.

High speed motion pictures which can be utilized with the combustion bomb or in a windowed 2-D motor provide the advantage of continuous observation throughout the burning process. However, image resolution limitations generally do not permit particles with diameters less than approximately 30 μm to be

resolved [11]. Depth of field is also limited if any appreciable magnification is employed. In addition, smoke and/or a large number concentration of particles above the burning surface can severely restrict the quality of the obtainable data. The latter problem can be minimized by restricting the percentage of aluminum in the propellants to low values.

The second part of the overall effort consists of a series of tests utilizing a small, 3-D, end-burning rocket motor. Simple opacity measurements will be used to determine the effects of motor operating conditions and propellant properties on exhaust particle concentrations. Angular scattering measurements from a laser light source will also be made to obtain the mean particle size and concentration [12, 13, 14]. Performance parameters such as thrust and characteristic velocity can also be measured. Additionally, exhaust residues will be collected for comparison with the light scattering measurements. The latter data will be used for examining the effects of nozzle contours and for comparison with the strand residue data from the combustion bomb tests. The major advantages of the small 3-D rocket motor tests are (a) the combustor and exhaust flow environments are realistic, and (b) mean particle size and concentration in the nozzle exhaust flow can be measured without interfering with the flow field. The major disadvantages of the 3-D rocket runs are (a) only mean particle size can be obtained by the light scattering techniques, and (b) the collection of particles from the

exhaust is more difficult than with the combustion bomb tests.

The third component of the overall effort consists of a series of runs utilizing a 2-D, windowed rocket motor. All of the experimental techniques applied to strand burners and end-burners will be utilized. The burning propellant will be observed with high speed motion pictures to determine time dependent behavior. Light scattering techniques will be applied to the nozzle exhaust. Exhaust residue will be collected for particle analysis. In addition to these techniques, the windowed 2-D rocket motor permits analysis by means of holography. Holograms exposed over the period of nano-seconds should allow 3-D photographic analysis to be conducted at any point in the flow including the chamber, throat, nozzle, and exhaust plume. The major advantages of 2-D windowed rocket experiments are : (a) resolution to less than 10 μm and excellent depth of field with holograms [15, 16], and (b) the combustor and exhaust flow environment are close to actual conditions. The major disadvantages of the 2-D windowed rocket experiment are: (a) the holograms provide a record of only an instant in the event and not a complete time history, and (b) the manual reduction of holographic data is time consuming. Data collected will be compared and correlated with the data obtained from the strand and end-burning experiments.

The results of the overall experimental program should: (a) define the strengths, weaknesses, and interrelationships

between the various diagnostic techniques employed, (b) provide detailed data on the performance and operating characteristics of a family of well-documented propellants, and (c) define the particle behavior and characteristics throughout the entire flow field.

The purpose of this investigation was to conduct the combustion bomb experiments with propellant strands as discussed above. High speed motion pictures and particle collection coupled with scanning electron microscope analysis were the principal diagnostic methods employed. The data obtained for later correlation with data from light scattering and holographic diagnostic techniques were: (a) propellant burning rates, (b) near-surface burning particle sizes and velocities, (c) postfire particle size distributions, (d) photographic resolution limitations, and (e) the relationships between observed burning particle behavior and postfire residue characteristics.

II. METHOD OF INVESTIGATION

Six solid propellants containing aluminum particles of different diameters were tested in a combustion bomb at two pressures. Postfire residue was collected and analyzed with a scanning electron microscope to determine postfire particle size distributions. High speed motion pictures were taken of the propellant deflagration to examine the time varying characteristics of the event. Data obtained from the residue analysis and high speed motion pictures were correlated to determine the effects of combustion pressure and initial aluminum size in the propellants.

III. EXPERIMENTAL APPARATUS

The combustion bomb used in this investigation was a two piece unit made from 347 stainless steel. It had a core volume of about 34 cubic inches and an inside diameter of 2 inches. Three optical quality glass windows, each one inch in diameter, were incorporated in the bomb. Two windows were located diametrically opposite to one another and were utilized for high speed photographic observation and back lighting of the burning strands. The third window was located 90 degrees between the other two and was used for side lighting. Due to high design operating pressures, the viewing diameter through the glass windows was reduced to one-half inch by the window cover plates. O-ring pressure seals were used around the windows and at the junction of the two piece unit. Figure 1 is a schematic and Figure 2 is a photograph of the combustion bomb.

The combustion bomb was pressure tested to 4500 psi. The maximum expected operating pressure is 3000 psi. In this investigation, the maximum pressure used was 1000 psi.

Pressurization of the combustion bomb, ignition of the propellant strands, and activation of the high speed camera were controlled from a remote control panel located behind a steel safety booth with a one inch thick plexiglass viewing window. The control booth was situated out of the line of sight of the combustion bomb windows as a safety precaution.

Figure 3 is a photograph of the control booth. Figure 4 is a photograph of the remote control panel. Figure 5 is a circuit diagram of the remote control panel.

The propellant strand ignition system consisted of two electrodes mounted on either side of the specimen mounting post. Between the electrodes a length of 0.008 inch diameter nickel-chromium ignition wire was connected. The ignition wire was in series with a variable resistor to control the current provided by a 12 volt DC wet cell battery. A continuity check circuit with a visual indicator light was also included.

The combustion bomb pressurization system was controlled from the remote control panel through a dome valve. The dome valve controlled the nitrogen flow from the compressed gas reservoir. A pressure tap and gauge were used to read the bomb pressure directly and could be viewed from the control booth. An exhaust port valve on the top of the bomb was manually set to control the rate of exhaust flow for smoke removal. The nitrogen flow was introduced through a porous plate in the bottom of the chamber of the bomb, passed up through the test section, and then vented to the atmosphere.

The high speed camera could be controlled through the remote control panel in either a manual or automatic mode. In the manual mode, the camera was activated when desired. In the automatic mode, the camera was activated through a timing

delay after the ignition circuit was closed. In this investigation, the manual mode was used.

For photographic observation, a Hycam model K2004E-115 high speed motion picture camera was used. Although various framing rates were examined in the preliminary tests, a rate of 5000 frames per second was selected for use throughout the investigation. A Red Lake Millimite TLG-4 oscillator was connected to the camera on all runs to provide timing marks on the film edge at the rate of 1000 per second.

The lens used on the camera was an Elgeet 77mm/f1.9 lens. The minimum focus distance for this lens is 3 feet. To position the camera closer for better resolution, a 1.625 inch extension tube was attached to the lens. With the extension tube, the front of the lens could be brought within one inch of the observation window of the combustion bomb and the focus distance was 5 inches. In this configuration the magnification was about 1X and the depth of field at f/4 was about 4 mm [17].

An SLM-1200 projector and a 650 watt focused flood light were used to provide side lighting and back lighting as required.

Figure 6 is a schematic and Figure 7 is a photograph of the layout of the experimental apparatus.

Movie film types included 7724 4X negative (ASA 400), 7222 2X negative (ASA 250), 7250 Ektachrome (ASA 250), and 7267 Kodachrome (ASA 25). The 7267 Kodachrome was the primary

film used in this investigation. 7250 Ektachrome was used in a few cases for comparison.

For collecting postfire residue, a stainless steel collection cup was built. The cup had an inside diameter of 1.75 inches, a wall thickness of 0.0625 inches, and a height of one inch. Three holes were drilled in the bottom of the cup to fit over the two ignition electrodes and the specimen mounting post. At the point of contact with the cup, the ignition electrodes were electrically installed to prevent a short in the ignition circuit. When installed in the bomb, the entire propellant strand was contained within the volume of the cup. There was one eighth of an inch of radial space between the outer radius of the cup and the inner radius of the bomb so as not to disrupt the flow of nitrogen for pressurization and postfire purge.

The residue collected was ultrasonically cleaned in an Electromation Model 250 ultrasonic cleaner. Ethanol was used as the bath. After cleaning, the particles were dried in a vacuum evaporator installed in a Hotpack Model 1262 refrigerator/oven. The vacuum was drawn with a CENCO Hyvac 2 roughing pump.

The dried particles prepared for electron microscopy were gold coated in a Denton Vacuum Evaporator with a DSM-5 sputter module. Particle size analysis was done on an Hitachi S-450 scanning electron microscope (SEM). Photographic records of SEM observations were recorded on Polaroid Type 52 Film.

To determine the percentage of metal recovered from the combustion of a propellant strand, the strand and the dried residue were weighed. The scale used was a Mettler Type H15 with a resolution capability of +/- 0.0001 grams.

IV. EXPERIMENTAL PROCEDURES

A. SAMPLE PREPARATION AND TEST CONDITIONS

Six propellants were selected for testing. The propellant formulations are listed in Table I. The first four propellants listed were specially formulated and provided by the Aerojet Solid Propulsion Company. They represent a family of the same composition by weight where the only variable was the size of the spherical aluminum particles. The last two propellants listed were provided by the Naval Weapons Center and contained only a small amount of Al_2O_3 particles as a metal additive.

Propellant strands were cut to a size that would fill the field of view of the high speed camera. The strands were cemented to stainless steel pedestals which fit into the propellant sample mounting post in the combustion bomb. Dimensions of the propellant strands are given in Figure 8. The tops of the strands were cut horizontally during the initial phase of testing. Subsequently, the tops were cut at a 45° angle to permit better observation of the burning surface.

Propellant strands were burned in a nitrogen environment within the combustion bomb. Four tests were conducted with each propellant: (1) particle collection at 500 psi, (2) particle collection at 1000 psi, (3) high speed motion pictures at 500 psi, and (4) high speed motion pictures at 1000 psi.

Particle collection and high speed motion pictures were not conducted in the same test. A flow of nitrogen was required through the combustion bomb during the high speed motion pictures to purge smoke from the combustion bomb so that the burning strand could be observed. Smoke and many of the particles were exhausted to ambient conditions by the purge, and it was found that the remaining particles collected in the bomb were not representative of the total postfire residue. Thus, for particle collection, the purge valve was closed during the combustion. Additionally, the particle collection cup completely encircled the propellant strand preventing observation through the combustion bomb windows. Figures 9a and 9b show propellant strands mounted for particle collection and high speed motion picture tests respectively.

Tables II and III summarize the test conditions for the particle collection and the high speed motion pictures respectively. Although a total of twenty-four runs were required to complete the investigation, additional tests are included in Tables II and III for discussion.

B. POSTFIRE RESIDUE COLLECTION AND TREATMENT

In preparation for the collection of postfire residue, the internal surfaces of the combustion bomb were cleaned. Acetone was used as a cleaning solvent. The particle collection cup was cleaned with ethanol in the ultrasonic cleaner.

The collection cup was positioned in the bomb and the propellant strand was placed in the mounting post. Nickel-chromium ignition wire was attached between the ignition electrodes and placed in contact with the entire top surface of the propellant strand. Prior to closing the bomb, a continuity check of the ignition circuit was conducted from the remote control panel.

With the combustion bomb sealed and the purge valve closed, the bomb was pressurized to the test pressure. The ignition circuit was then closed to ignite the propellant strand.

After the burning was complete, the bomb was allowed to remain pressurized and undisturbed for at least five minutes to permit particles to settle into the collection cup. The purge valve was then opened a small amount to slowly relieve the pressure in the bomb and to prevent disturbance of the collected postfire residue.

The bomb was opened and the collection cup was placed inverted into a 50 ml beaker. Ethanol was poured into the beaker to cover the cup. The beaker was then placed in a bath of ethanol in the ultrasonic cleaner and treated for five minutes to wash the residue off the collection cup and to separate contaminants such as carbon or incompletely reacted material from the Al/Al_2O_3 particles.

After ultrasonic treatment, the collection cup was removed from the beaker and the remaining solution was left undisturbed for fifteen minutes to allow particles to settle. This settling time was based on Stoke's law which relates the equality

between the gravitational and the drag forces on a particle falling through a liquid at constant velocity. Table IV lists settling times for Al_2O_3 particles of various diameters in 2 cm of ethanol [5].

At the end of the settling time, all but 5 mm of the ethanol in the beaker was carefully poured off. Clean ethanol was added to the beaker to a depth of 2 cm, and the residue was treated with the same procedures for a second and third time.

With all but 5 mm of ethanol drained from the beaker after the third cleaning cycle, the particle sample was ready to be dried. This was accomplished in the oven at 80° C while under a vacuum. Fifteen minutes was allowed for drying the particles.

C. SEM SAMPLE PREPARATION AND MICROSCOPY

The technique for mounting the postfire residue on SEM sample holders was found to be just as important as the technique for washing and drying the residue if good quality photomicrographs of postfire residue particles were to be obtained. Techniques for mounting propellant residue on SEM sample holders are discussed in the literature [5]. The technique chosen for this analysis was to mount the residue on a thin layer of epoxy on the SEM sample holder. The sample holder for SEM microscopy was an aluminum pedestal about 12 mm in diameter. The surface of the pedestal was generally too rough to spread an ultra-thin, even layer of epoxy. To provide a smooth surface, the pedestal was prepared by first sanding with a number

"O" grit emery cloth and then polishing with a 15 μm Al_2O_3 slurry on a broadcloth. The surface was then rinsed with ethanol.

Spreading a layer of epoxy of proper thickness on the prepared pedestal became a matter of experience after the results of previous efforts had been observed. In general, it was desired that the epoxy layer be no higher than the equator of spherical particles. If this condition were achieved, actual particle diameters could be observed and measured. If the particles were more deeply immersed in the epoxy, a dome which was smaller than the actual diameter was observed and measurements were inaccurate. In the other extreme, a particle that was in contact with the epoxy only at its pole could be readily observed since there was no problem with shadows below the particles when observed with the SEM. In general, it was found that ultra-thin, uniformly smooth layers of epoxy provided the best results.

As an example of poor SEM sample preparation, refer to Figures 10a and 10b which are photographs from test number 1500250180. They show postfire residue that has been inadequately cleaned and also a layer of epoxy that is too thick and uneven. Figures 11a and 11b are photographs from test number 1520090480. They show a similar condition of a thick and uneven epoxy layer, however in this case the particles have been properly cleaned.

Two types of epoxy were tried. The first was a clear epoxy that hardened in five minutes. The second was a clear epoxy that hardened in twenty-four hours. The latter, Chem Tech T-88, was the easiest to use. A small quantity was placed on a polished pedestal with a glass rod. Then a razor blade was used to spread the epoxy by holding the razor blade at a forty-five degree angle with respect to the pedestal surface and drawing the razor blade across the pedestal while pressing with moderate force. Additional sweeps of the razor blade were necessary when the layer of epoxy was uneven or streaked.

After a uniformly thin layer of epoxy was spread, the dried postfire residue was scattered on the epoxy. This was accomplished by holding a 50ml beaker containing the residue at an angle over the pedestal and tapping the beaker with a glass rod. The residue spilled over the lip of the beaker in a fine shower of particles and was randomly distributed on the epoxy. Any particles that adhered to the inside surface of the beaker were coaxed out with the glass rod. The intent was to achieve an uncluttered, uniform surface distribution of particles on the pedestal. This desired distribution was easier to obtain when the mean particle diameter was greater than 50 μm. For mean diameters less than 50 μm, the particles tended to adhere to one another and the resulting surface distribution tended to be more dense and more closely packed.

After the epoxy cured, the sample was gold plated using the DSM-5 sputter module. The thin layer of gold that was applied measured 100 to 200 Angstroms in thickness. A layer of this thickness did not obscure the surface details of particles which had diameters greater than 1 μm. The gold coating was conductive and prevented the sample from charging by conducting the electrical charge from the surface to the grounded aluminum pedestal. A charged particle appears to have a surrounding halo, which is very bright on the CRT and eventually masks the particle. An additional benefit of plating is that gold is usually a better emitter of secondary electrons than the underlying sample and thus provides enhanced image detail. As an example of particle charging, refer to Figure 12. These are photographs from test number 1515280380 in which the SEM sample was not gold plated.

The postfire particle samples were examined with the SEM at an accelerator voltage of 15 kV and magnifications from 50X to 2000X. A series of photomicrographs were taken with the SEM of each of the samples. Each series consisted of the following: (a) one large scale view at 90° incidence to present an overview of particle size distribution and the surface density of particles on the sample holder, (b) two small scale oblique views at 15° incidence to show the manner in which the particles were imbedded in the epoxy layer, and (c) two small scale views at 90° incidence corresponding respectively to the same local areas that were photographed in the oblique

views. The latter two views were utilized to count particles and measure particle diameters. All five photographs in each series were automatically labeled by the SEM with a scale factor in microns.

D. HIGH SPEED MOTION PICTURES

The selected combination of camera lens and lens extension tube resulted in approximately a 5 inch focal length, which located the face of the lens just outside the window of the combustion bomb with about one inch of clearance for focusing movement of the camera/lens system. The focal length was as short as possible to provide the best resolving power. The camera was rigidly mounted to an aluminum bracket that could be traversed along a rail aligned with the diametrically opposed windows of the combustion bomb.

Prior to a test, the eyepiece of the camera was focused on the crosshairs of the accessory focusing screen. Rough focusing on the propellant strand was done by moving the entire camera. Fine focusing was done with the lens focusing ring. To ensure that the entire thickness of the propellant strand was contained within the depth of field, the ignition wire was selected as the point of sharpest focus.

Two sources of external lighting were used as required. The 1200 watt lamp was used for side lighting and the 650 watt lamp was used for either side or back lighting.

A framing rate of 5000 frames per second was used on all tests. External illumination and f/stop were dependent on

the type of film used. These parameters were determined by practice runs and are listed in Table III.

The Millimite timer was set at 1000 cycles per second for all tests. The timing marks recorded on the edge of the film were required to determine the actual framing rate and thus the elapsed time for an observed event. One hundred foot rolls of film were used for all tests and the selected framing rate was attained after about 65 feet of film were exposed.

A brass scale that measured 5 mm high was attached to the right ignition electrode so that it could be seen in the field of view of the camera. This provided a known length scale for the high speed motion picture data reduction. With a propellant strand mounted and wired for ignition, the combustion bomb was sealed and pressurized to the test pressure. The purge valve on the top of the bomb was opened slightly to allow a flow of nitrogen through the bomb while maintaining the desired pressure. The required flow rate of the purging flow to prevent smoke accumulation in the combustion bomb was determined from practice runs. A higher flow rate was required at 1000 psi than at 500 psi. Once the apparatus was set for the test, the high speed camera was controlled from the remote control panel. The camera was started manually at the same instant that the ignition circuit was closed. In this fashion the entire duration of the deflagration was recorded.

To ascertain the resolution capability of the high speed motion pictures, the USAF 1951 resolution target was utilized.

Various film types were tested. For most film types, the resolution target was photographed twice: (1) through the window of the combustion bomb, and (2) with the window removed. Table V lists the resolution target test conditions.

V. RESULTS AND DISCUSSION

A. POSTFIRE PARTICLE SIZE ANALYSIS

Determination was made of the percentage of metal recovered in the particle collection and preparation process. Before a particle collection test, the propellant strand was weighed. Knowing the percentage of aluminum by weight, the weight of aluminum in the strand was calculated. After the postfire residue had been ultrasonically treated and dried, the residue was weighed. The weight of the particles recovered was compared with the initial weight of aluminum. In a test case using the sample from test run 1445180480, the following data were obtained:

1. Strand weight, 0.3257 gr
2. Initial aluminum weight, 0.0163 gr
3. Recovered particle weight, 0.0021 gr
4. Percentage recovered, 12.9%

Other particle samples were compared visually with this sample, and the quantity recovered appeared about the same in all cases.

Considering the relative positions of the collection cup and the propellant strand in the combustion bomb, it was felt that the percentage of particles collected was representative of the total sample. The residue on the walls of the collection cup was very similar in appearance to that deposited on the combustion bomb walls. It would be possible

to collect a larger percentage of the particles if a taller collection cup were used. The internal dimensions of the combustion bomb would permit a cup with a height of about three and one-half inches to be mounted in the same manner as the one used.

The SEM photomicrographs of the postfire particle specimens for the test conditions specified in Table II are presented in Figures 13 through 24.

To plot initial particle size distribution, forty particles were chosen from each test and measured. To obtain a random and unbiased sample, particles were selected from the intersections of a fourteen by sixteen line grid superimposed over the 3½ by 4 inch Polaroid prints. Diameter measurements were made utilizing the scale at the bottom of each photograph. Plots of particle distributions for the test conditions specified in Table II are presented in Figures 25 through 36.

The plots indicate a bi-modal particle size distribution. The bi-modality is typical for aluminum combustion products. Experimental data from previous investigations suggest that condensed phase oxidation of aluminum contributes to coarse residue, whereas vapor phase oxidation results in fine residue [5]. Shedding of fine particles by burning agglomerates is another possible mechanism. Due to the bi-modal character of these particle size distributions, two average diameters are presented on each plot. One applies to the fine particle

distribution and the other to the coarse particle distribution. For the WGS-7, NWC-1, and NWC-2 propellants with initial metal powder mean diameters of about 8 μm, bimodal particle size distributions were not discerned. For these propellants the average diameter of the entire sample is given in the respective figure.

The number of particles which must be sized from the SEM photographs in order to obtain a statistically valid sample size depends upon a number of conditions: (a) percentage of residue that is collected, (b) how the residue is collected and washed, (c) how the residue is distributed on the SEM sample holder, and (d) how the particles in the photographs are selected for counting. One thousand particles have been counted by some investigators [5], but fewer may be used.

To determine how closely the forty particle distributions would compare with distributions for larger numbers of particles, two samples were selected for more detailed analysis. Approximately 220 particles were measured in each of the tests. Comparisons of the 40 particle distributions with the 220 particle distributions are shown in Figures 37 and 38. The computed average diameters of fine and coarse particle distributions between the respective samples was in good agreement, although the larger sample in both cases generated slightly smaller average diameters. These results indicated that the forty particle samples provided at least closely representative size distributions for the total particulate residue.

A plot was constructed of the average initial aluminum particle diameter in the propellant versus the average postfire particle diameter. This data is presented in Figure 39. A reference line with unity slope was superimposed on the data as an aid in size comparison. The data indicated that the mean diameter in the coarse particle distribution of the postfire residue closely matched the initial aluminum size in the cast propellants. The mean diameters in the fine postfire particle distributions increased slightly with increasing aluminum size. These results appear to indicate that little agglomeration is occurring and that many of the aluminum particles which leave the surface are rapidly quenched. Preliminary results from tests at the Aerojet Solid Propulsion Company with the same propellants have indicated that no significant agglomeration occurs and that metal combustion procedes almost to completion (i.e., yields primarily Al_2O_3) [18]. Al_2O_3 particles typically have smooth surfaces when compared to quenched aluminum particles. Almost all particles collected in this study were quite smooth, which agrees with the Aerojet results.

B. HIGH SPEED MOTION PICTURE ANALYSIS

One of the objectives of this investigation was to evaluate the strengths and weaknesses of the diagnostic techniques employed. It is intended to compare these capabilities with those of light scattering and holographic techniques to be

to be utilized in later phases of this experimental program. An area of interest was the maximum resolution capability of high speed motion pictures. The procedures used to photograph the USAF 1951 resolution target were discussed in Section IV. Results from tests 1515310580 and 1615310580 are presented in Figure 40 (type 7222-2X film). Figure 40a and 40b show a comparison of resolution target photographs taken with and without the combustion bomb window in place where the maximum resolution was 70 μm and 60 μm respectively. Figure 40c is a photograph taken in test 1745030480 (type 7250 film) without the combustion bomb window where the maximum resolution is 50 μm. Based on the resolution target tests, the maximum resolution expected in this investigation through the combustion bomb window was 60 μm. It was noted when focusing the camera for the resolution target tests that the maximum resolution through the camera optics was 15 μm. The difference between this and the results obtained on film were attributed to the limiting resolution capability of the film and/or to camera vibration.

Figures 41 and 42 are prints of typical frames from high speed motion picture tests 1415250580 (WGS-5A, 500 psi) and 1100250580 (WGS-5A, 1000 psi) respectively. A more dense particle distribution in the gas stream and more smoke are apparent in the test at the higher pressure. In addition, Figure 42 is an example of an uneven burning surface caused by the hot ignition wire falling against the side of the

propellant during the ignition sequence. Stages in the general behavior of the aluminum can be seen in the photographs. What appeared to be molten aluminum particles/agglomerates were observed on the propellant surface before particle ignition. The particles/agglomerates appeared as regions more brightly illuminated than the surrounding surface area. The vertical movement of the particles began with an apparent ejection from the propellant surface into the gas stream. In some cases this ejection was a rapid "pop-up" and in others it took place much more slowly as if there were some adhesion near the surface. As the particles left the surface, they ignited, and the diameters of the burning particles became larger than before ignition. Once ignited and separated from the surface, the particles moved with approximately constant velocity in the gas stream and exhibited a typical tail of flame pointing away from the surface. In this investigation, the general behavior of the aluminum was more easily observed for the propellants with initial aluminum particle diameters greater than 50 μm and at a pressure of 500 psi. As initial aluminum particle diameters decreased and pressure increased, the texture of the gas stream above the surface became less granular in appearance, and individual particles could not be readily distinguished from the uniformly bright sheet of flame. Additionally, more smoke was present at 1000 psi to obscure the surface. Smaller particles would probably be more easily observed for propellants formulated with even a

lesser percentage of aluminum to reduce the number concentration of aluminum particles above the burning surface.

Diameters of burning particles were measured in the region between the propellant surface and 4 mm above the surface. The diameters of these spherical flame envelopes were significantly larger than the diameters of the aluminum particles cast in the propellant. In general, the diameters of the burning particles were 7 to 12 times larger than the initial aluminum particles. Figure 43 is a plot of burning particle diameter versus initial aluminum particle diameter. The two propellants with the larger initial aluminum sizes showed increases in burning particle diameters as pressure increased. This result is in contrast to the mean postfire data in Figure 39 where minimal pressure dependence was observed. The large apparent size of the burning particles requires further investigation. Some possible explanations can account for the observed difference in diameters between burning particles and postfire residue. The burning particles could be large agglomerates with small flame envelopes that burn and shed mass until they reduce in size to much smaller particles. However, it would be quite unlikely that all four aluminized propellants would yield nearly the same ratios of initial-to-burning-to-final mean residue diameter and that the residue diameters are always nearly the same as the initial aluminum size. The burning particles could be small particles with very large flame envelopes. However, the particle sizes

near the surface before ignition occurred were nearly the same size as the burning particles. This result remains unresolved at this time. A sample of propellant has been provided to the Naval Weapons Center, China Lake. The Aerotherochemistry Division will take a high speed motion picture and conduct a particle collection experiment of propellant WGS-6A using their apparatus for comparison with the Naval Postgraduate School data.

Figure 44 is a plot of apparent burning particle diameter versus mean postfire particle diameter. The smaller particles of the distribution increased slightly in size with the apparent burning diameter as they did with initial aluminum size. This is not surprising considering the correlation obtained between burning and initial size shown in Figure 43. The apparent burning diameters of the coarse particle increased in a non-linear manner with mean postfire diameter.

The average velocities of several burning particles were measured in the region from the surface to 4 mm above the surface. Figures 45, 46, and 47 are plots of burning particle average velocity versus burning particle diameter for propellants WGS-5A, WGS-6A, and WGS-7A respectively. For the other propellants, velocity data were not obtained due to the inability to distinguish individual particles from the dense, brightly lit flame pattern. A linear least squares fit was applied to the velocity data points. The velocity of the particles decreased as the diameter increased, as expected.

This was a consistent trend for both particles from an individual propellant and for particles from propellant to propellant. The velocity of a particlar burning particle was approximately constant in the gas stream except in some cases in close proximity to the surface where it was noted to be slower. Representative values are shown in Figures 45 and 46.

The burning rates of the propellants were determined by measuring motion picture framing rates and the position of the burning surface for 1 mm increments over a 3 mm length near the center of the propellant strand. This region was selected to allow a steady state burning rate to be developed and to avoid heat transfer effects near the bottom the the propellant strand due to the stainless steel mounting pedestal. Figure 48 is a plot of burning rate versus initial aluminum particle diameter. The burning rates were relatively constant at a given pressure with a very slight increase as initial aluminum particle diameter decreased. The burning rates at 1000 psi were 17 to 19% greater than at 500 psi. These burning rates may not agree with burning rates obtained with larger propellant strands or in motors. Propellant strand diemensions can affect the burning rate through varying heat transfer effects and cross-flow velocities. 2-D and 3-D motors with larger propellant grains can also generate different burning rates.

Having determined the burning rates for both pressures tested, the exponent for the burning rate equation ($r = ap_c^n$)

was calculated for each propellant. The exponents are listed in Table VI.

VI. CONCLUSIONS AND RECOMMENDATIONS

Film resolution capabilities and propellant strand burning characteristics were determined for future comparison with results obtained using 2-D and 3-D propellant configurations with the additional diagnostic techniques of light scattering and holography.

Postfire particle size distributions were bi-modal in character. The mean diameters of the fine postfire particle distributions were approximately 10 μm in all cases, and increased slightly with increasing initial aluminum size. The mean diameters of the coarse postfire particle distributions were approximately the same size as the initial aluminum cast in the propellant, implying that little surface agglomeration and rapid quenching occurred.

The technique developed for collecting and preparing postfire residue for SEM analysis was satisfactory. Spectral analysis of postfire residue to determine composition could possibly provide additional data to correlate with fine and coarse postfire particle size distributions.

A minimum particle size of 60 μm could be observed through the window of the combustion bomb with the camera/lens system employed. The resolution was improved to 50 μm without the bomb windows. An area of potential improvement could be in the use of color film with an ASA in the range of 160 so that

a higher f/stop could be used with the same lighting to produce better resolution. Improving the rigidity of the camera installation could be another factor for enhancing resolution.

High pressure (1000 psi) and small initial aluminum size (less than 50 μm) limited the utility of high speed motion pictures. High burning rates, number concentration of burning particles on the surface and in the gas stream, and smoke generation, all contribute to this problem. Improvement in this area could possible be made with the use of aluminized propellants with less than 5% aluminum burning by weight.

The apparent diameters of burning particles in the gas stream were 7 to 12 times larger than the diameters of the initial aluminum cast in the propellant and of the mean diameters of the postfire residue. This result requires further investigation.

The velocity of any particular burning particle was nearly constant in the gas stream once it departed the region very near the burning surface. Smaller particles traveled at higher velocities as expected.

Propellant burning rates were approximately constant at a given pressure with only a slight increase for propellants with smaller initial aluminum size. Burning rates at 1000 psi were approximately 17% higher than at 500 psi.

TABLE I

PROPELLANT COMPOSITION

Propellant Designation	Binder % Weight	Oxidizer % Weight	Metal % Weight	Mean Metal Diamter, μm
WGS-5A	HTPB 12	AP 83	Al 5	75-88
WGS-6A	HTPB 12	AP 83	Al 5	45-62
WGS-7A	HTPB 12	AP 83	Al 5	23-27
WGS-7	HTPB 12	AP 83	Al 5	7-8
NWC-1[1]	HTPB 12	AP 87	Al_2O_3 1.0	8
NWC-2[1]	HTPB 12	AP 87.5	Al_2O_3 0.5	8

Note:
1. *Approximate formulation*

TABLE II

PARTICLE COLLECTION TEST CONDITIONS

Test Number	Propellant Type	Pressure PSI
1445240480	WGS-5A	500
1515280380	WGS-5A	500
1500250180	WGS-5A	500
1445180480	WGS-5A	1000
1030030580	WGS-6A	500
1600170480	WGS-6A	1000
1215030580	WGS-7A	500
1400240480	WGS-7A	1000
1100030580	WGS-7	500
1500210480	WGS-7	1000
1230010580	NWC-1	500
1520090480	NWC-1	500
150010580	NWC-1	1000
1200110580	NWC-2	500
1615100580	NWC-2	1000

TABLE III

HIGH SPEED MOTION PICTURE TEST CONDITIONS

Test Number	Propellant Type	Pressure PSI	Film Type	f/STOP	EXTERNAL LIGHT
1545050480	WGS-5A	500	EKTACHROME 7250	4.0	650 W SIDE
1600260480	WGS-5A	500	KODACHROME 25	1.9	1200 W SIDE 650 W BACK
1500300480	WGS-5A	1000	KODACHROME 25	1.9	1200 W SIDE 650 W BACK
1415010580	WGS-6A	500	KODACHROME 25	1.9	1200 W SIDE 650 W BACK
1415250580	WGS-6A	500	KODACHROME 25	1.9	1200 W SIDE 650 W BACK
1315010580	WGS-6A	1000	KODACHROME 25	1.9	1200 W SIDE 650 W BACK
1100250580	WGS-6A	1000	KODACHROME 25	1.9	1200 W SIDE 650 W BACK
1300250580	WGS-7A	500	EKTACHROME 7250	5.6	1200 W SIDE 650 W BACK
1700300480	WGS-7A	1000	KODACHROME 25	1.9	1200 W SIDE 650 W BACK
1345250580	WGS-7	500	KODACHROME 25	1.9	1200 W SIDE 650 W BACK

TABLE III
(continued)

Test Number	Propellant Type	Pressure PSI	Film Type	f/STOP	EXTERNAL LIGHT
1615300480	WGS-7	1000	KODACHROME 25	1.9	1200 W SIDE 650 W BACK
1500250580	NWC-1	500	KODACHROME 25	1.9	1200 W SIDE 650 W BACK
1145250580	NWC-1	1000	KODACHROME 25	1.9	1200 W SIDE 650 W BACK
1530250580	NWC-2	500	KODACHROME 25	1.9	1200 W SIDE 650 W BACK
1215250580	NWC-2	1000	KODACHROME 25	1.9	1200 W SIDE 650 W BACK

Note:
1. *The Frame rate for all tests was 5000 pictures per second.*

TABLE IV

PARTICLE SETTLING TIMES

PARTICLE DIAMETER, μm	SETTLING TIME, SEC
1	13072
2	3268
3	1452
4	817
5	523
10	131
15	58
20	33
25	21
30	15
40	8.1
50	5.2
60	3.6
70	2.7
80	2.0
90	1.6
100	1.3

NOTE: Settling times apply to a 2 cm depth of ethanol.

TABLE V

RESOLUTION TARGET TEST CONDITIONS

TEST NUMBER	FILM TYPE	WINDOW IN PLACE	PICTURES PER SEC	F/STOP	EXTERNAL LIGHT
1630250580	KODACHROME 25	NO	50-250	1.9	650 WATT BACK LIGHT
1645250580	KODACHROME 25	YES	50-250	1.9	650 WATT BACK LIGHT
1745030480	EKTACHROME 7250	NO	50-250	4	650 WATT BACK LIGHT
1700250580	EKTACHROME 7250	YES	50-250	4	650 WATT BACK LIGHT
1630310580	4X 7224	NO	50-250	5.6	650 WATT BACK LIGHT
1530310580	4X 7224	YES	50-250	5.6	650 WATT BACK LIGHT
1515310580	2X 7222	NO	50-250	4	650 WATT BACK LIGHT
1615310580	2X 7222	YES	50-250	4	650 WATT BACK LIGHT

TABLE VI

BURNING RATE EXPONENTS

PROPELLANT TYPE	BURNING RATE EXPONENT
WGS-5A	0.301
WGS-6A	0.273
WGS-7A	0.275
WGS-7	0.272
NWC-7	0.247
NWC-2	0.299

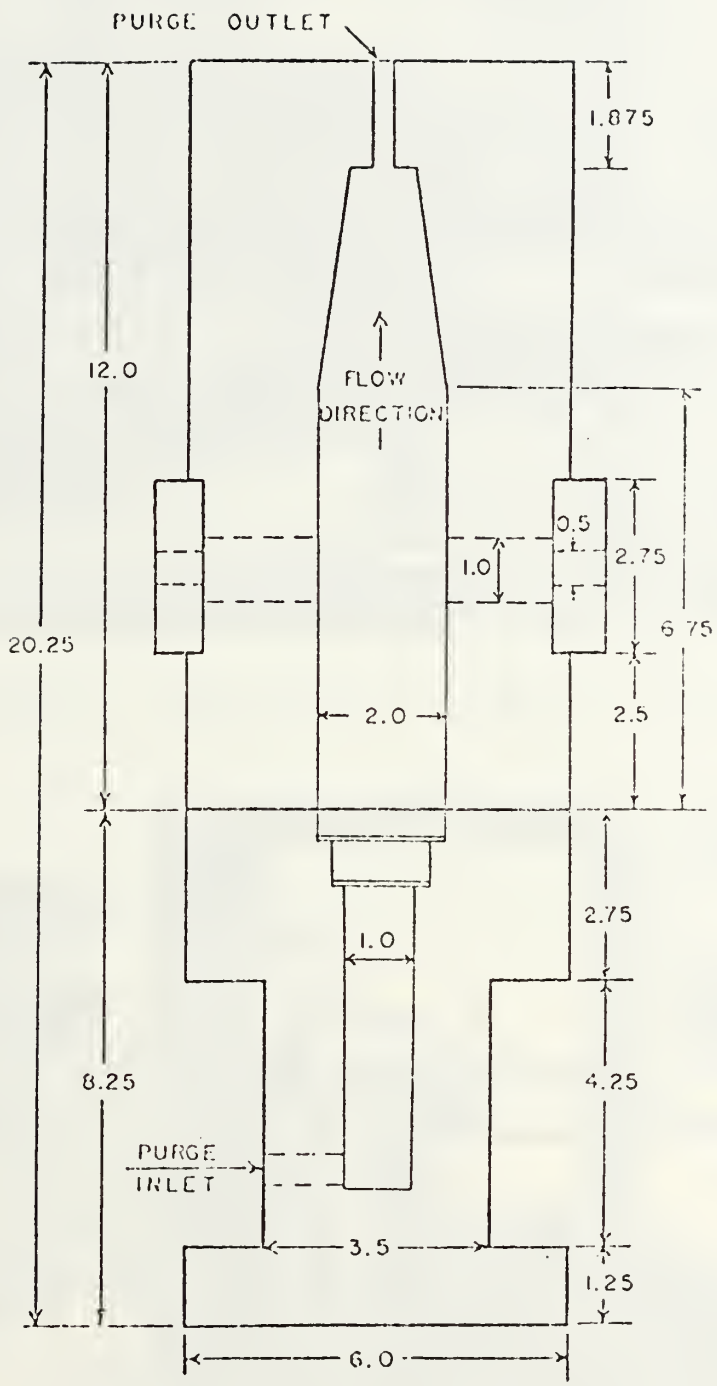

Figure 1.
Schematic of Combustion Bomb

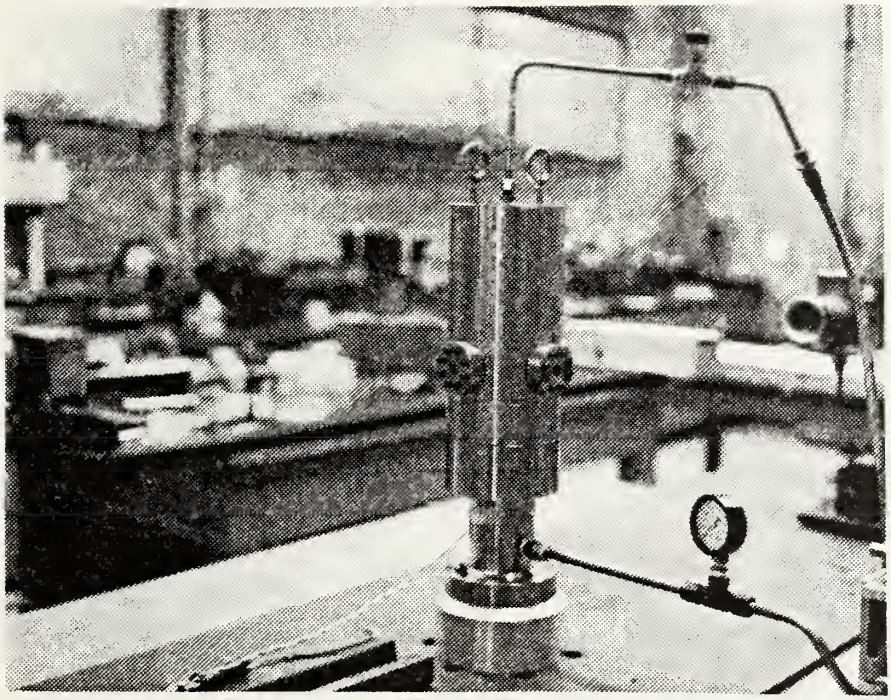

FIGURE 2. Photograph of Combustion Bomb

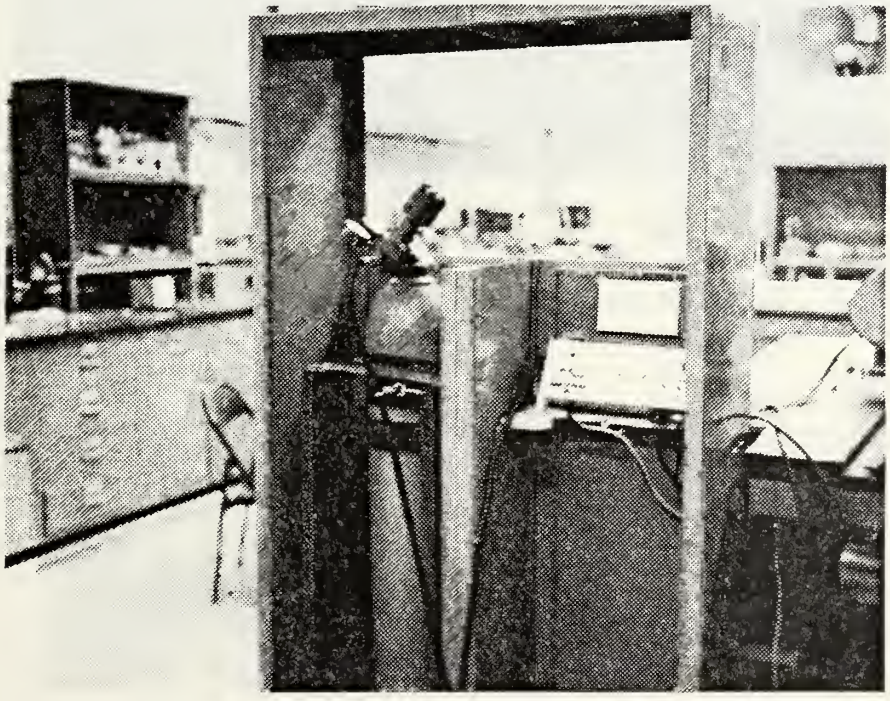

FIGURE 3. Photograph of Control Booth.

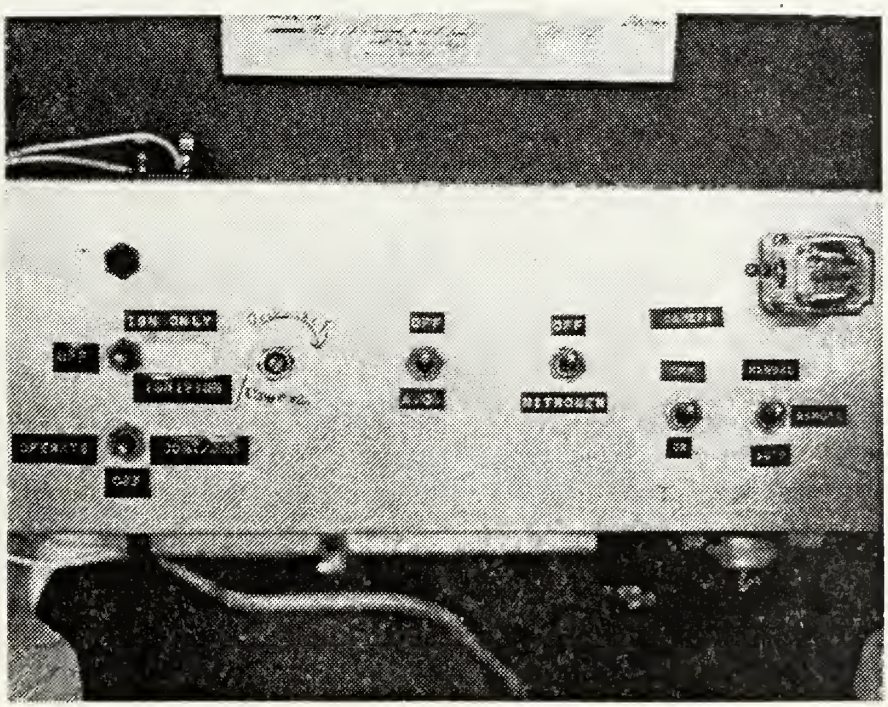

FIGURE 4. Photograph of Remote Control Panel

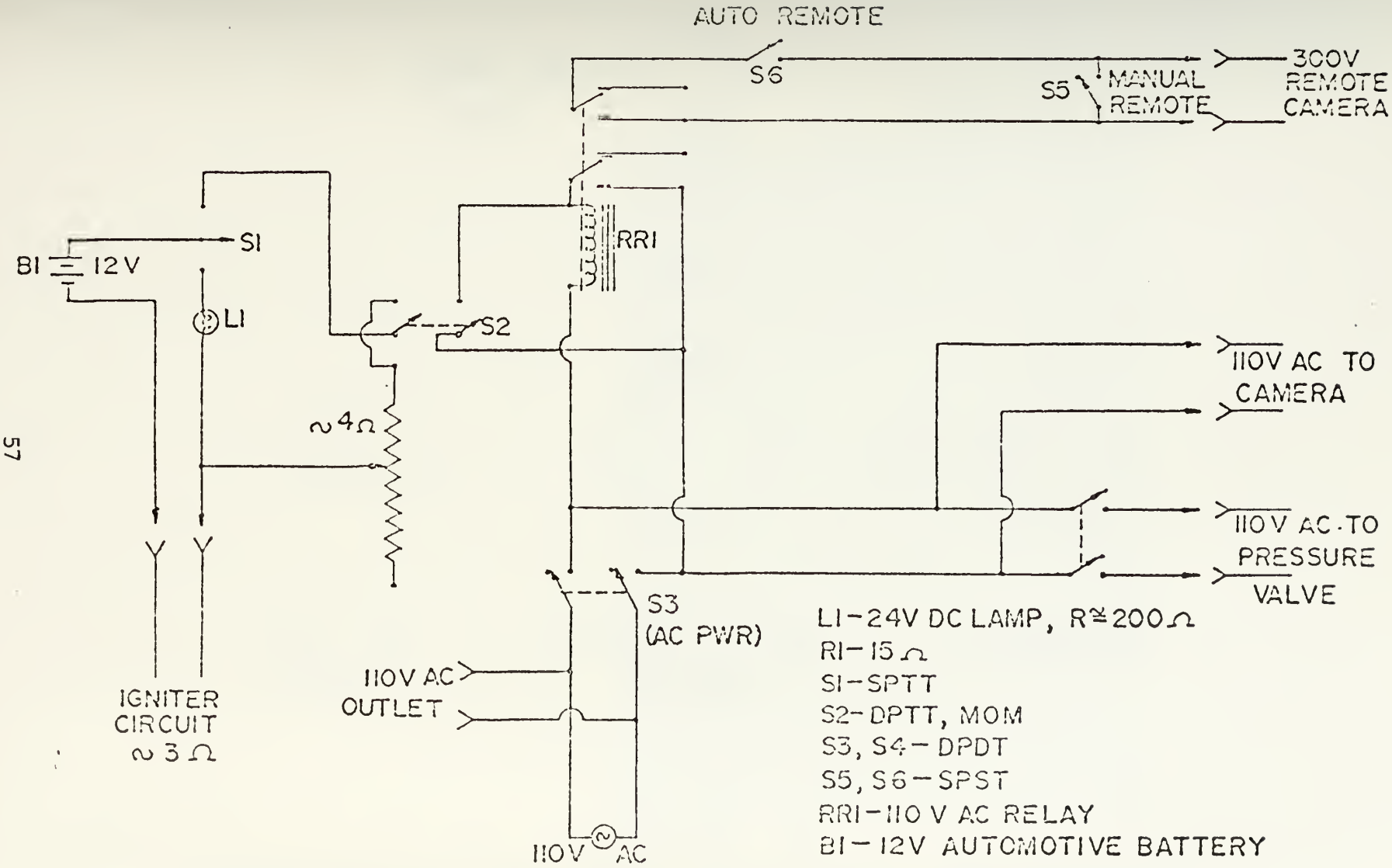

Figure 5. Circuit Diagram of Remote Control Panel

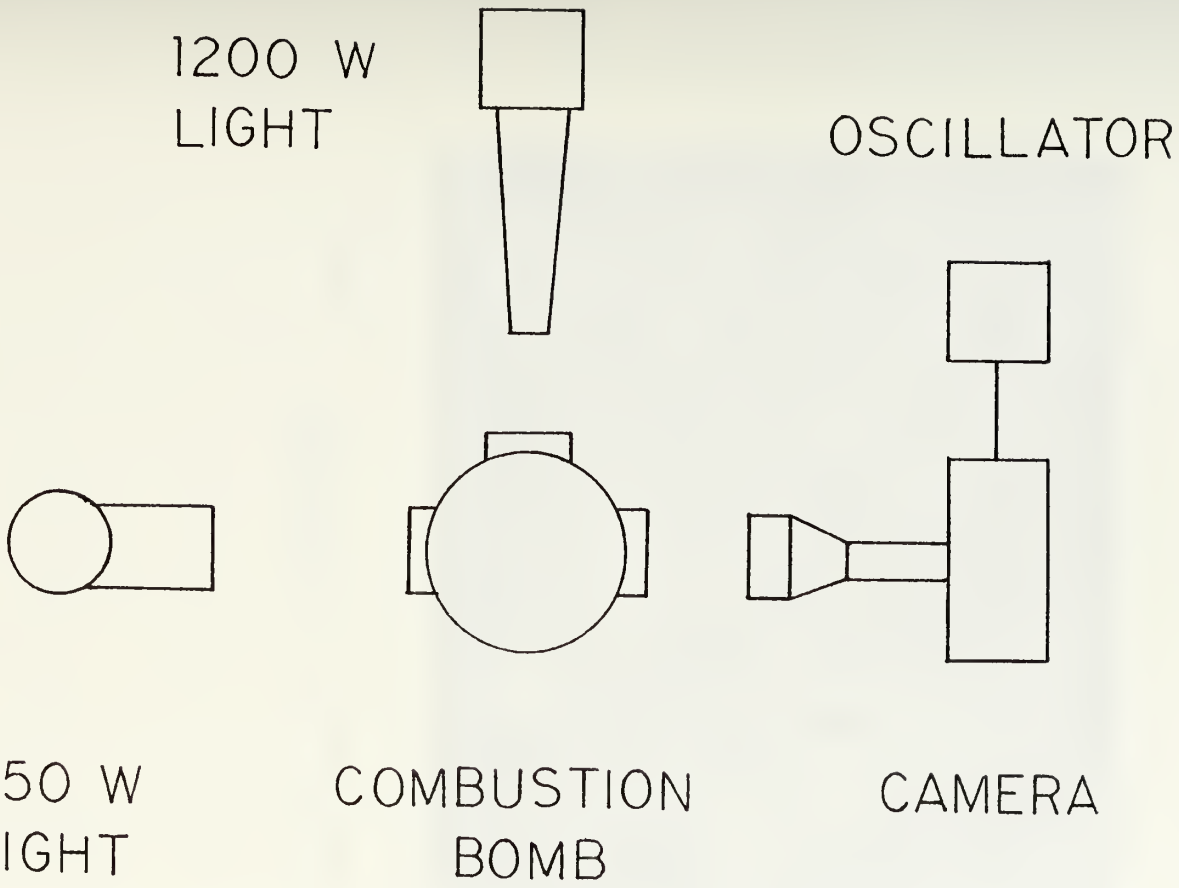

FIGURE 6
SCHEMATIC OF EXPERIMENTAL APPARATUS

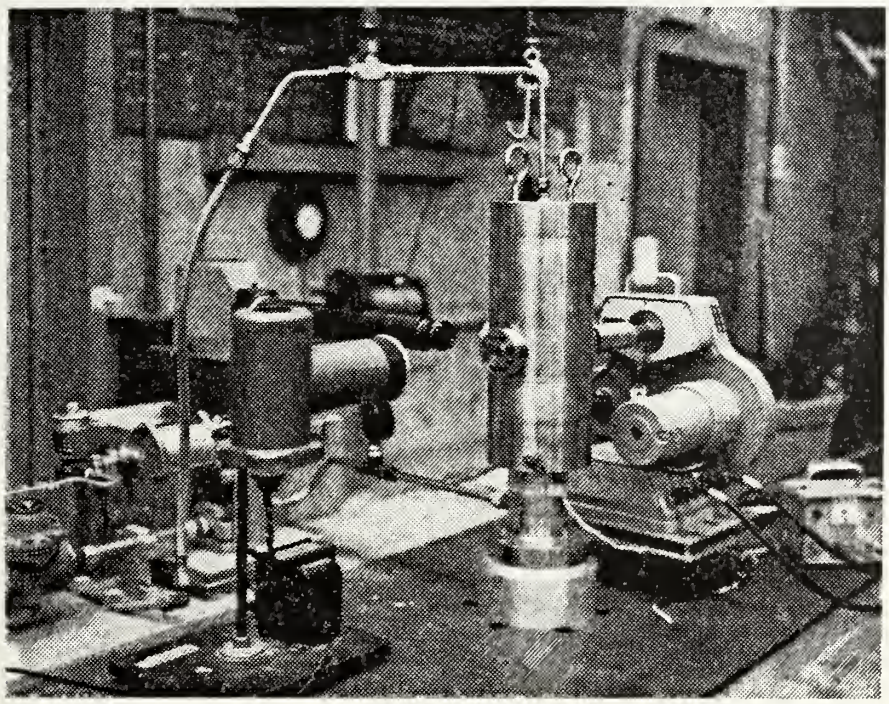

FIGURE 7. Photograph of Experimental Apparatus

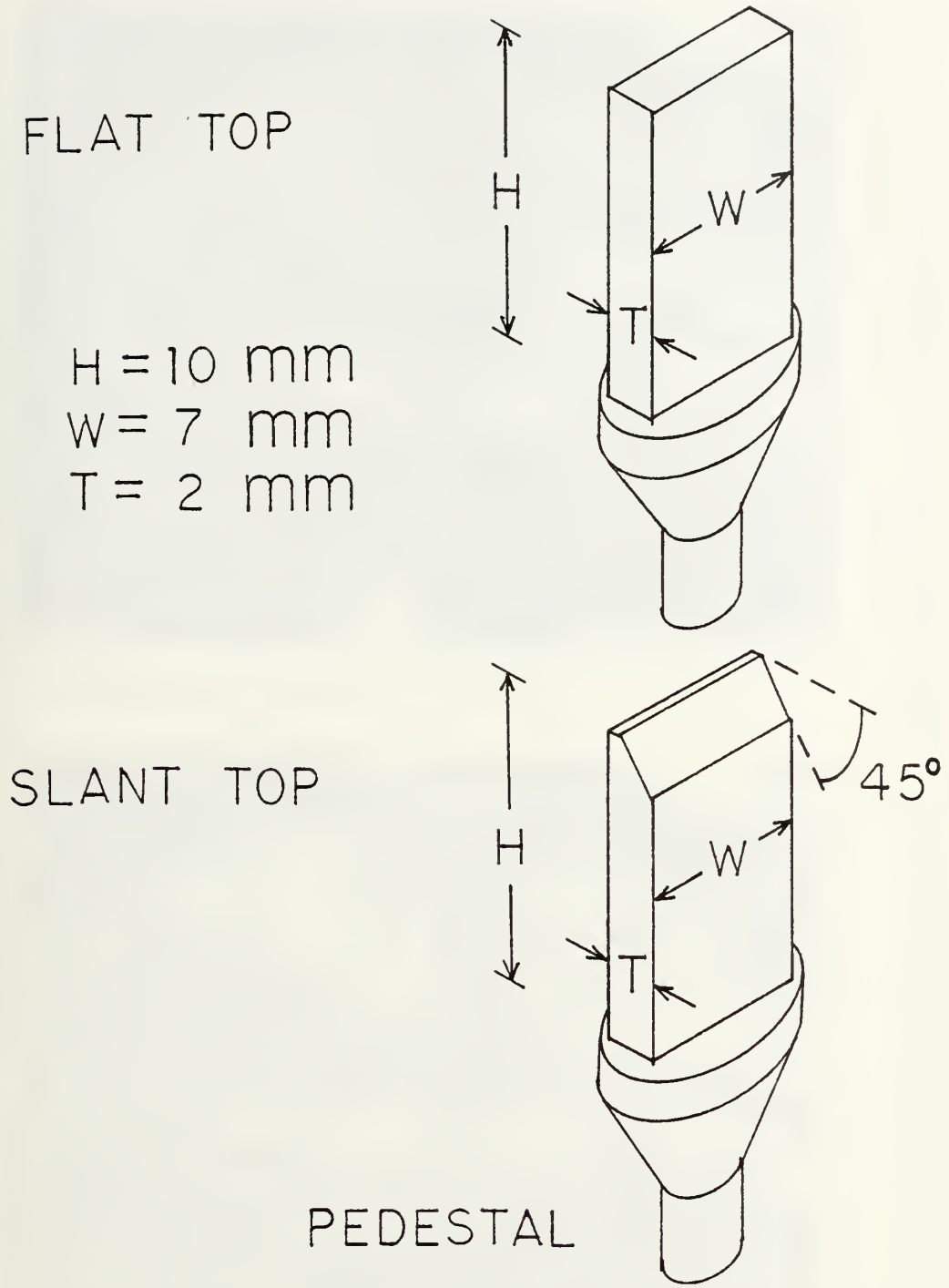

FIGURE 8
PROPELLANT STRAND DIMENSIONS

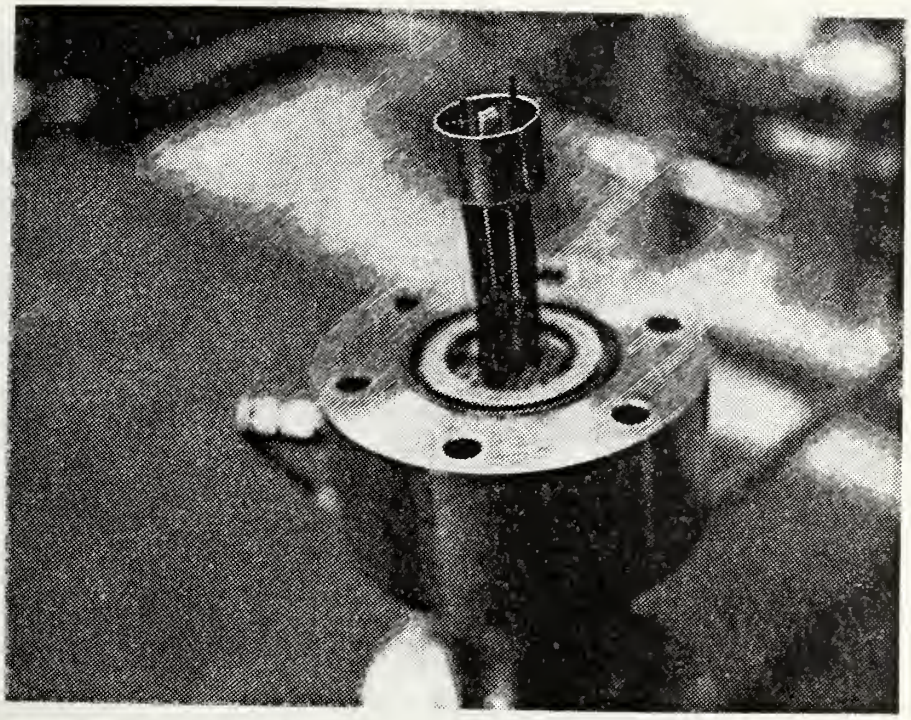

(a) Postfire Residue Collection

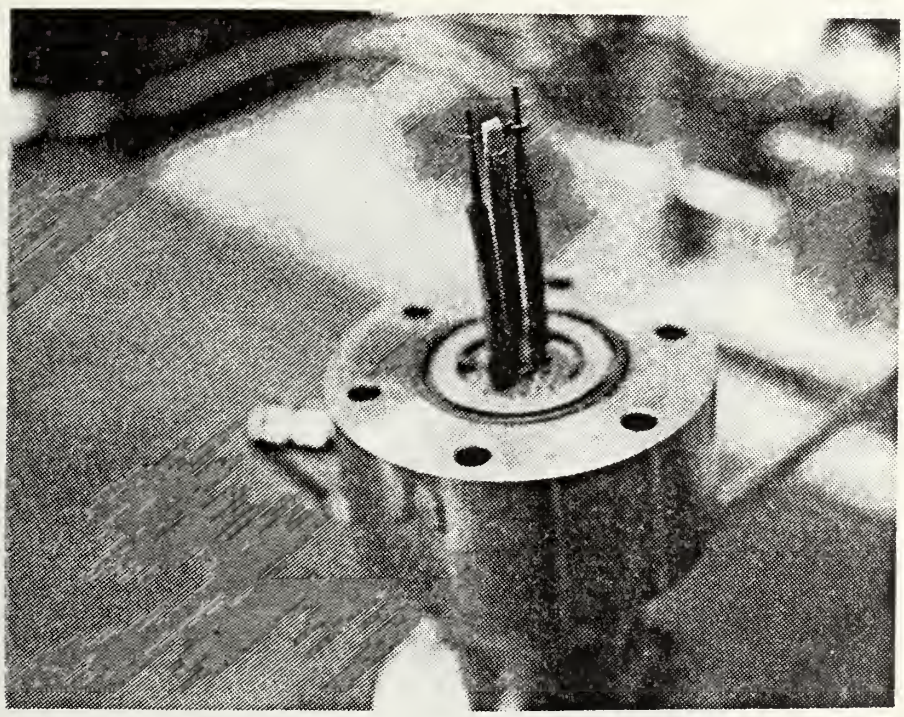

(b) High Speed Motion Pictures

FIGURE 9. Photographs of Propellant Strands Mounted in Combustion Bomb

(a) Inadequately Cleaned Postfire Residue

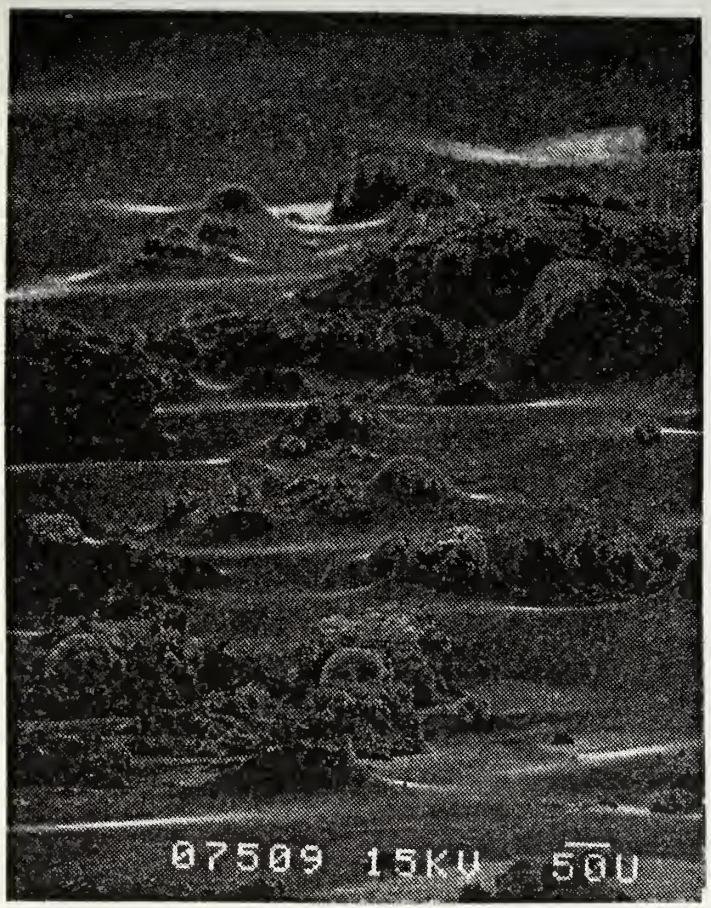

(b) Thick, Uneven Epoxy Layer

FIGURE 10. Examples of Poor SEM Sample Preparation (1500250180)

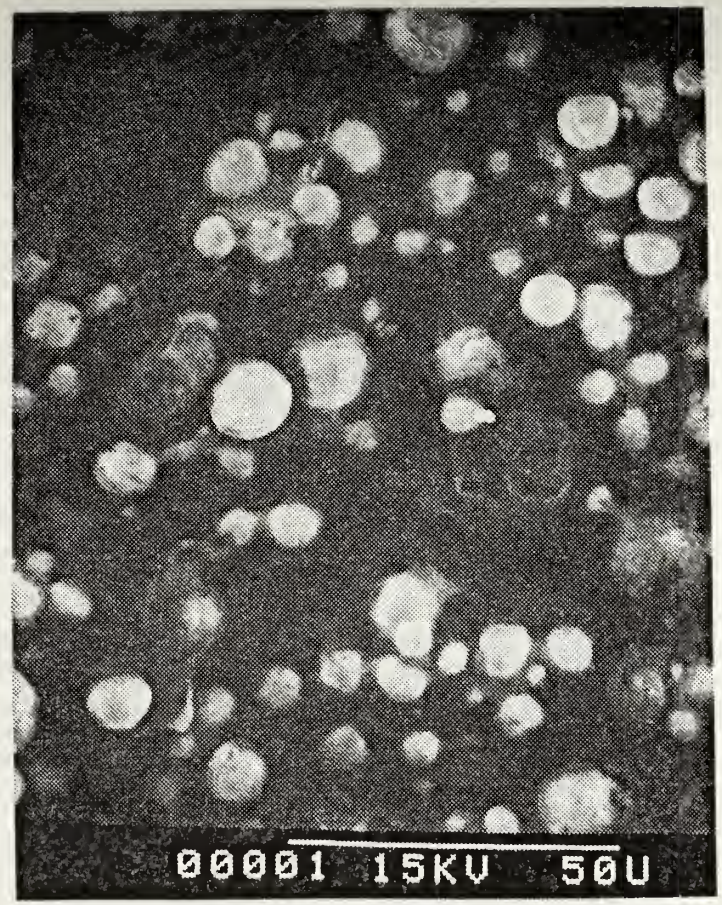

(a) Adequately Cleaned Postfire Residue

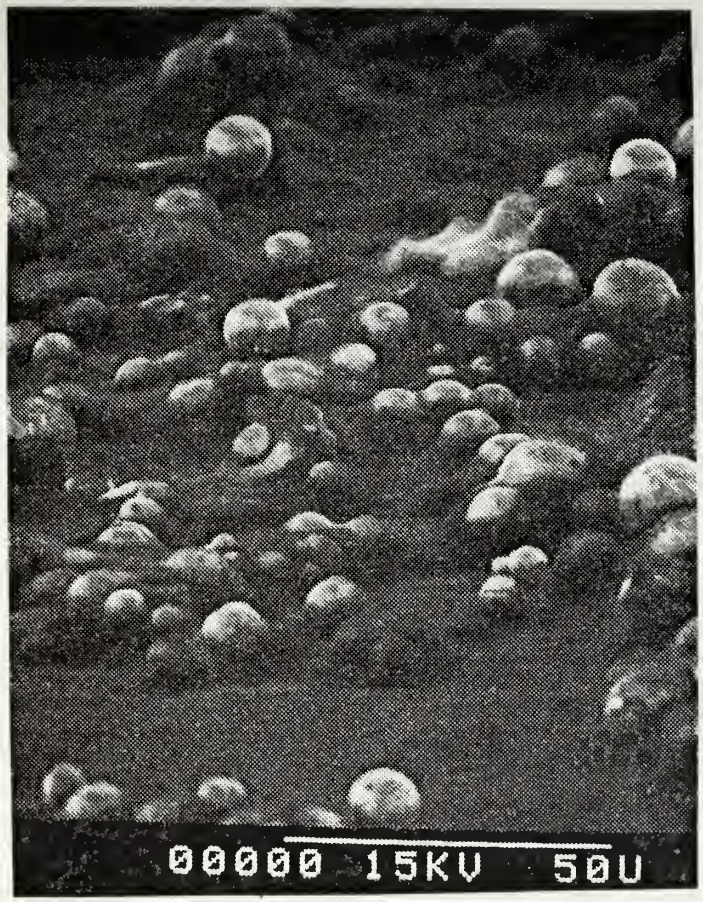

(b) Thick, Uneven Epoxy Layer

FIGURE 11. Examples of Poor SEM Sample Preparation (1520090480)

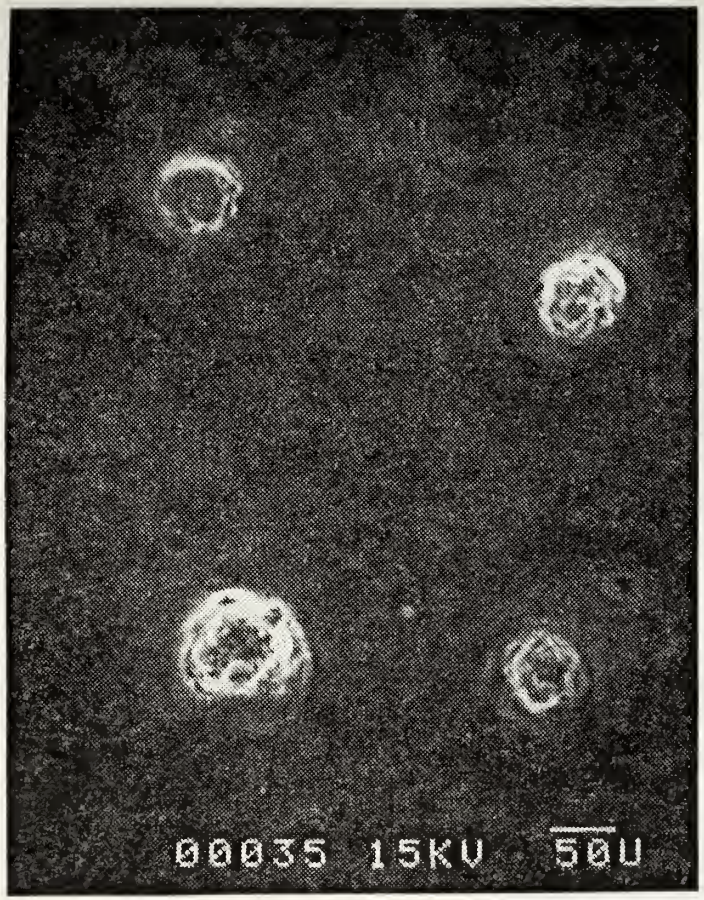

(a)

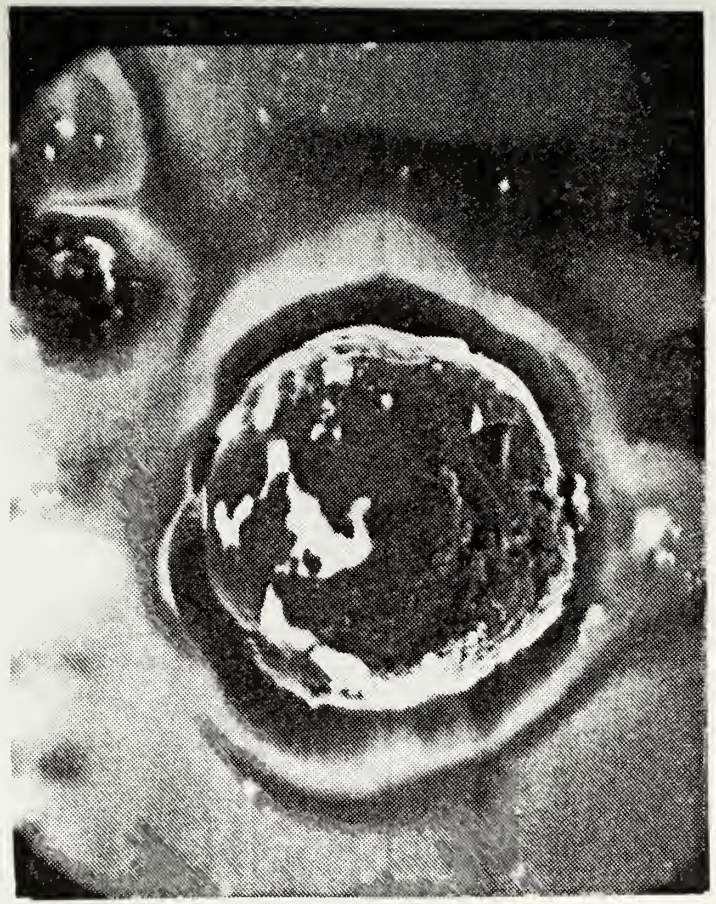

(b)

FIGURE 12. Examples of SEM Sample Charging (1515280380)

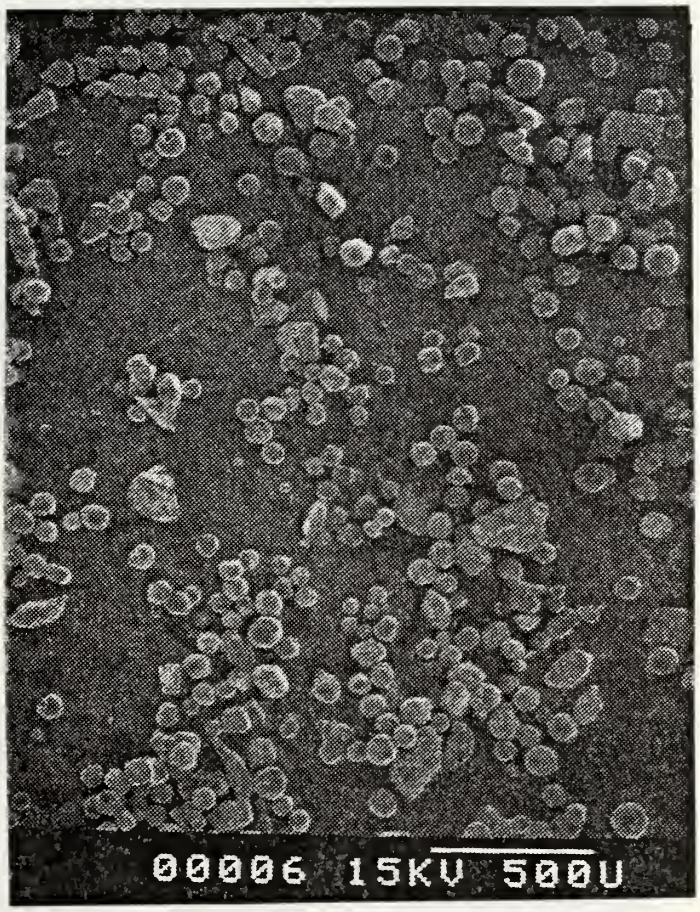

(a)

FIGURE 13. Photomicrographs of Postfire Residue (1445240480, WGS-5A, P_c = 500 psi)

(b)

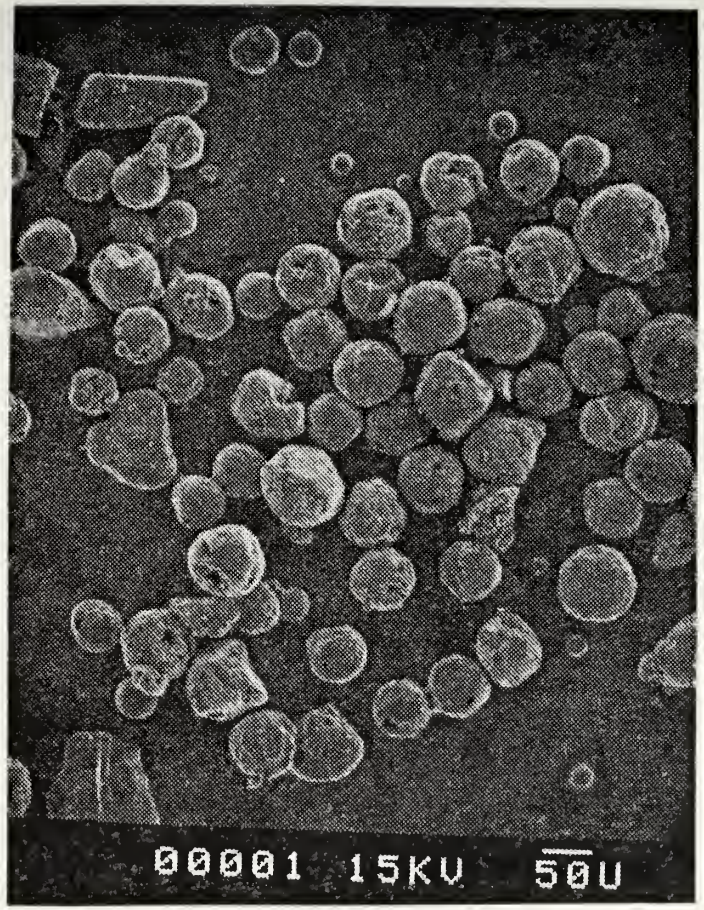

(c)

(d)

(e)

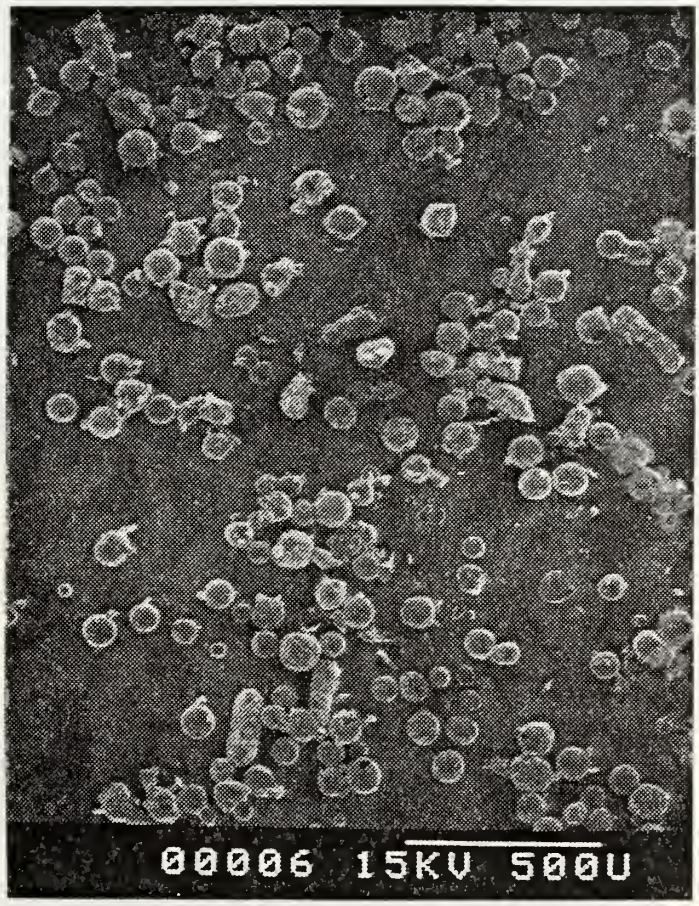

(a)

FIGURE 14. Photomicrographs of Postfire Residue (1445180480, WGS-5A, P_c = 1000 psi)

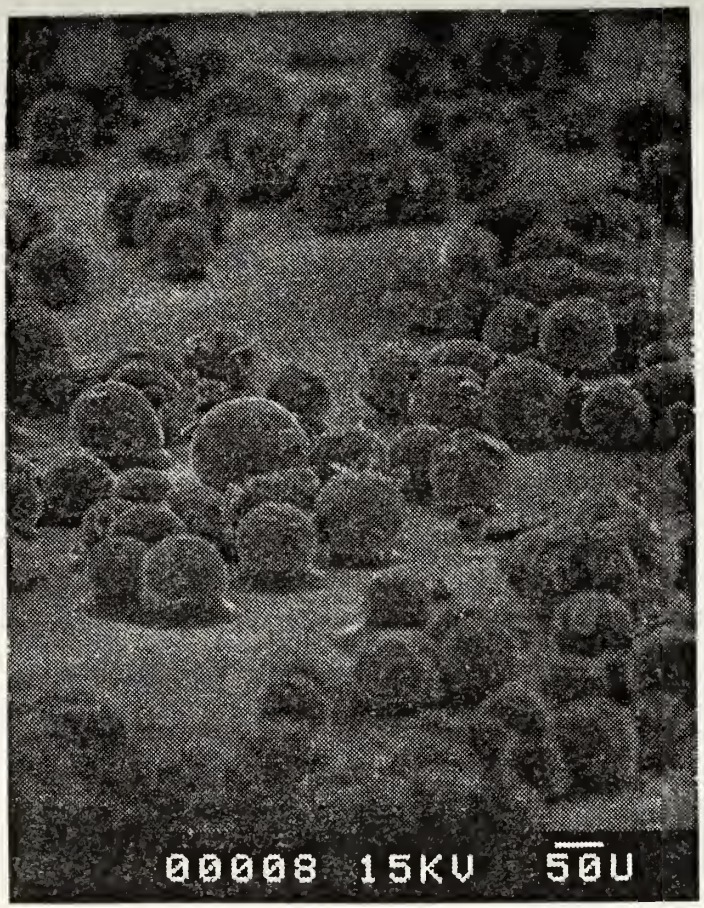

(b)

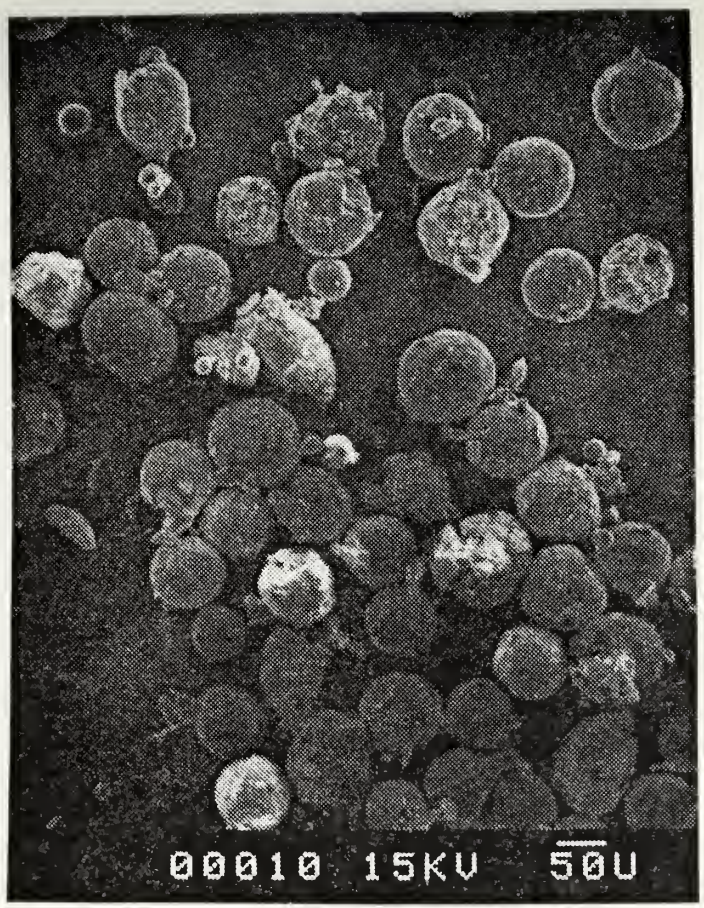

(c)

(d)

(e)

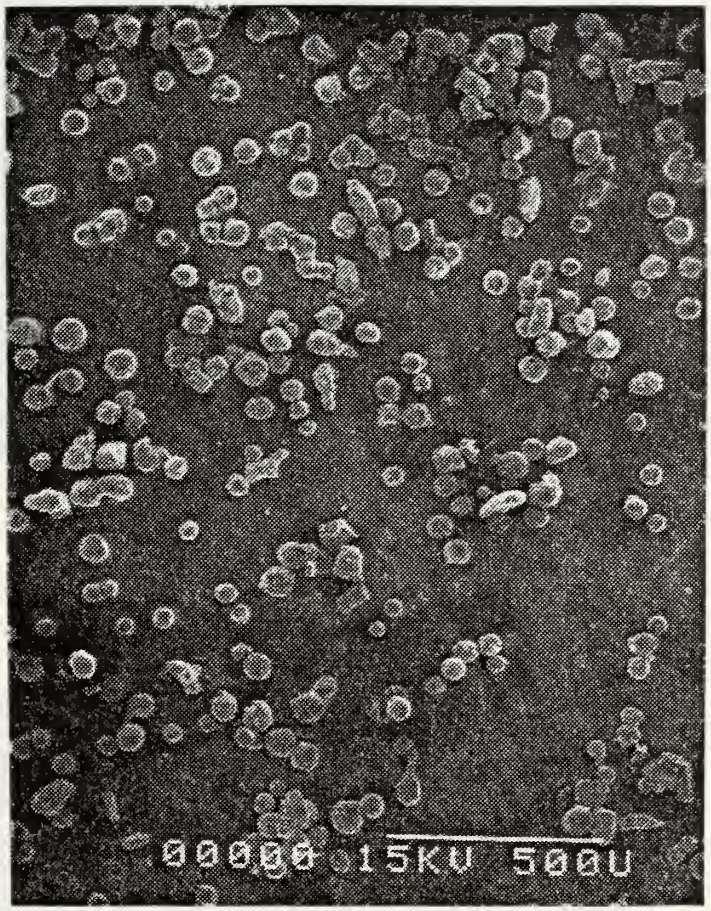

(a)

FIGURE 15. Photomicrographs of Postfire Residue (10030030580, WGS-6A, P_c = 500 psi)

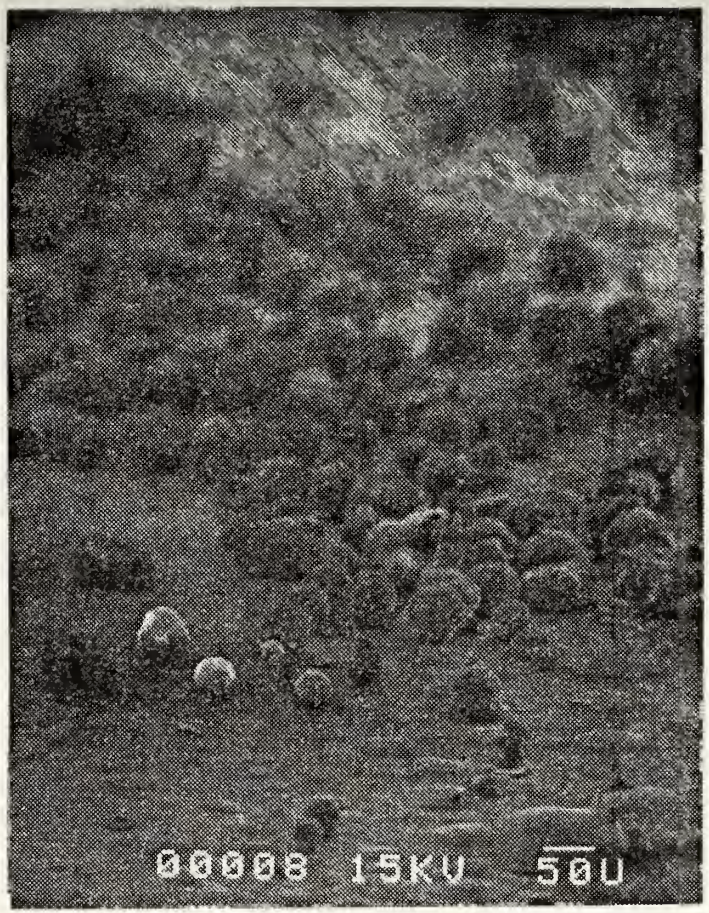

(b)

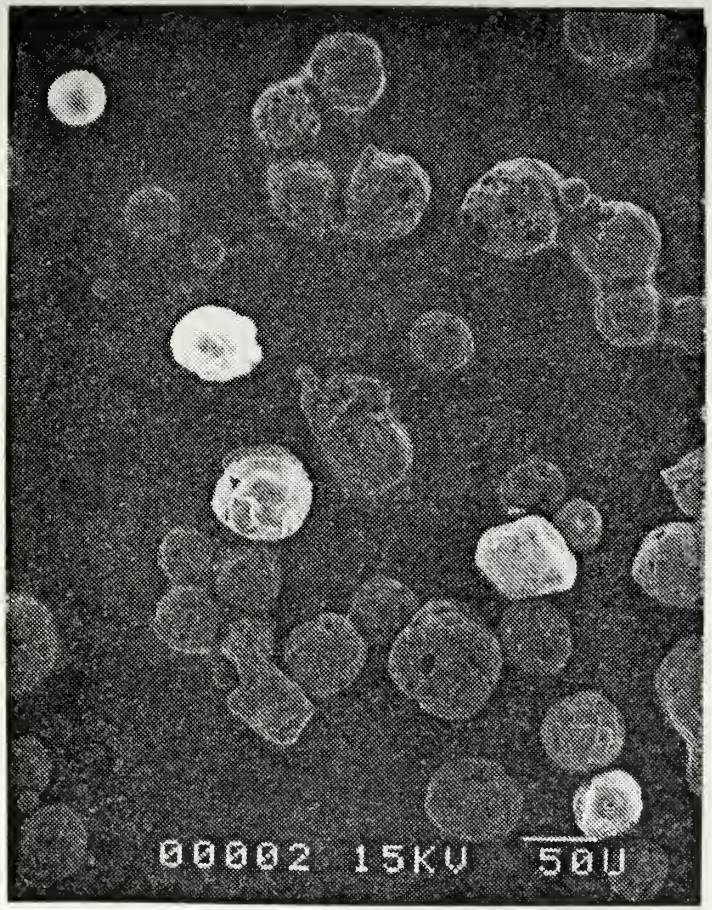

(c)

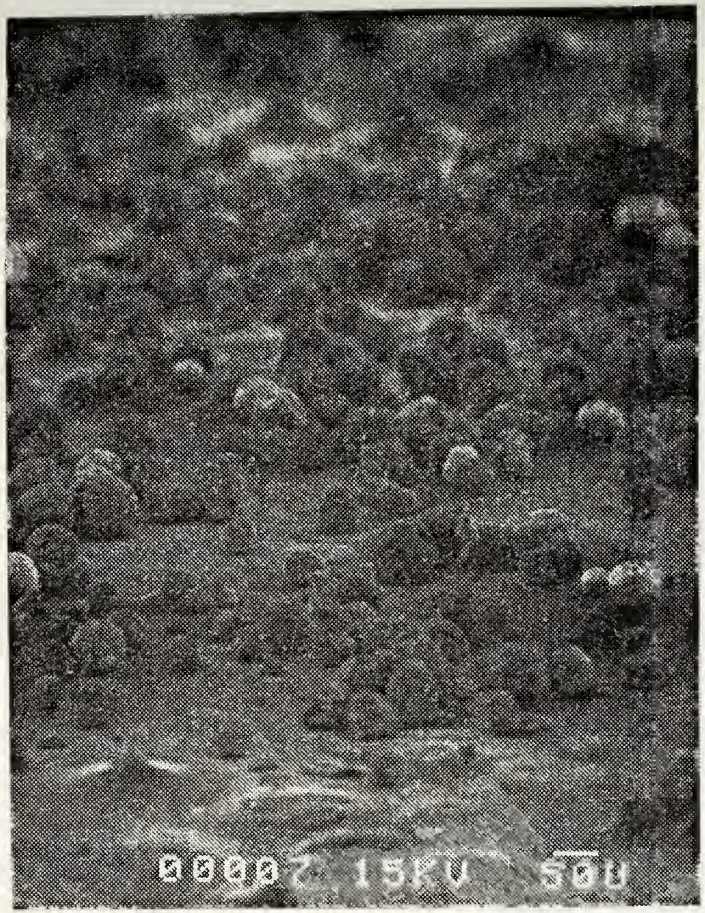

(d)

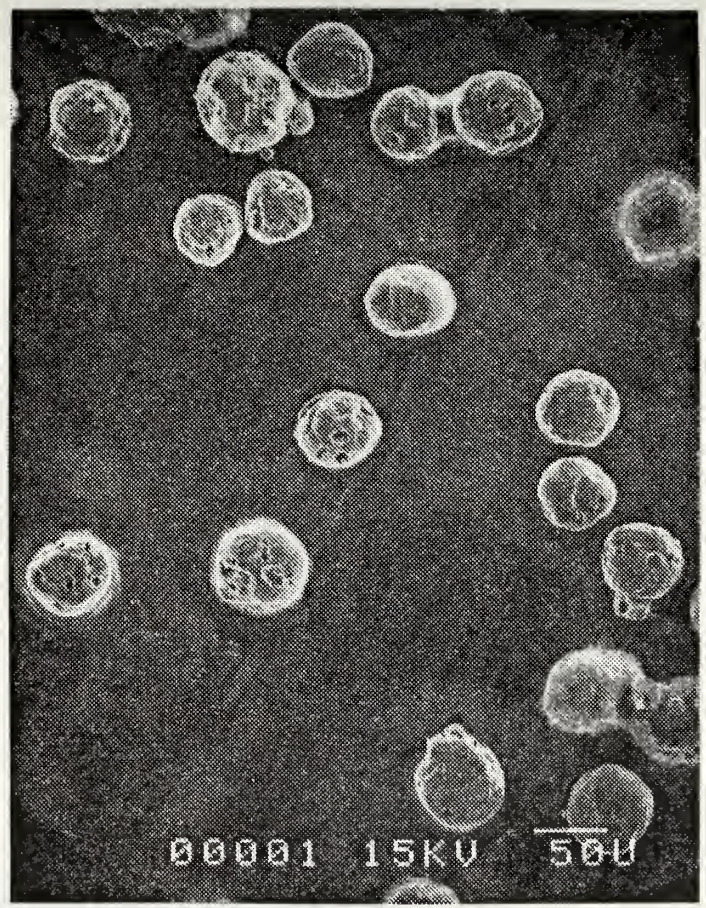

(e)

(a)

FIGURE 16. Photomicrographs of Postfire Residue (160017040, WGS-6A, P_c = 1000 psi)

(b)

(c)

(e)

(d)

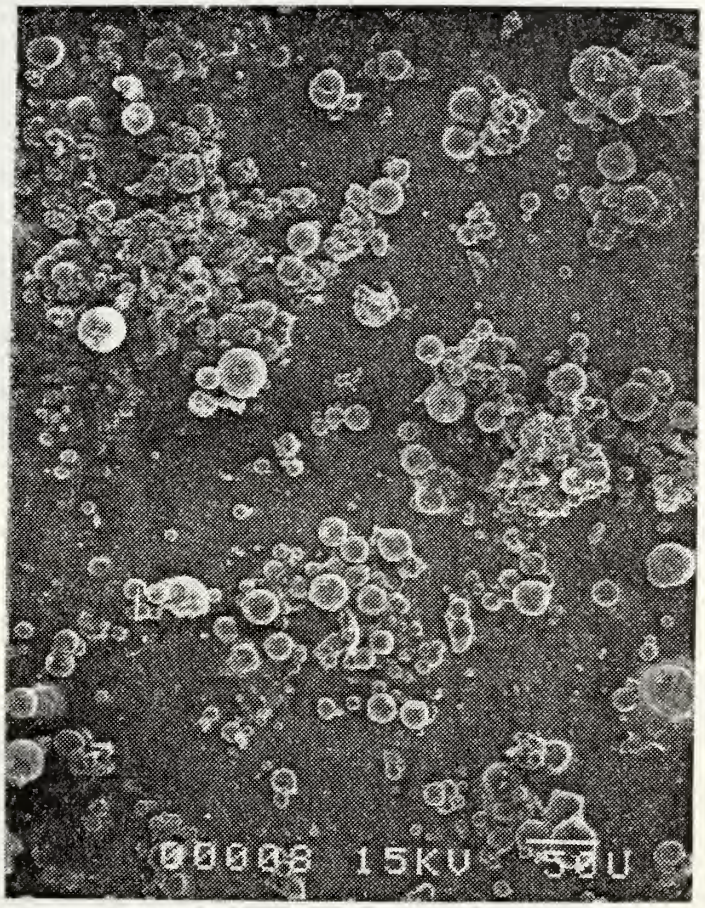

(a)

FIGURE 17. Photomicrographs of Postfire Residue (1215030580, WGS-7A, P_c = 500 psi)

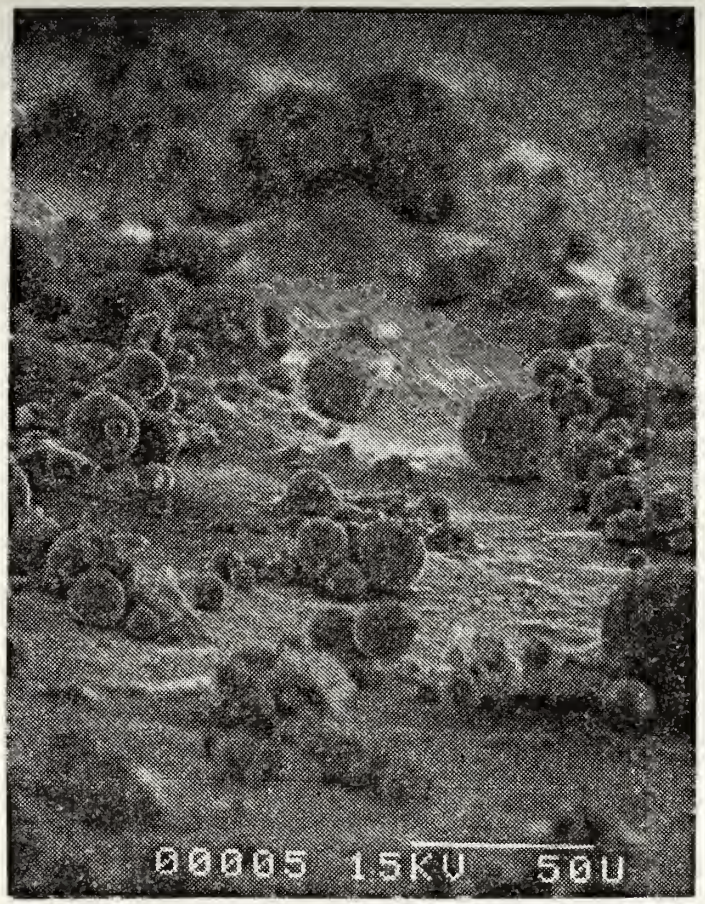

(b)

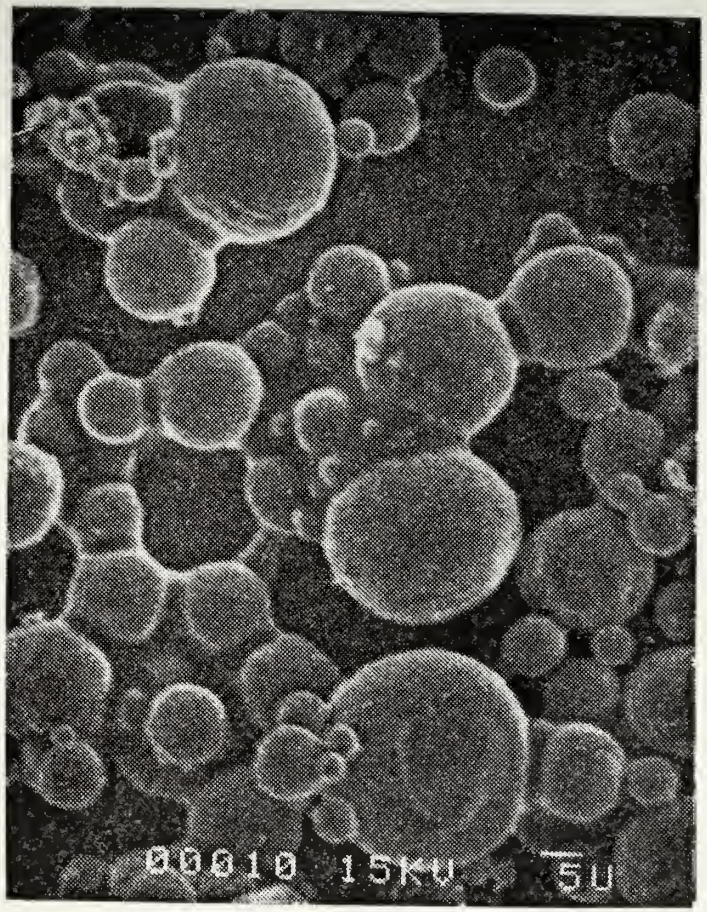

(c)

(e)

(d)

(a)

FIGURE 18. Photomicrographs of Postfire Residue (1400240480, WGS-7A, P_c = 1000 psi)

(b)

(c)

(d)

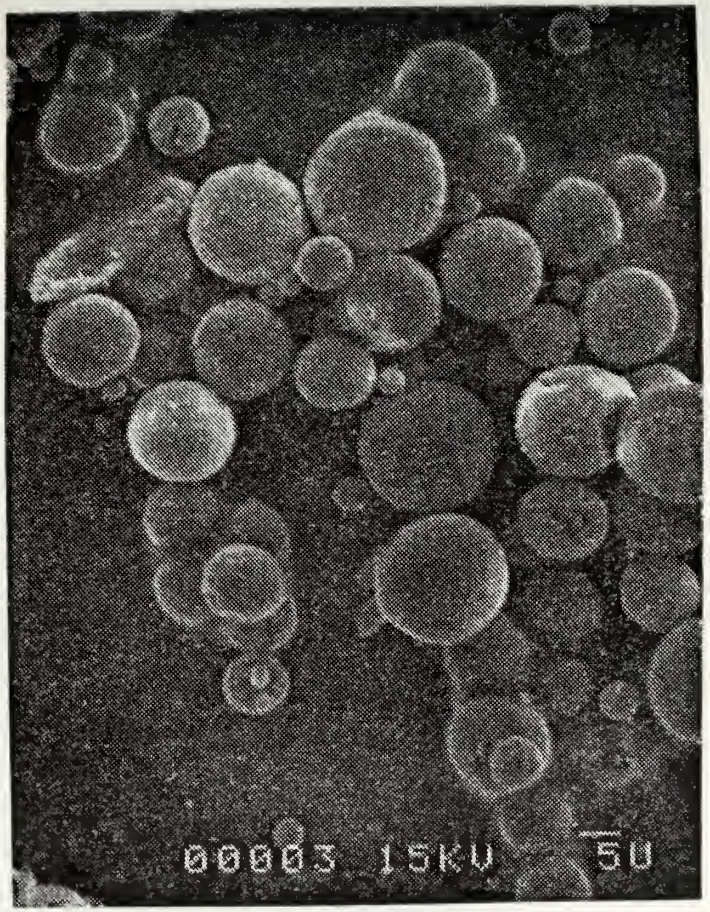

(e)

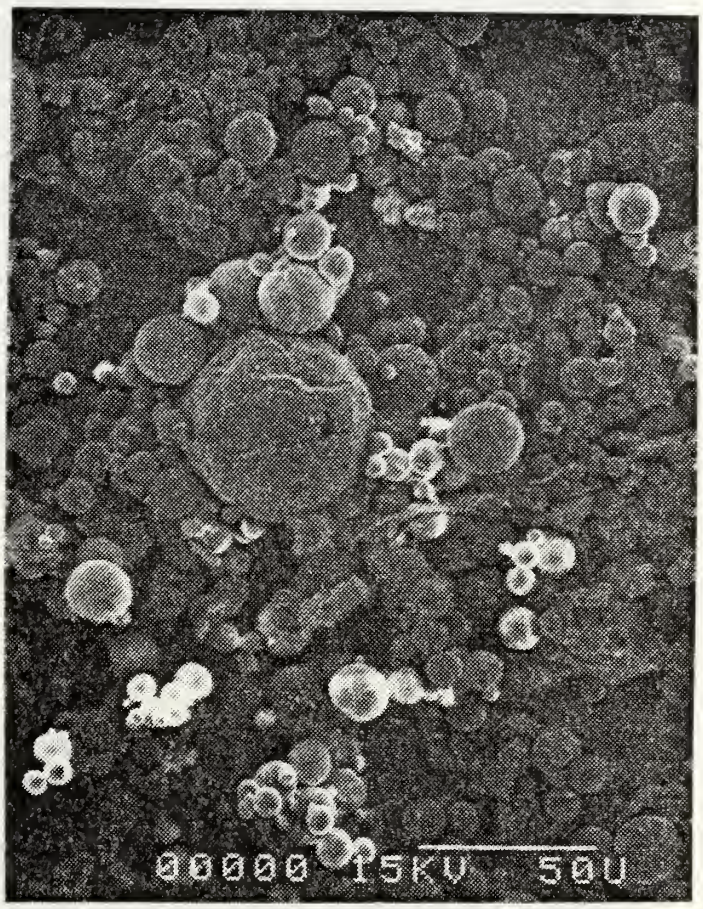

(a)

FIGURE 19. Photomicrographs of Postfire Residue (1100030580, WGS-7, P_c = 500 psi)

(b)

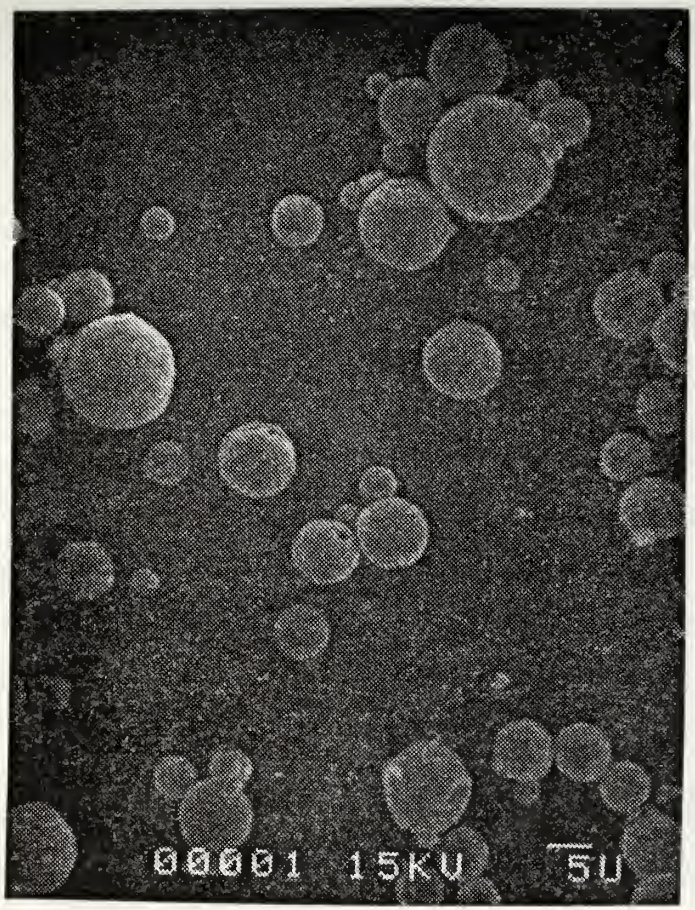

(c)

(d)

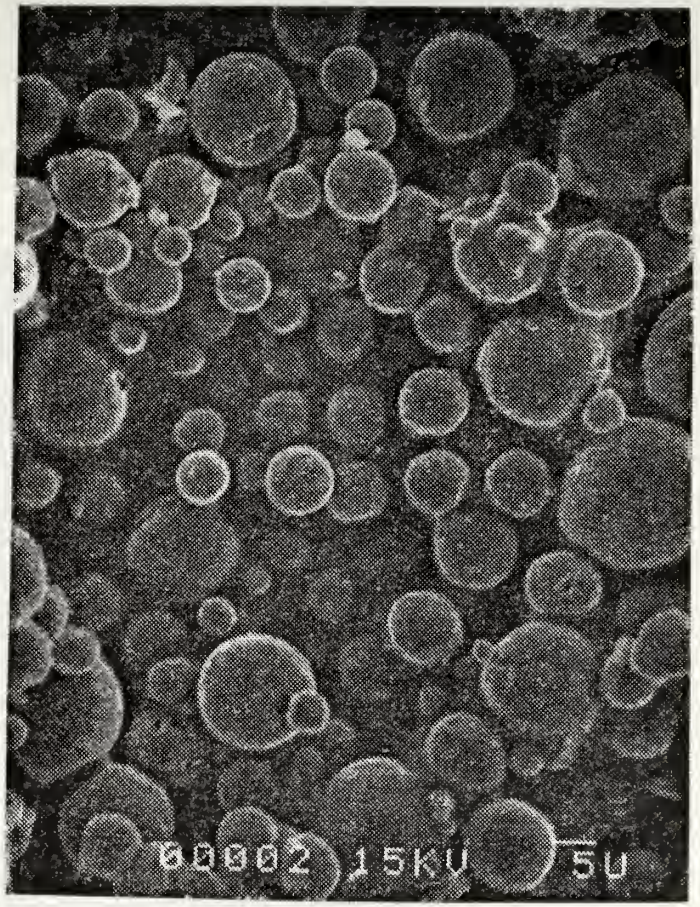

(e)

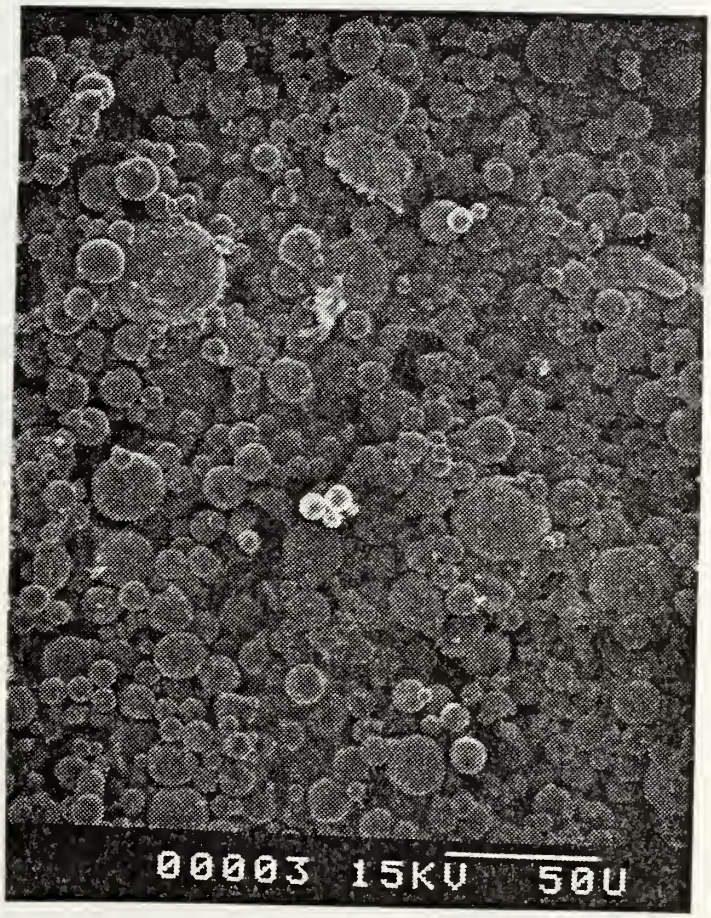

(a)

FIGURE 20. Photomicrographs of Postfire Residue (1500219480, WGS-7, P_c = 1000 psi)

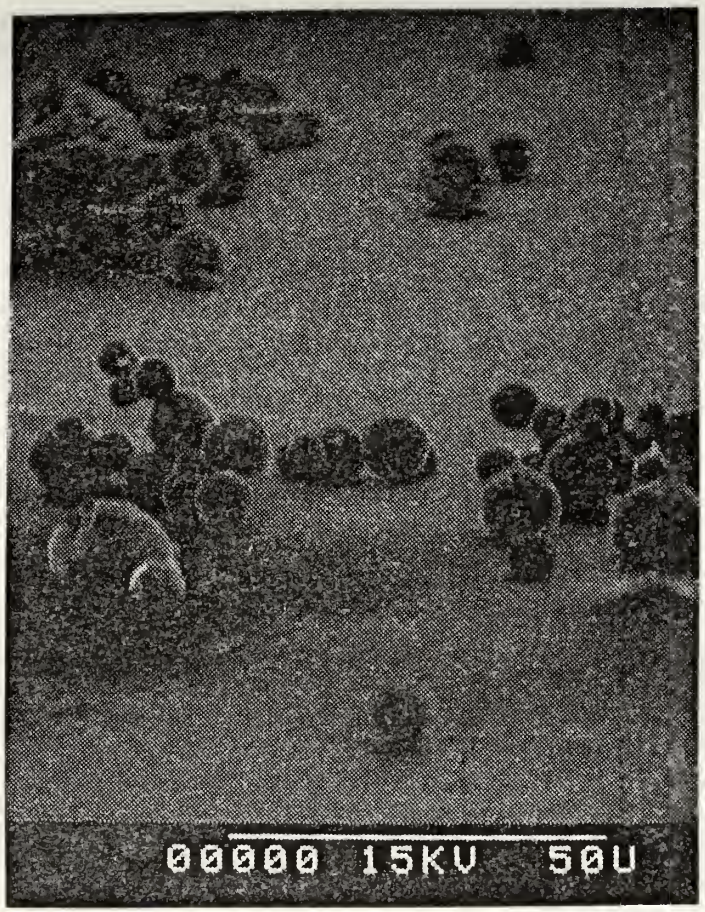

(b)

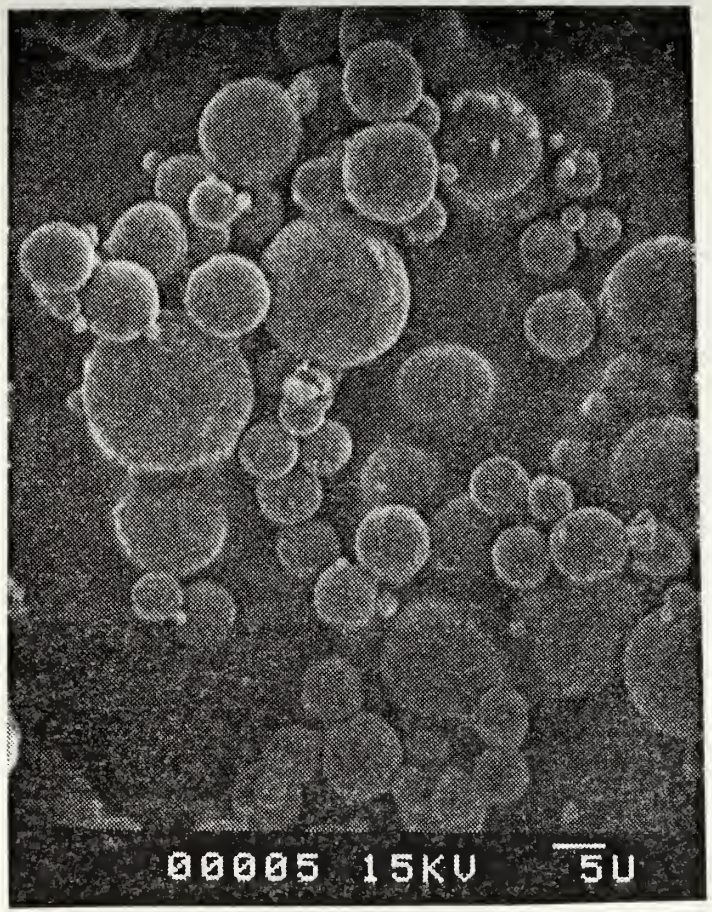

(c)

(d)

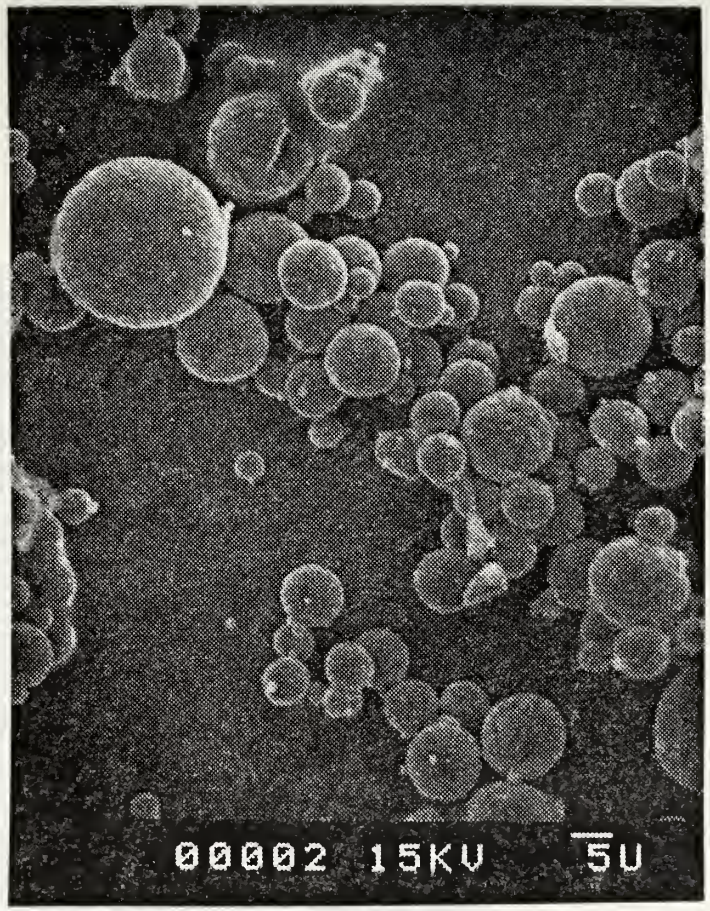

(e)

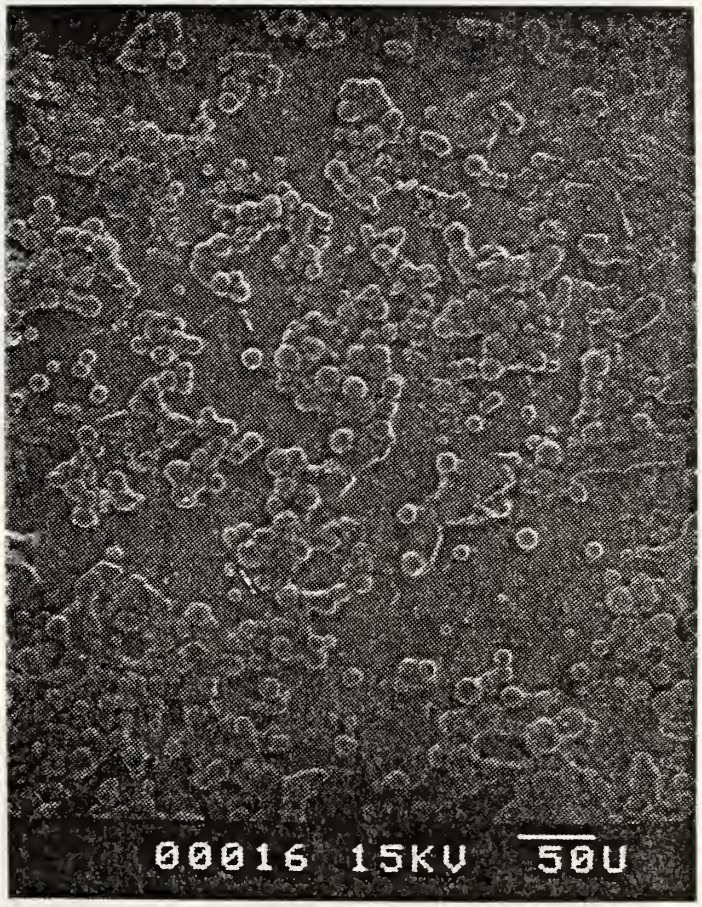

(a)

FIGURE 21. Photomicrographs of Postfire Residue (1230110580, NWC-1, P_c = 500 psi)

(b)

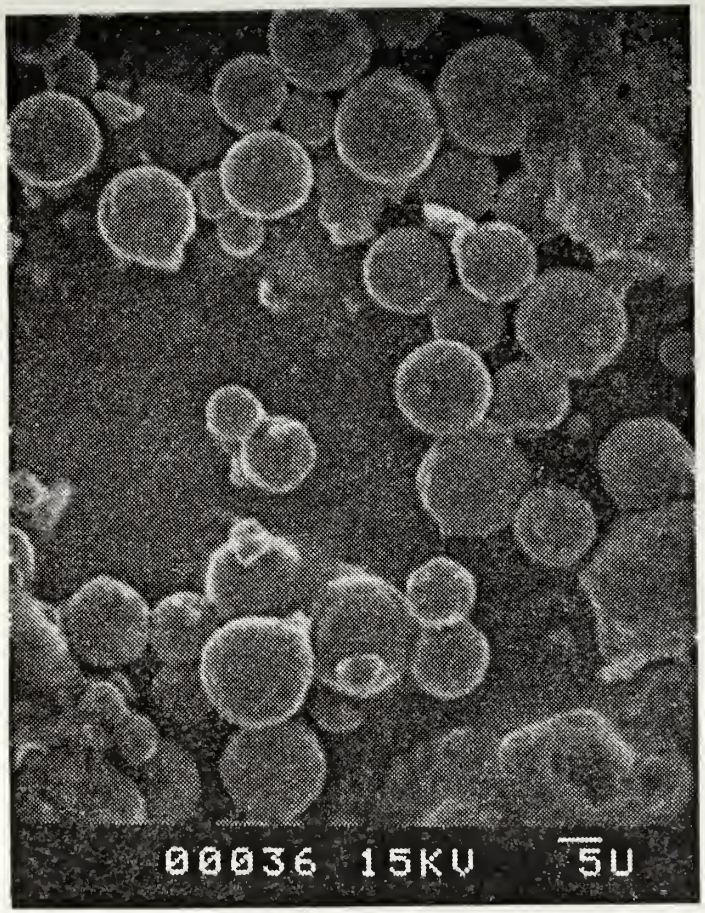

(c)

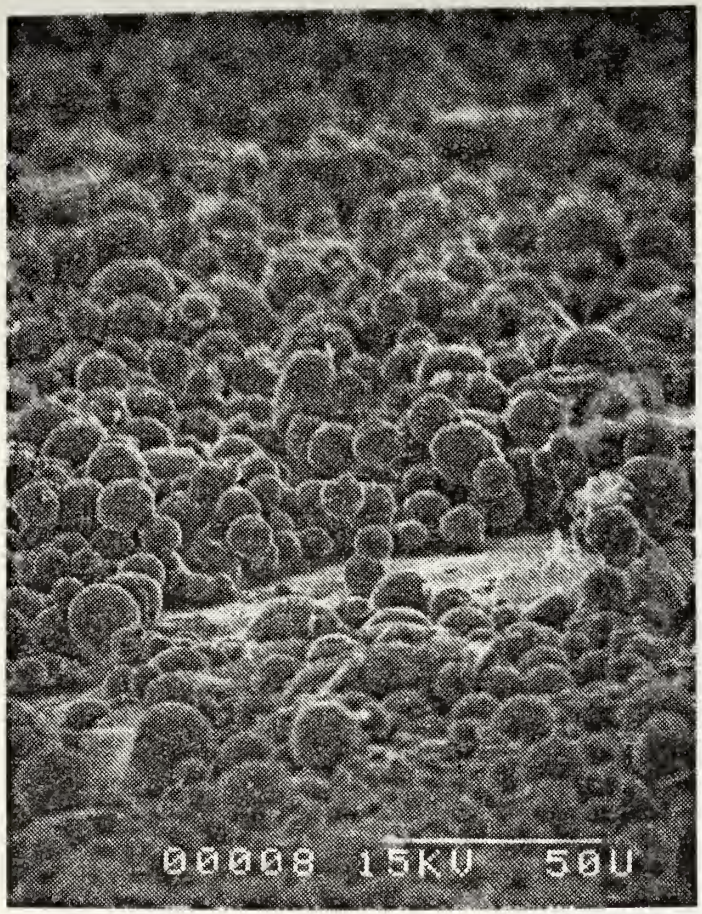

(d)

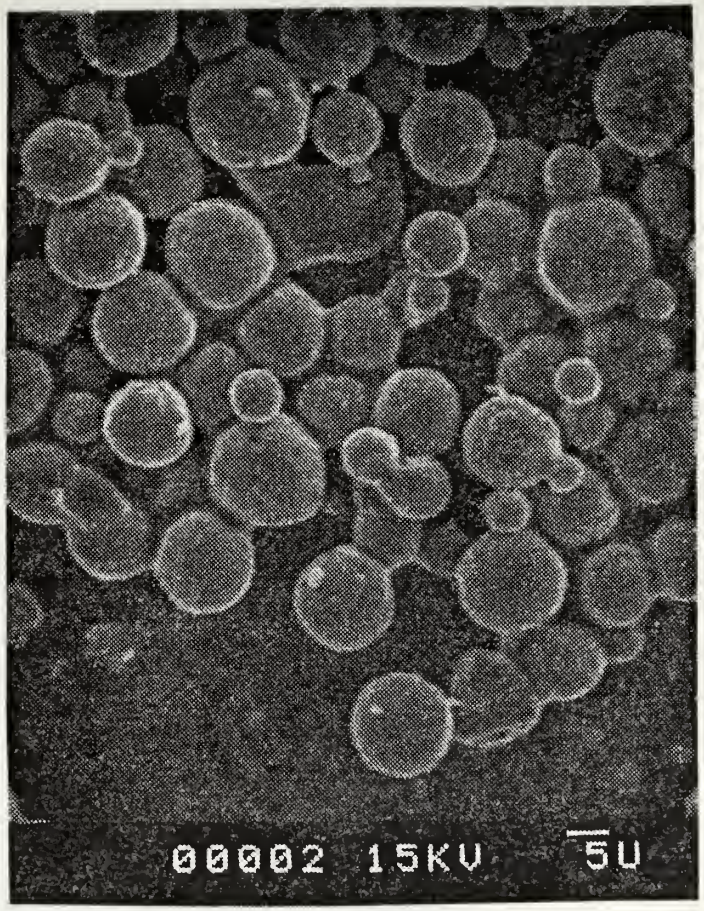

(e)

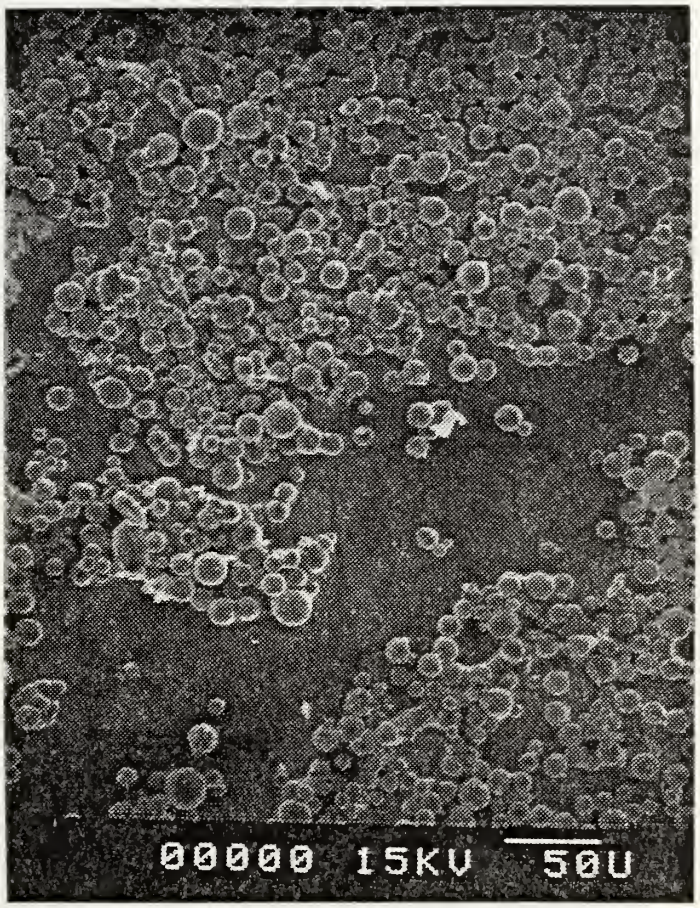

(a)

FIGURE 22. Photomicrographs of Postfire Residue (150010580, NWC-1, P_c = 1000 psi)

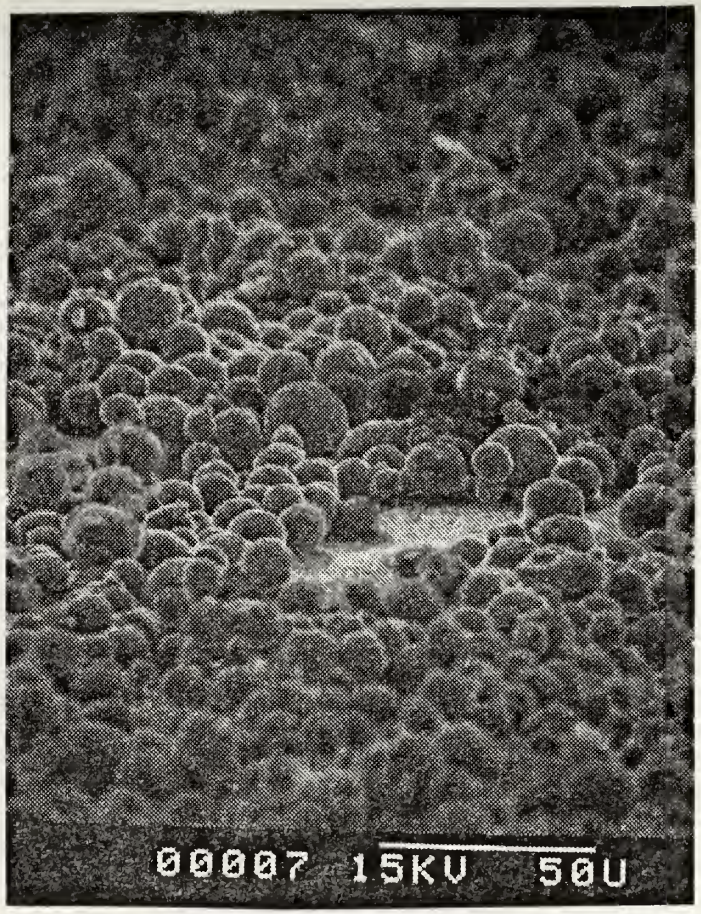

(b)

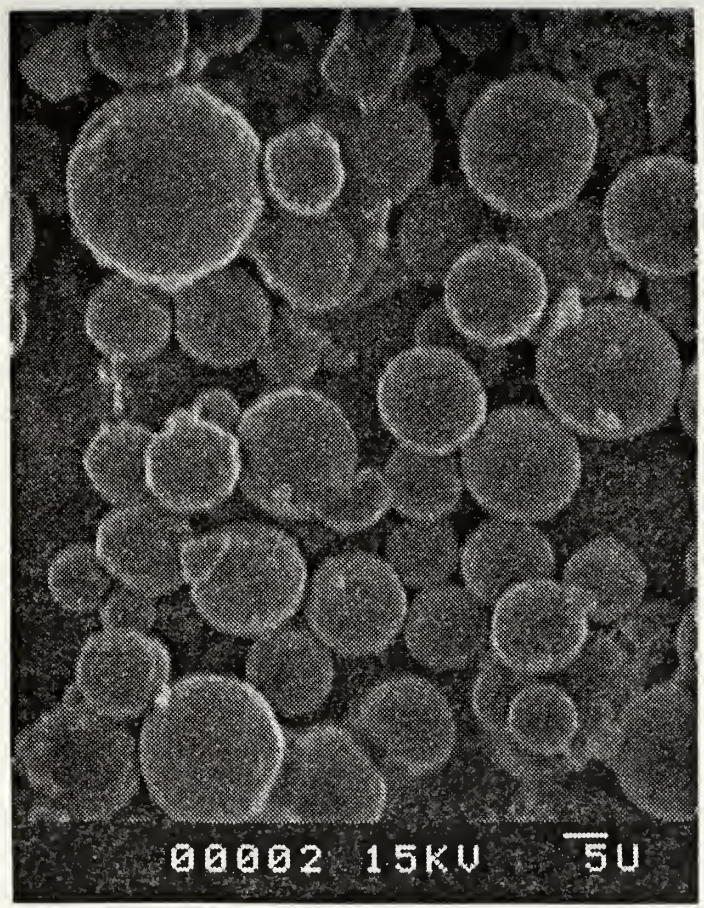

(c)

(d)

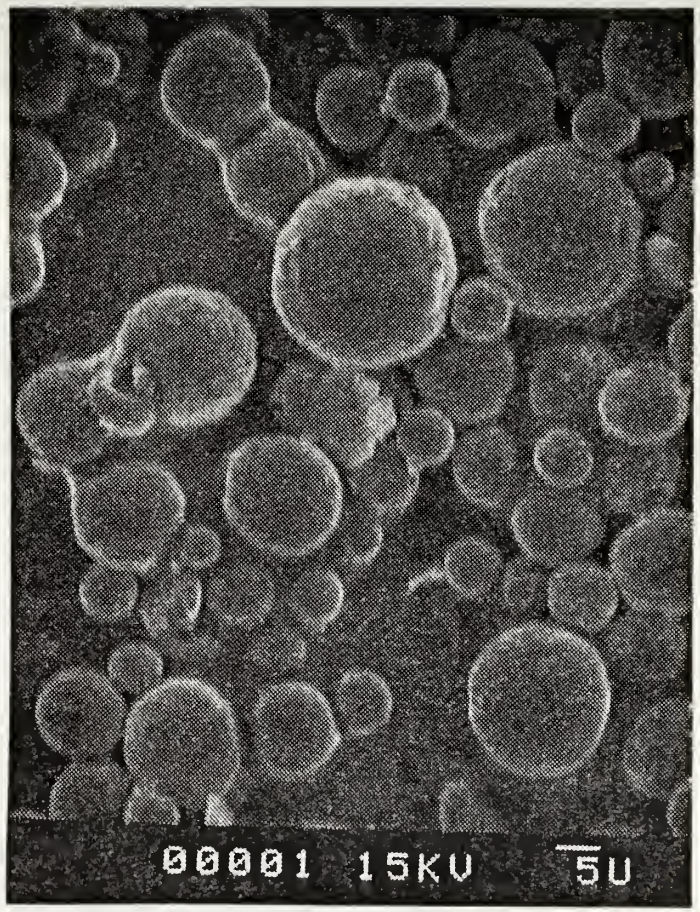

(e)

(a)

FIGURE 23. Photomicrographs of Postfire Residue (1200110580, NWC-2, P_c = 500 psi)

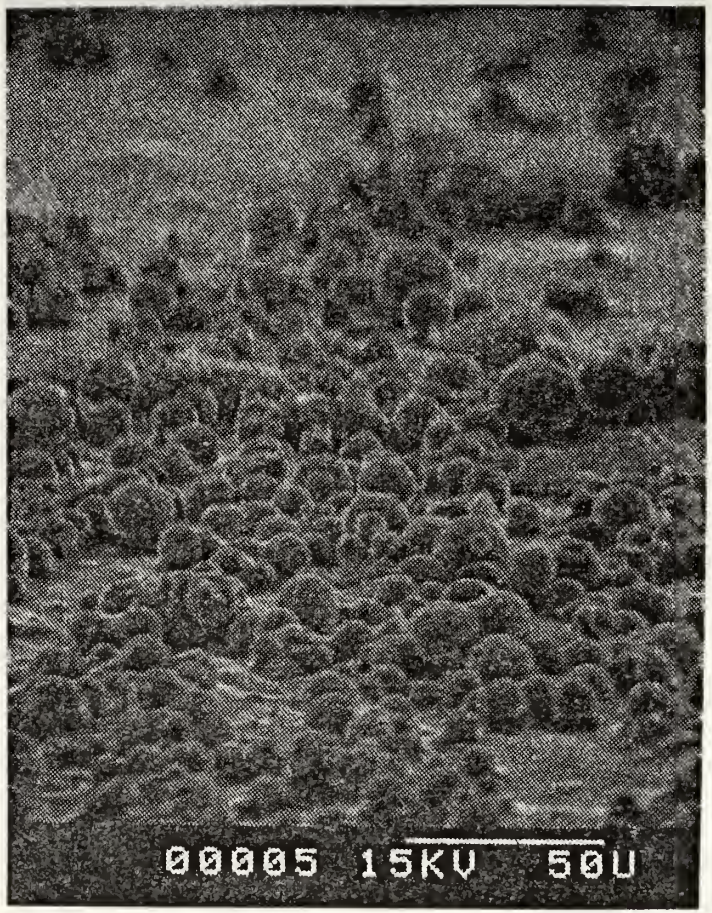

(b)

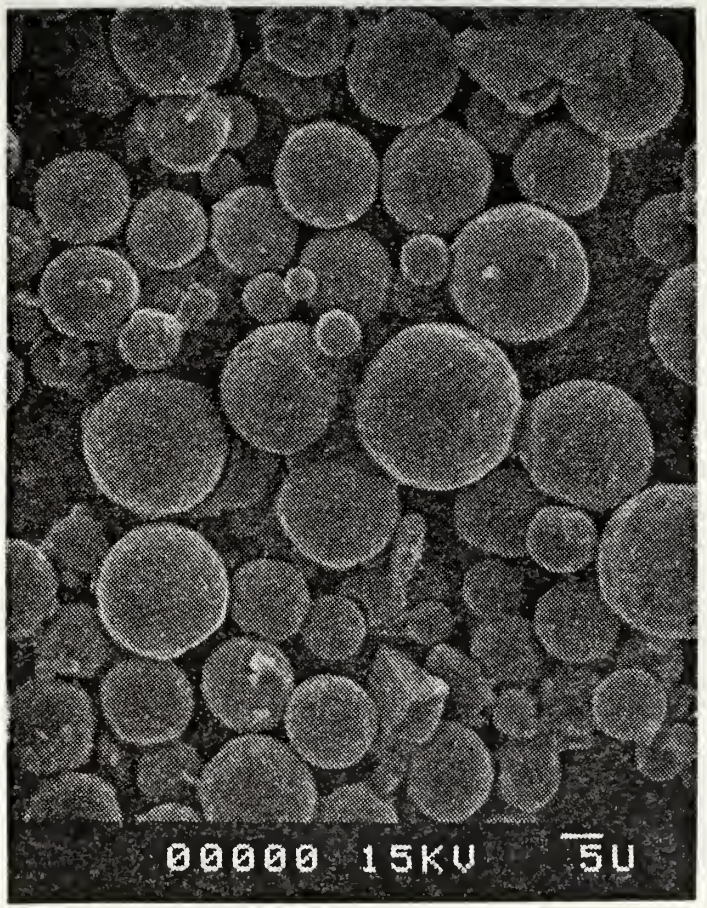

(c)

(d)

(e)

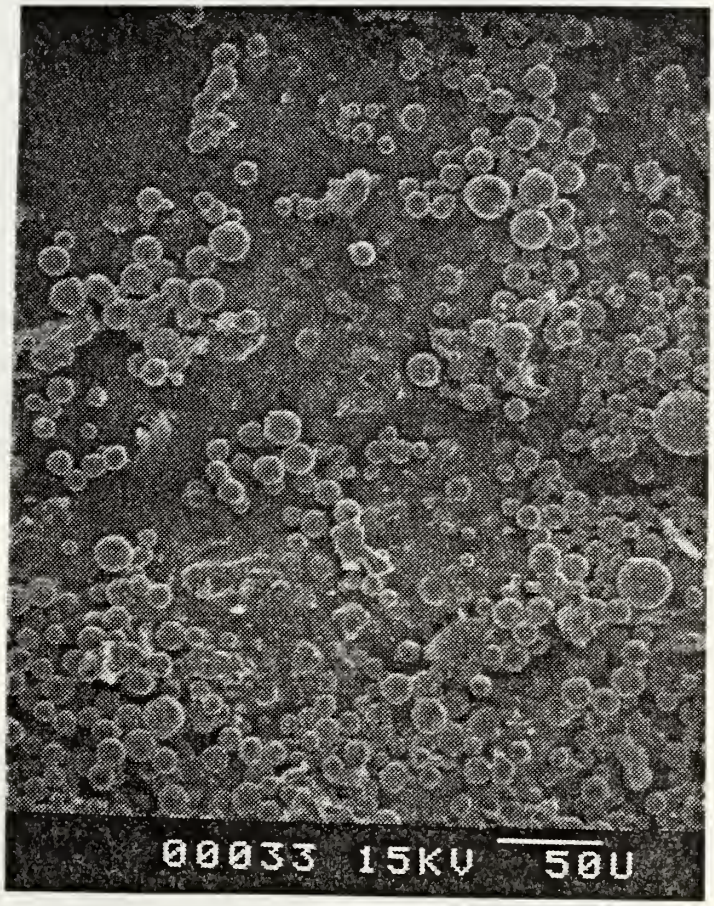

(a)

FIGURE 24. Photomicrographs of Postfire Residue (1615100580, NWC-2, P_c = 1000 psi)

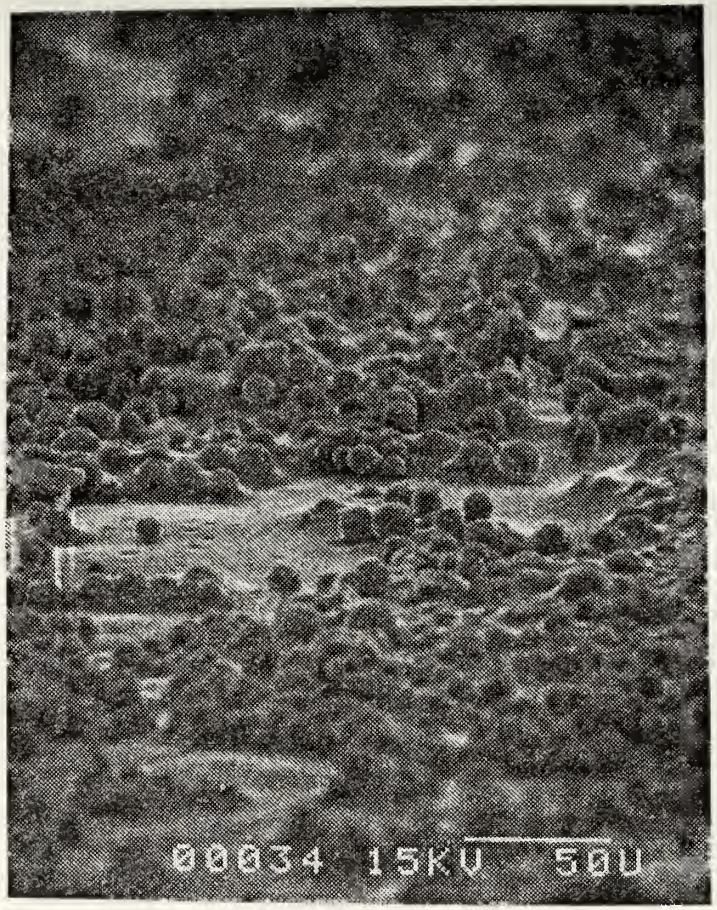

(b)

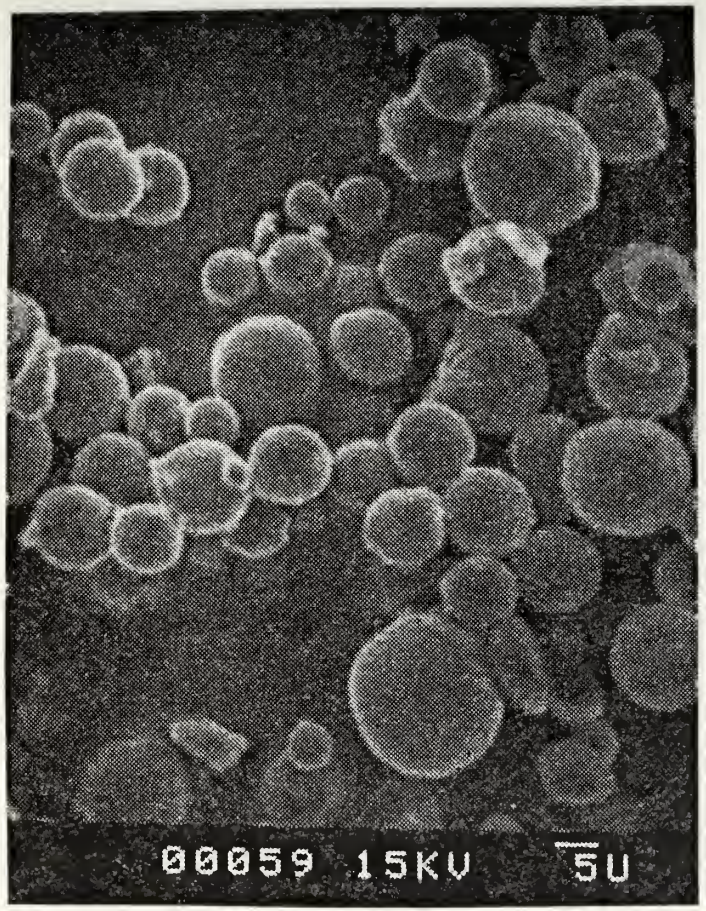

(c)

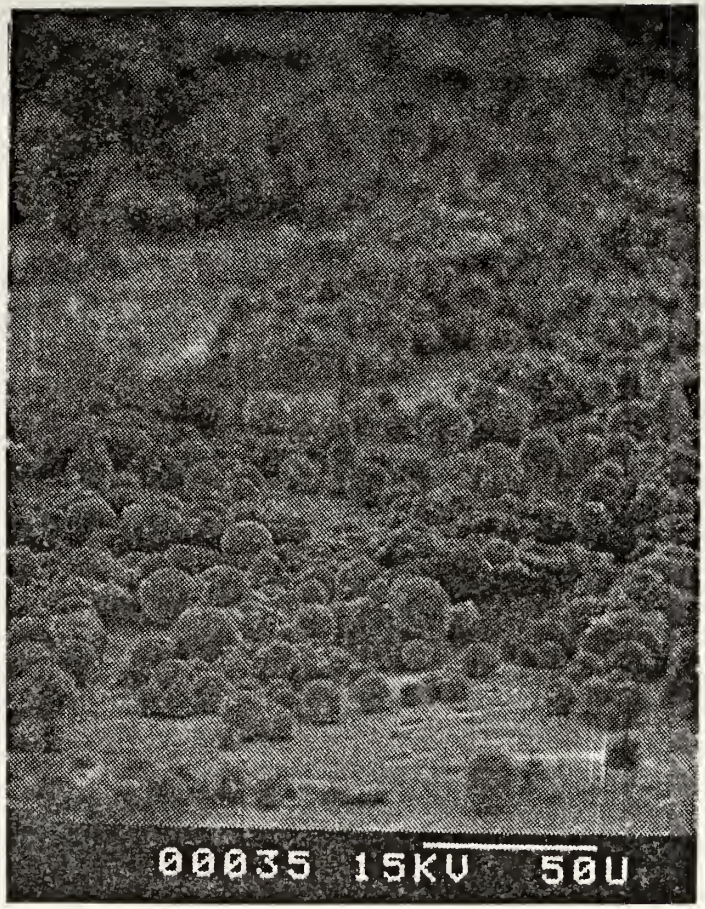

(d)

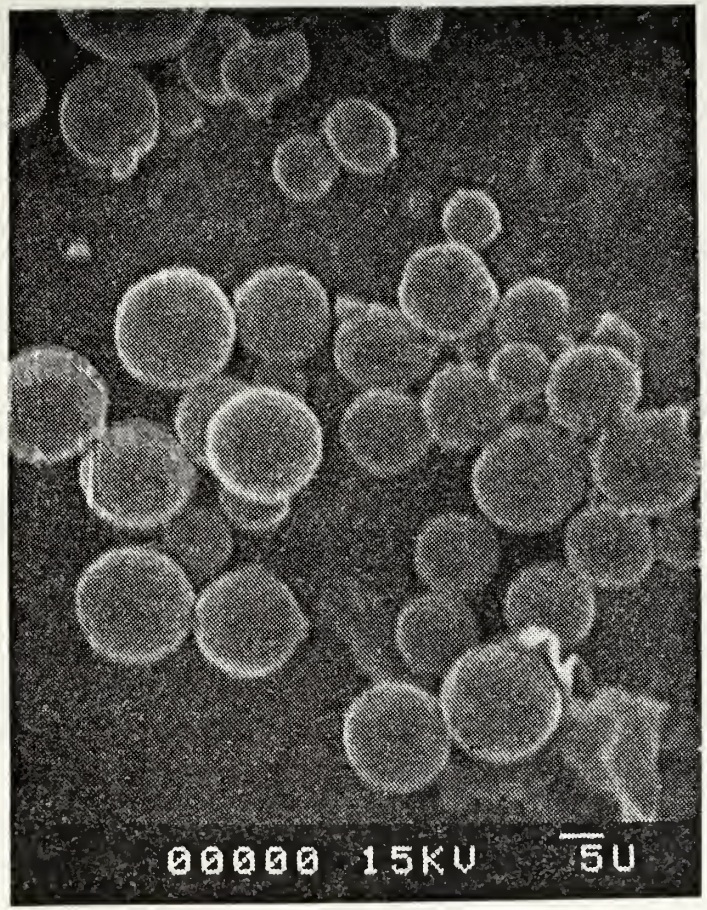

(e)

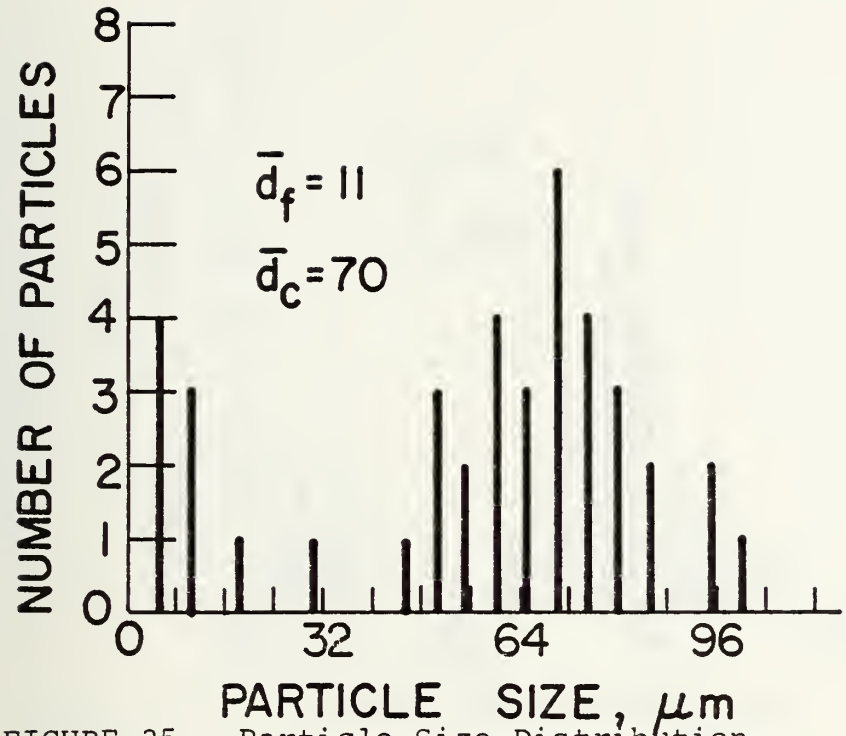

FIGURE 25. Particle Size Distribution (1445240480, WGS-5A, P_c = 500 psi)

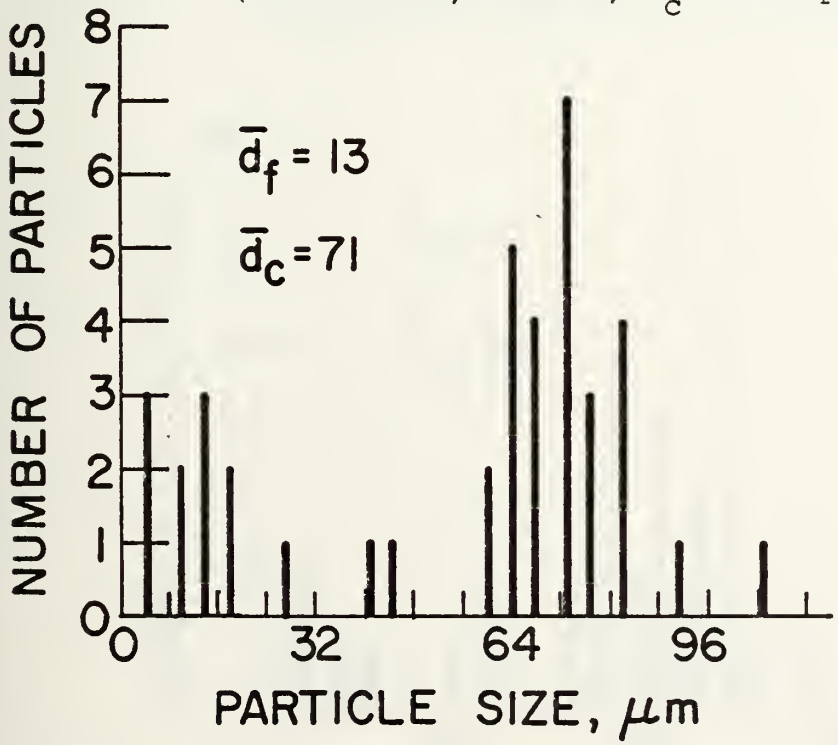

FIGURE 26. Particle Size Distribution (1445180480, WGS-5A, P_c = 1000 psi)

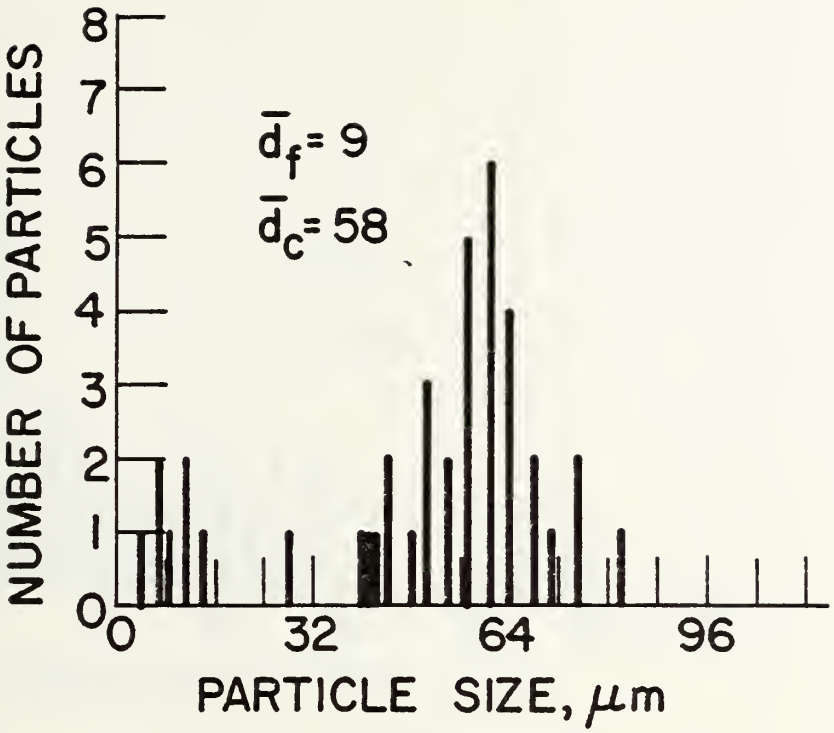

FIGURE 27. Particle Size Distribution (1030030580, WGS-6A, P_c = 500 psi)

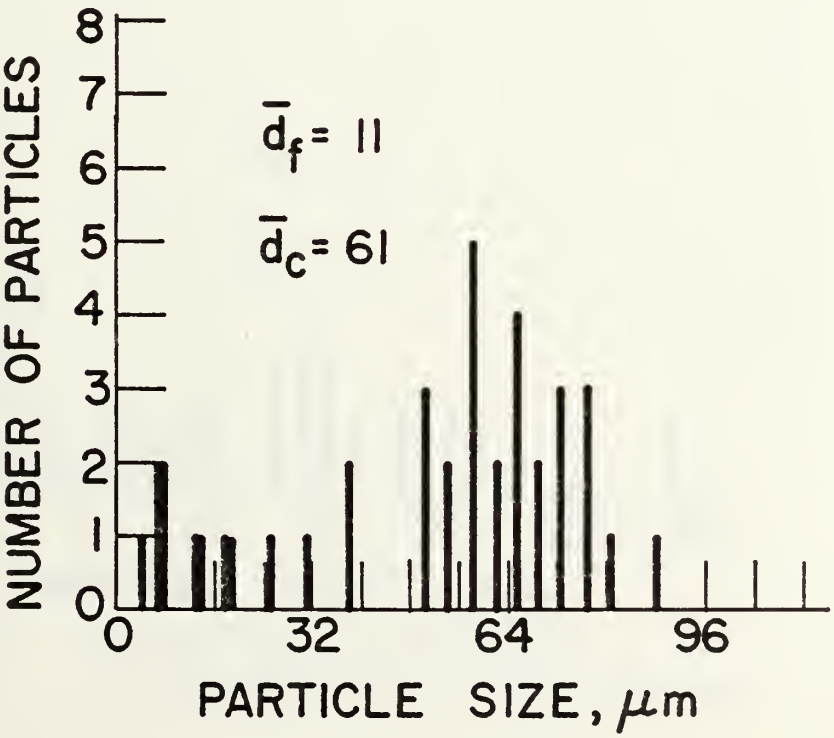

FIGURE 28. Particle Size Distribution (1600170480, WGS-6A, P_c = 1000 psi)

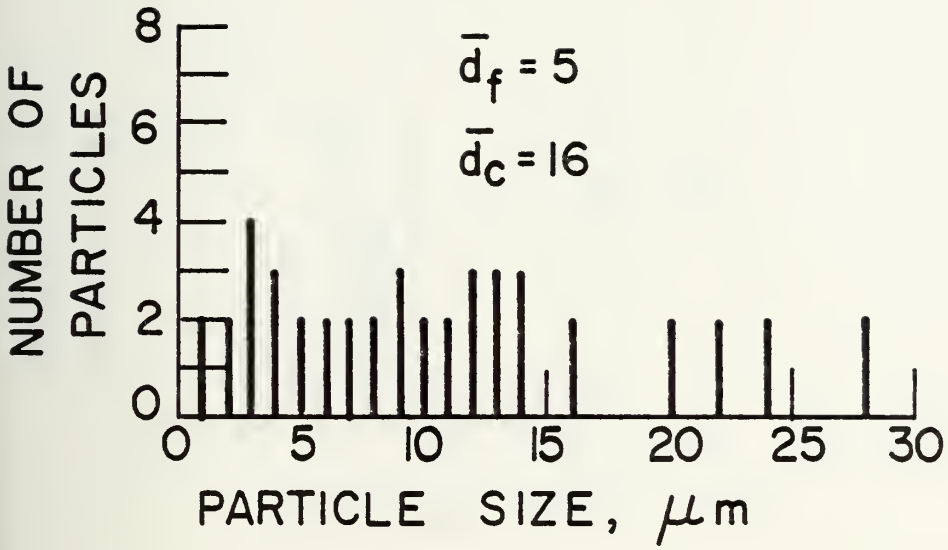

FIGURE 29. Particle Size Distribution (1215030580, WGS-7A, P_c = 500 psi)

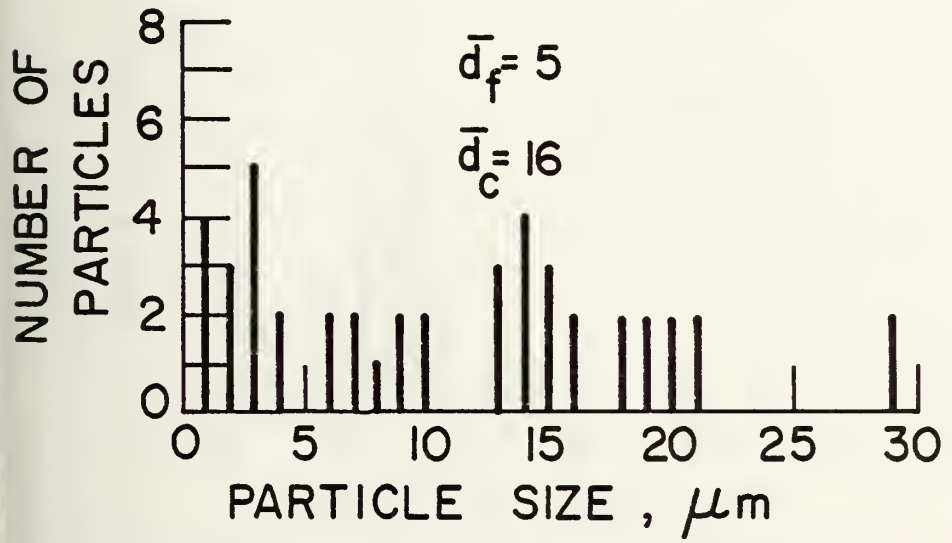

FIGURE 30. Particle Size Distribution (1400240480, WGS-7A, P_c = 1000 psi)

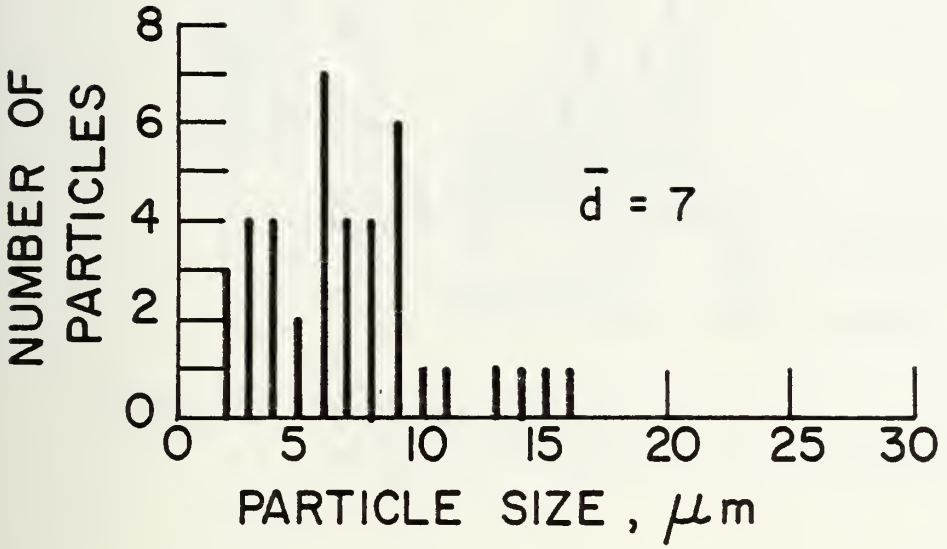

FIGURE 31. Particle Size Distribution (1100030580, WGS-7, P_c = 500 psi)

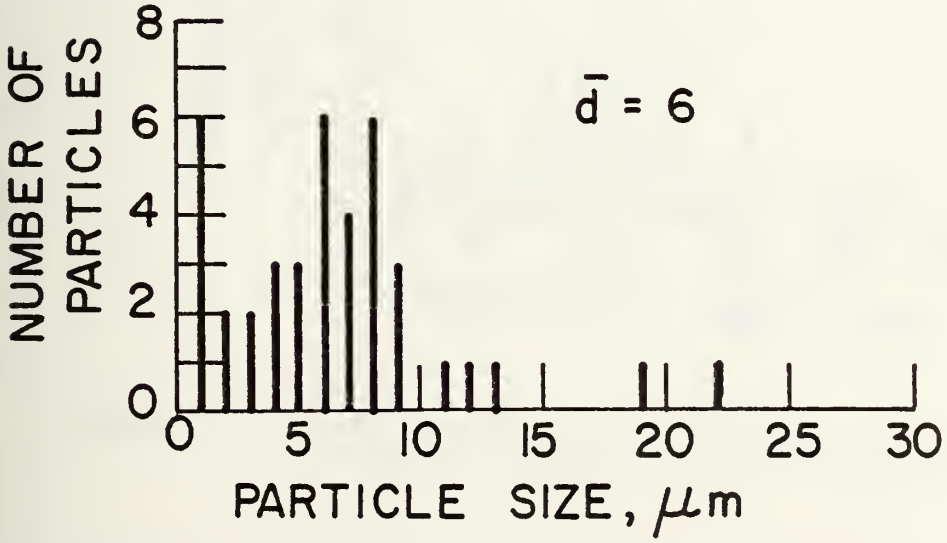

FIGURE 32. Particle Size Distribution (1500210480, WGS-7, P_c = 1000 psi)

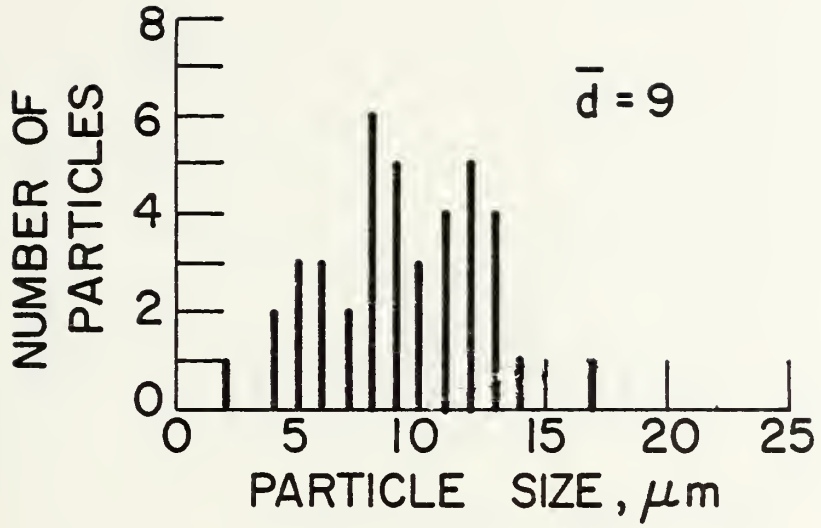

FIGURE 33. Particle Size Distribution (1230110580, NWC-1, P_c = 500 psi)

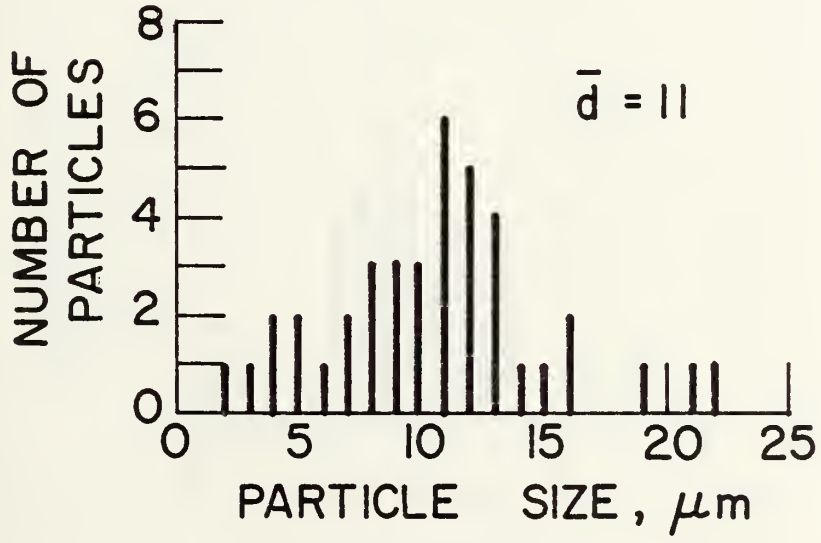

FIGURE 34. Particle Size Distribution (1500100580, NWC-1, P_c = 1000 psi)

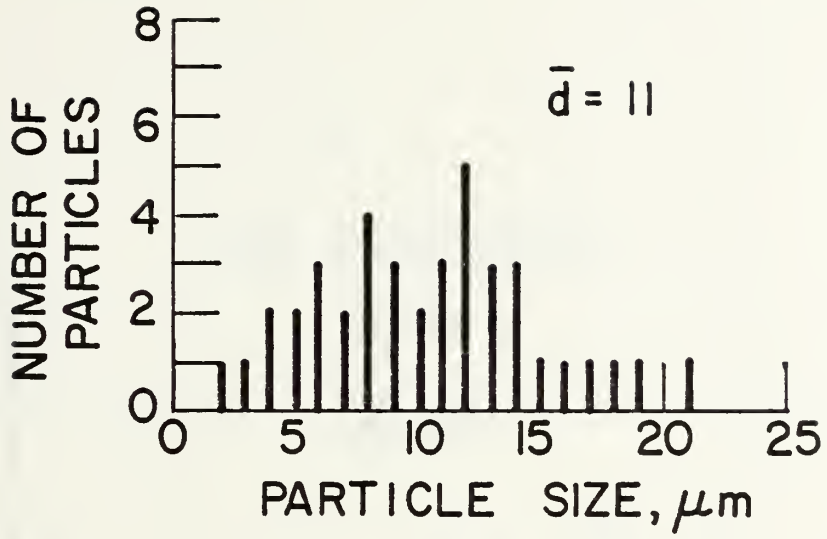

FIGURE 35. Particle Size Distribution (1200110580, NWC-2, P_c = 500 psi)

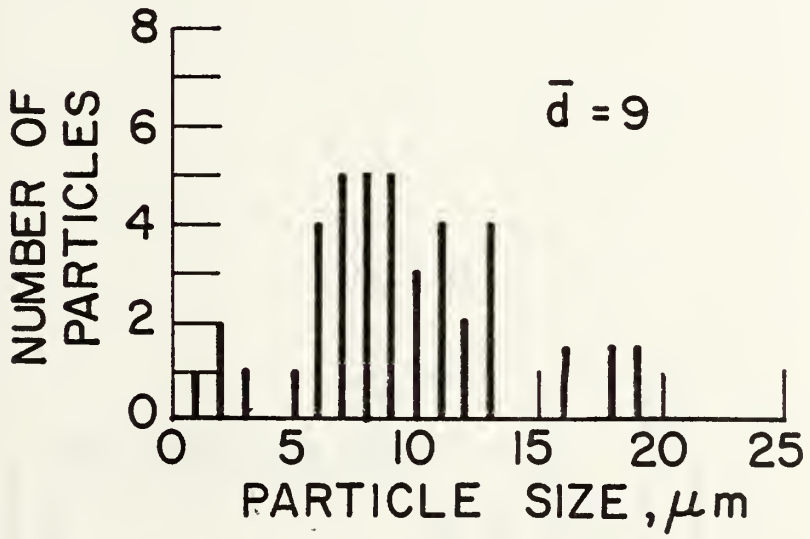

FIGURE 36. Particle Size Distribution (1615100580, NWC-2, P_c = 1000 psi)

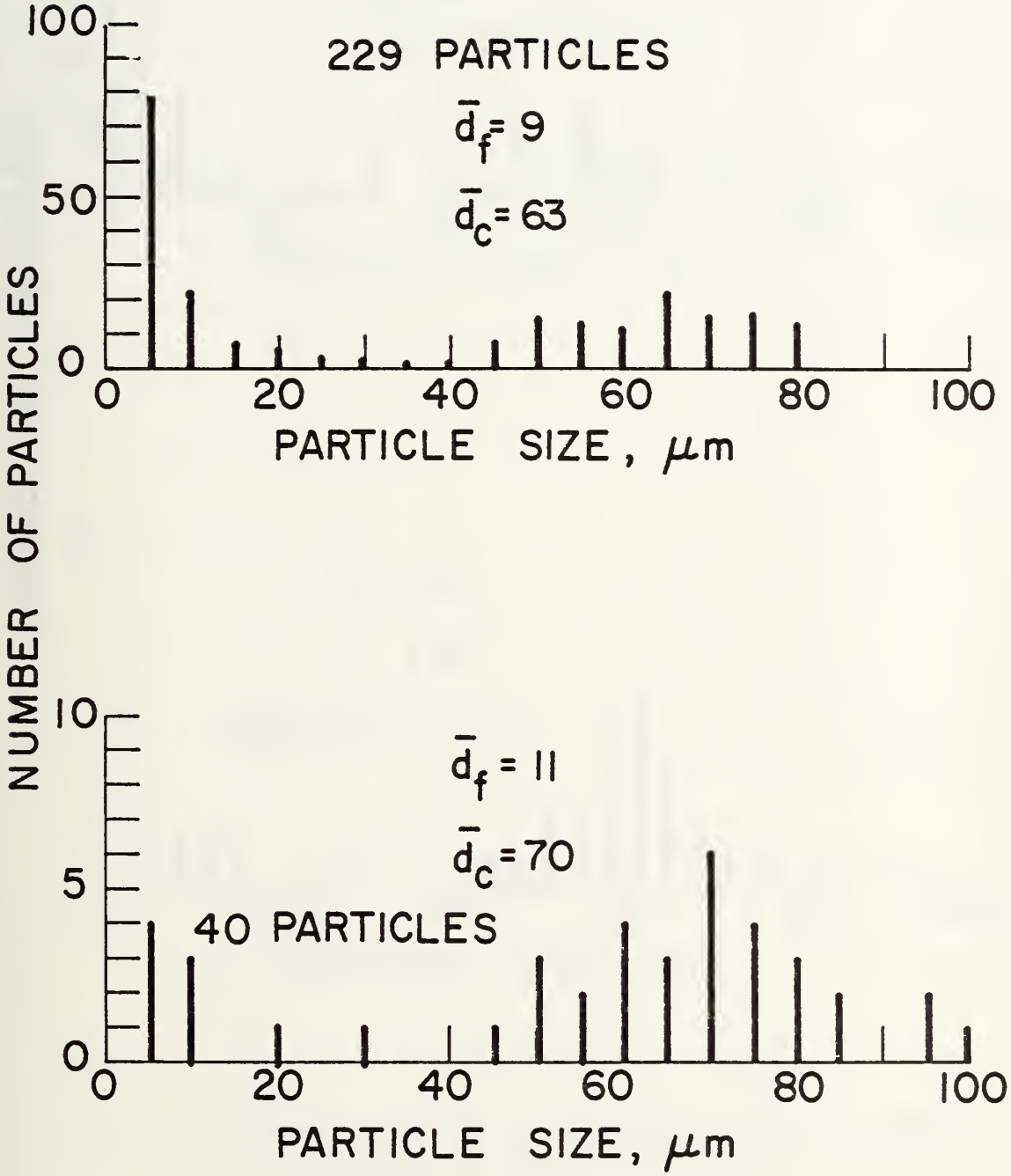

FIGURE 37. Comparison of 40 and 220 Particle Sample Distributions (14452400480, WGS-5A, P_c = 500 psi)

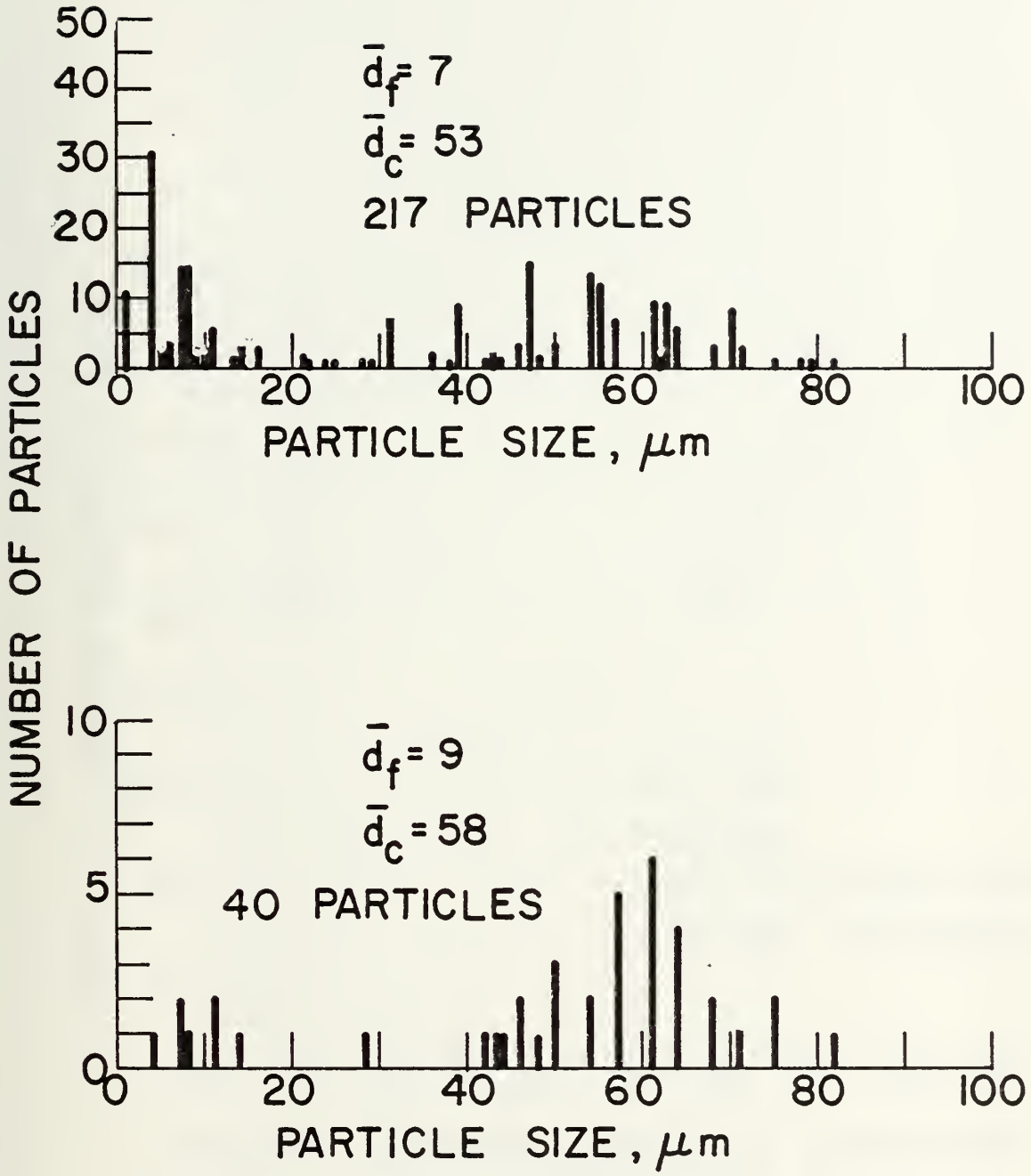

FIGURE 38. Comparison of 40 and 220 Particle Sample Distributions (1030030580, WGS-6A, P_c = 500 psi)

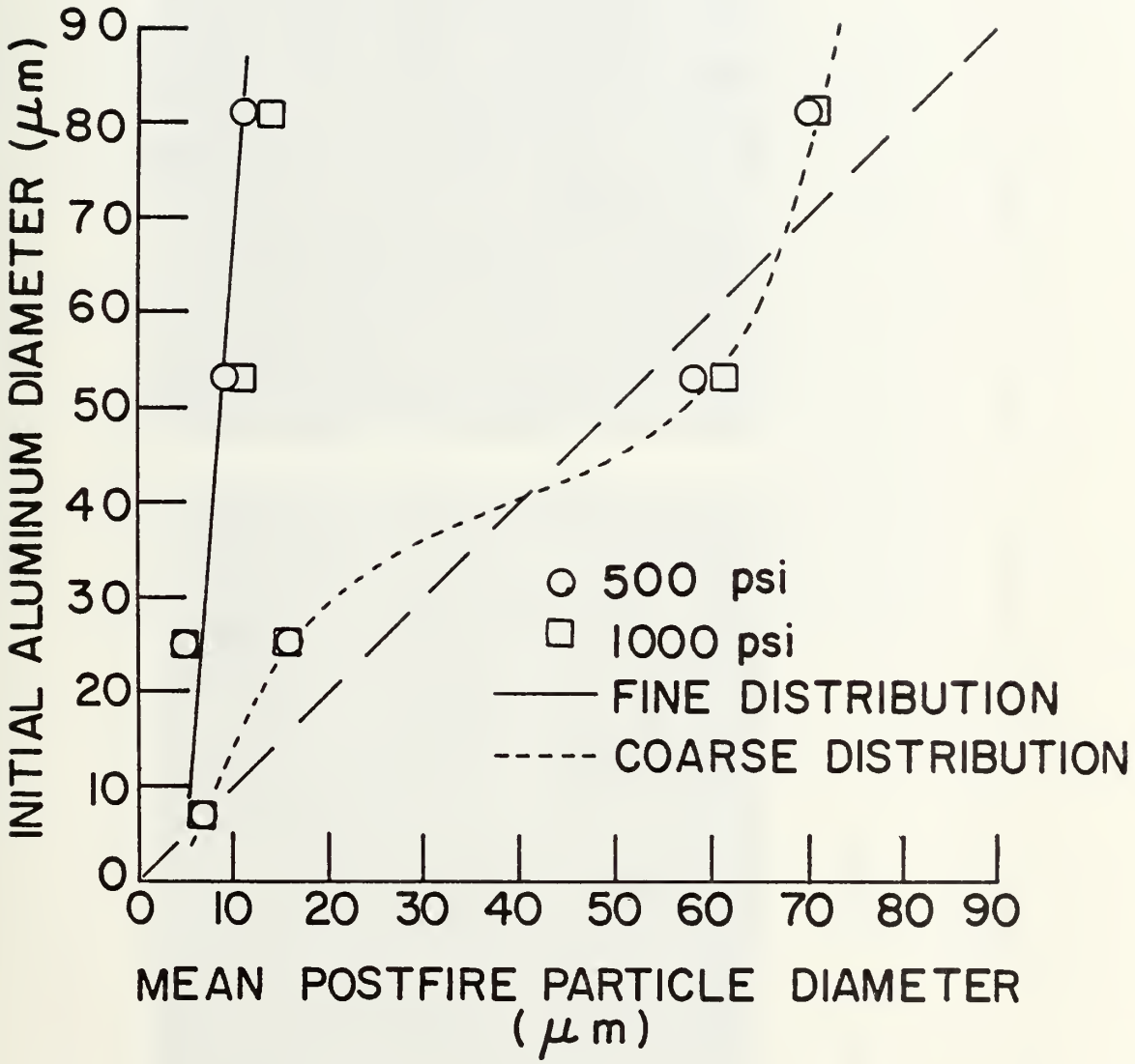

FIGURE 39. Initial Aluminum Particle Diameter Versus Mean Postfire Particle Diameter

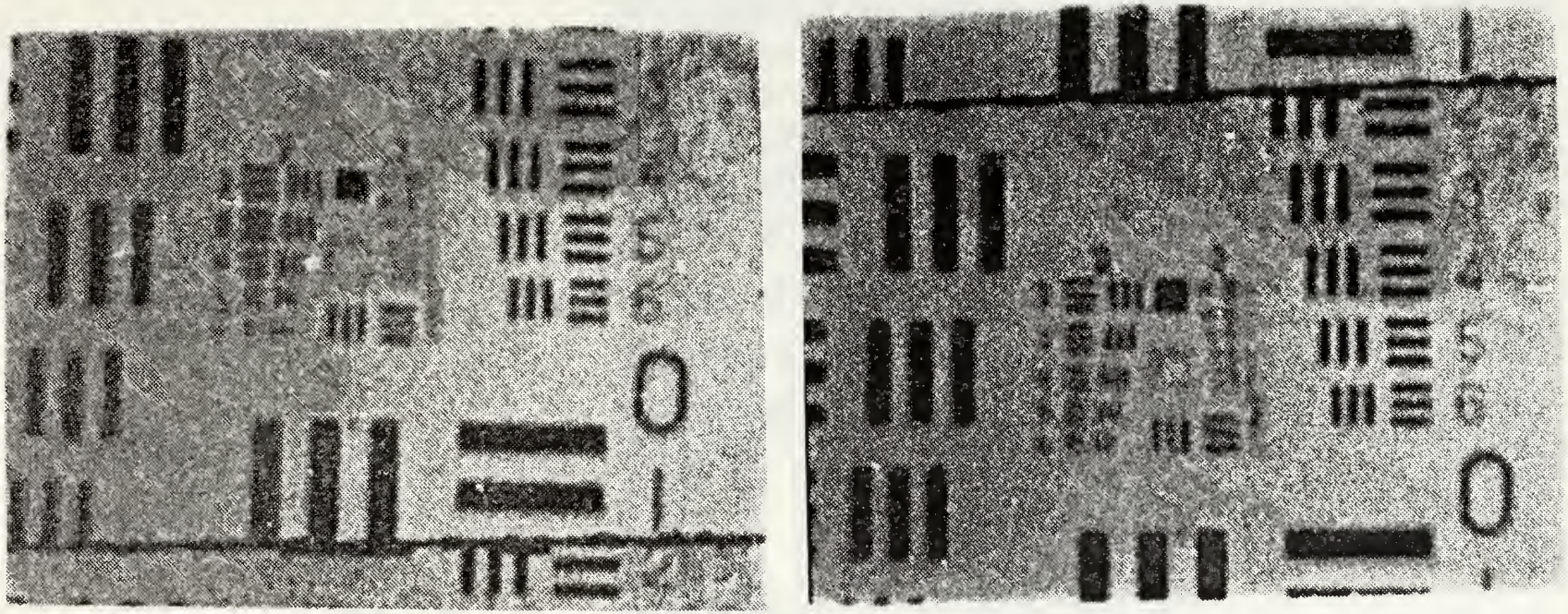

(a) Through window

(b) Without Window

FIGURE 40. Photographs of Resolution Target

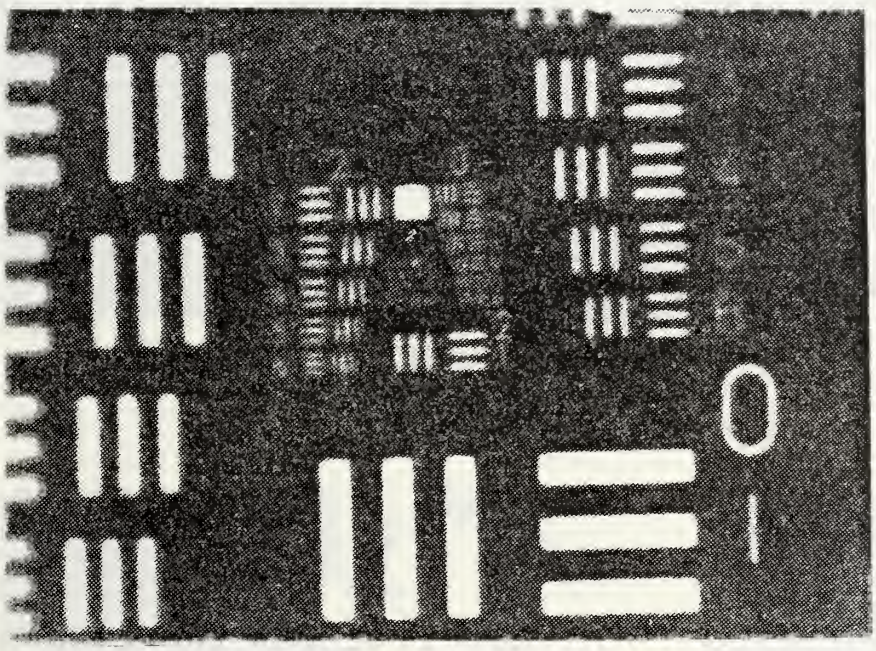

(c) Without window

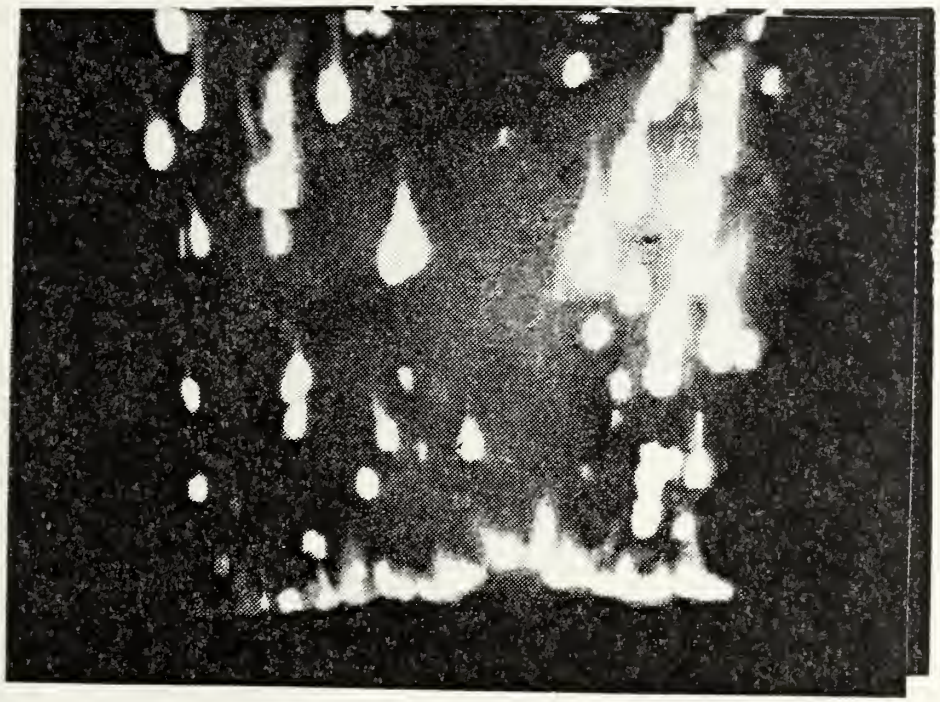

FIGURE 41. High Speed Motion Picture Frame
(1415250580, WGS-5A, 500 psi)

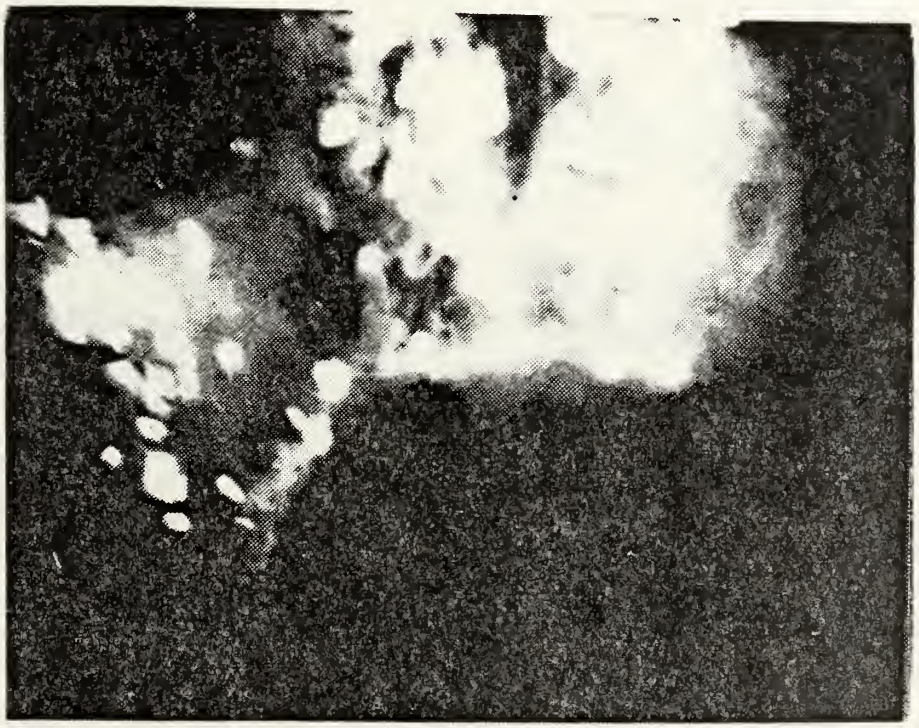

FIGURE 42. High Speed Motion Picture Frame
(1100250580, WGS-5a, 1000 psi)

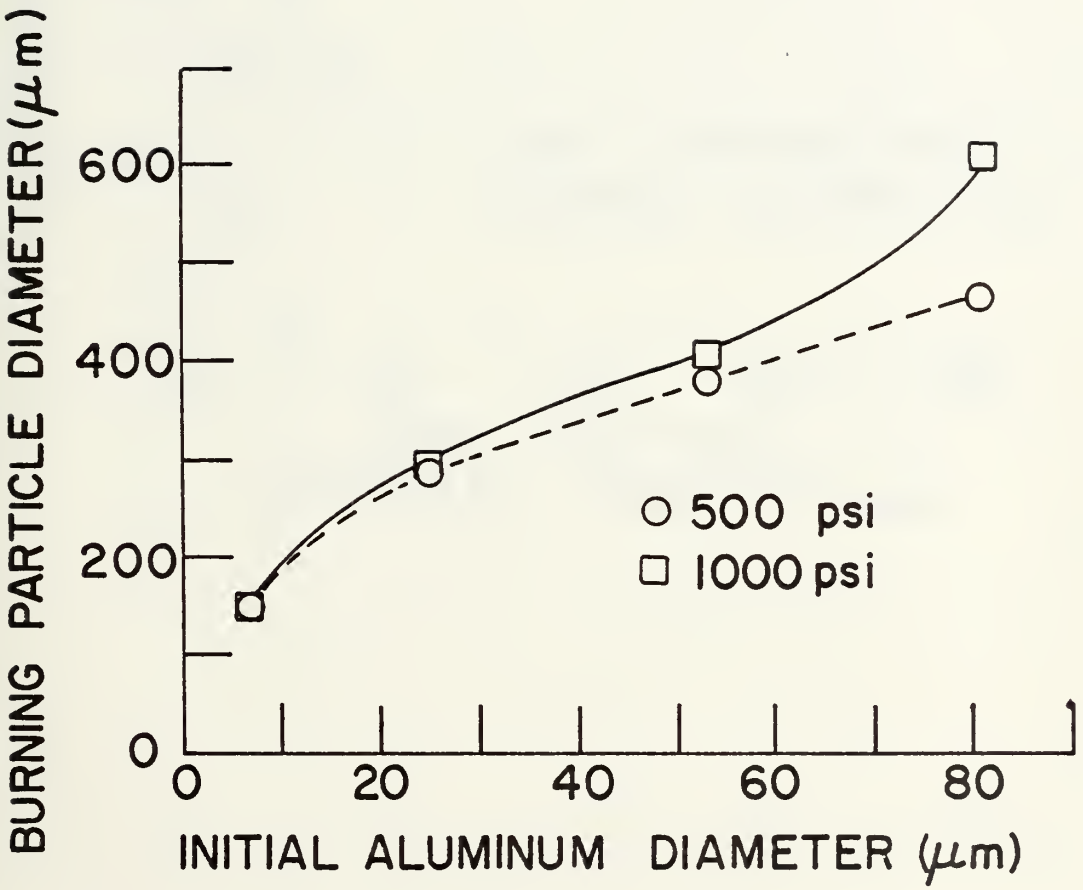

FIGURE 43. Burning Particle Diameter Versus Initial Aluminum Particle Diameter

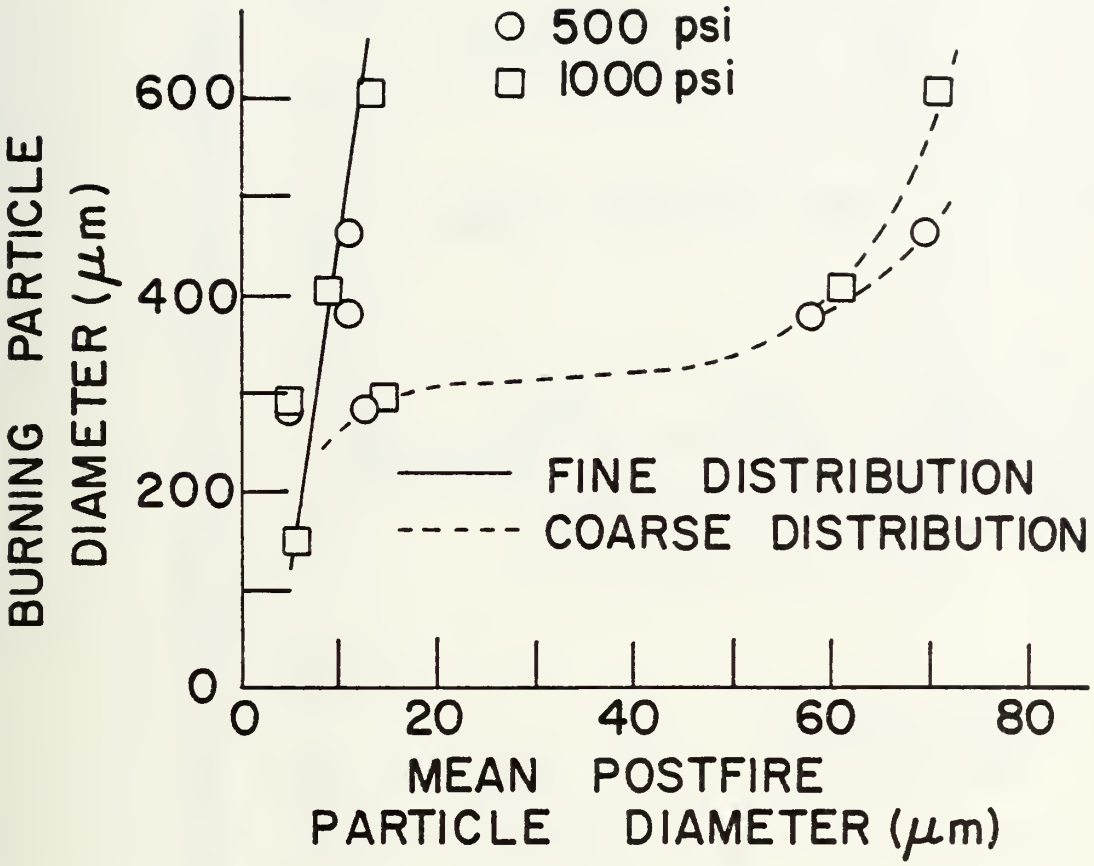

FIGURE 44. Burning Particle Diameter Versus Mean Postfire Particle Diameter

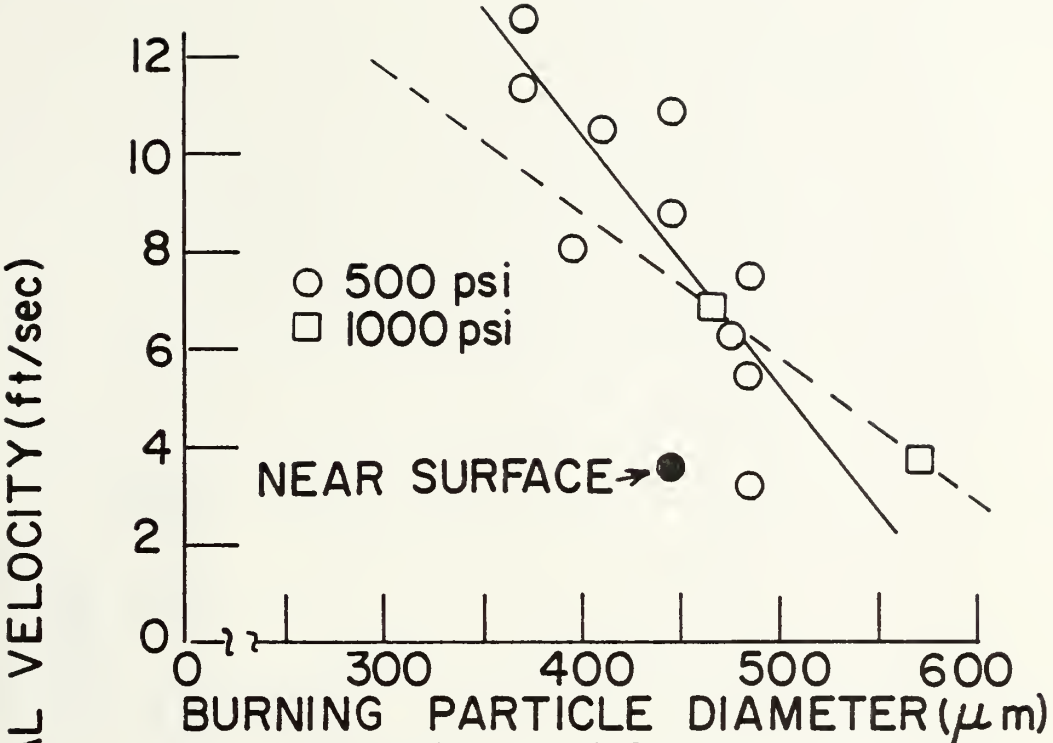

FIGURE 45. Burning Particle Average Velocity Versus Burning Particle Diameter for Propellant WGS-5A

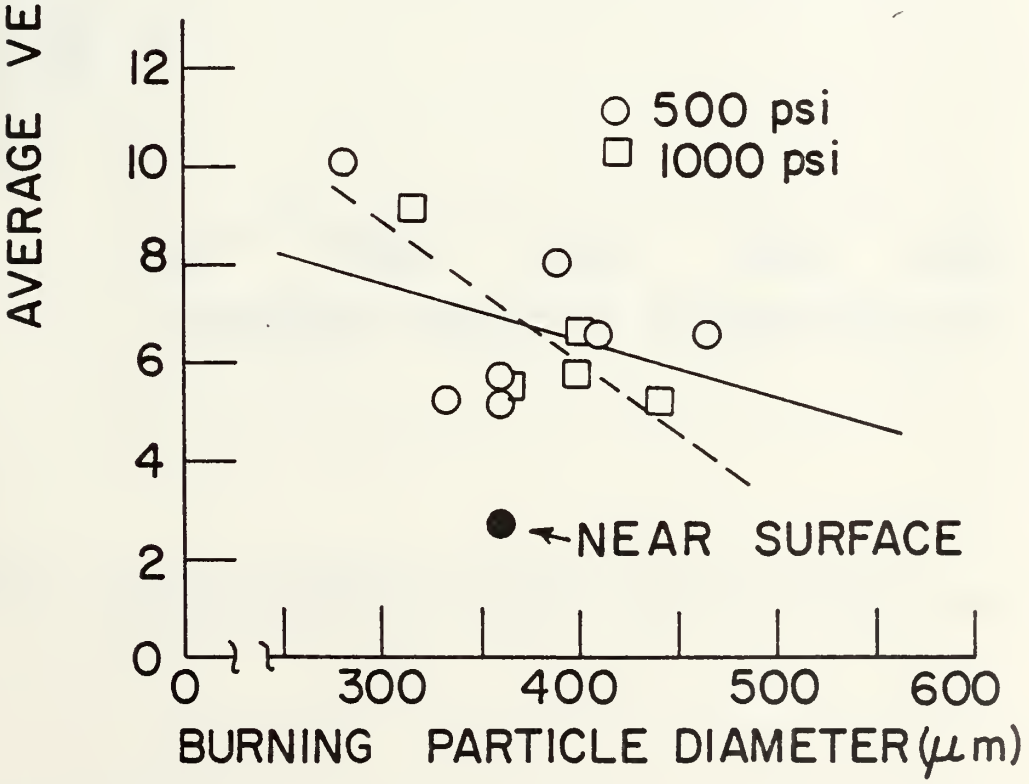

FIGURE 46. Burning Particle Average Velocity Versus Burning Particle Diameter for Propellant WGS-6A

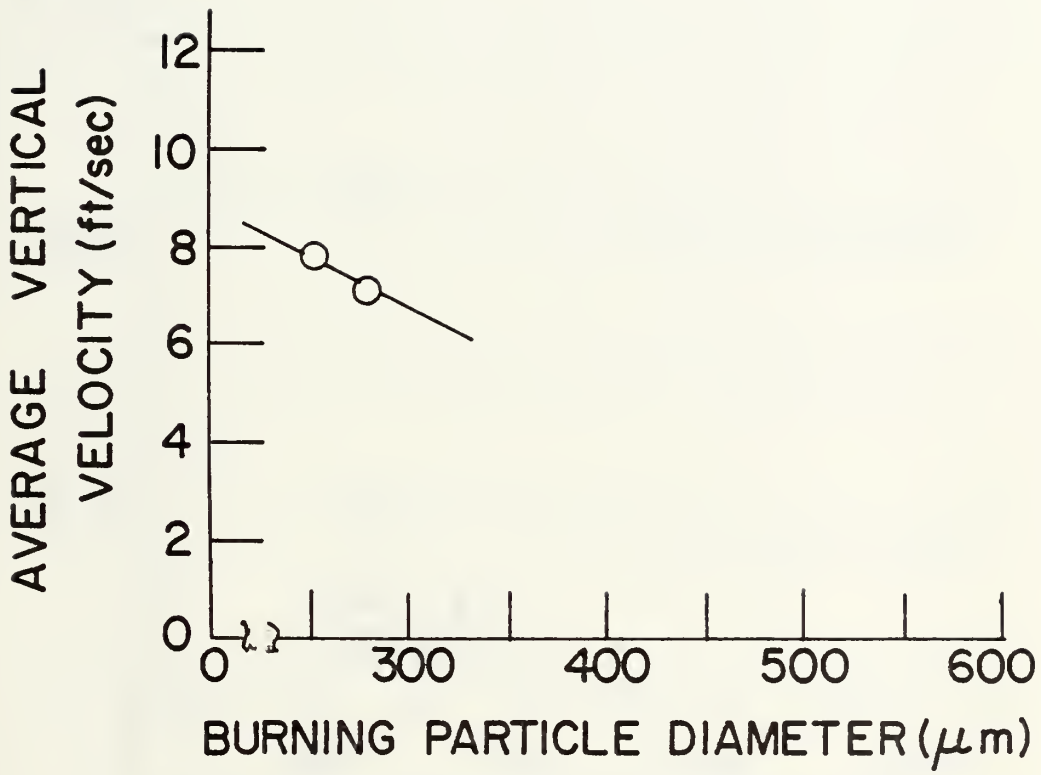

FIGURE 47. Burning Particle Average Velocity Versus Burning Particle Diameter for Propellant WGS 7-A

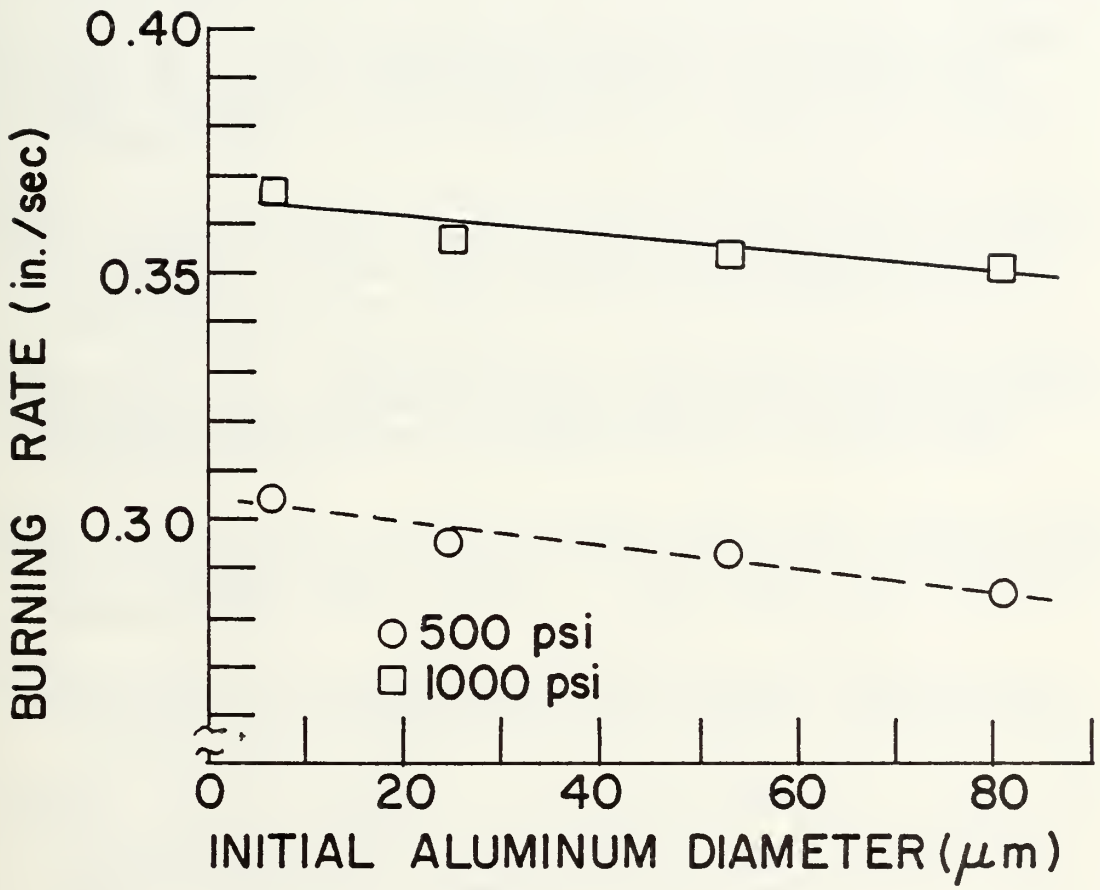

FIGURE 48. Burning Rate Versus Initial Aluminum Diameter

REFERENCES

1. Price, E. W., Sigman, R. K., and Sambamurthi, J. K., "Behavior of Aluminum in Solid Propellant Combustion," 1977, Georgia Institute of Technology, Atlanta, Ga., USA, 1977, AFOSR-TR-0468.

2. Derr, R. L., Churchill, H.L., and Fleming, R. W., "Aluminum Behavior in Solid Propellant Combustion," AFRPL-TR-74-13, Air Force Rocket Propulsion Laboratory, Edwards, Ca.

3. Barrere, M., "Recent Experimental Results on the Combustion of Aluminum and Other Metals," Proceeding of AGARD Meeting on the Reactions of Gases and Solids, October 1969.

4. Gany, A., and Caveny, L. H., "Agglomeration and Ignition Mechanism of Aluminum Particles in Solid Propellants," Proceedings of the 17th International Symposium on Combustion, August 1978.

5. Kraeutle, K. J., "Applications of Particle Size Analysis in Combustion Research," AIAA Paper 77-978, July 1977, American Institute of Aeronatics and Astronautics, New York, N.Y.

6. Gany, A., Caveny, L. H., and Summerfield, M., "Aluminized Solid Propellants Burning in A Rocket Motor Flow Field," AIAA Journal, Vol. 16, No. 7, July 1978, pp. 736-739.

7. Caveny, L. H., and Gany, A., "Breakup of Al/Al_2O_3 Agglomerates in Accelerating Flow Fields," AIAA Paper 79-0300, AIAA Aerospace Science Meeting, January 1979.

8. Geisler, R. L., Kinkead, S. A., and Beckman, C. W., "The Relationship Between Solid Propellant Formulation Variables and Motor Performance," AIAA Paper No. 75-1199, October 1975, American Institute of Aeronautics and Astronautics, New York, N.Y.

9. Micheli, P. L., and Schmidt, W. G., "Behavior of Aluminum in Solid Rocket Motors," Report AFRPL-TR-77-29, Aerojet Solid Propulsion Company, Sacramento, Ca., December 1977.

10. Caveny, L. H., and Gany, A., "Aluminum Combustion Under Rocket Motor Conditions," AGARD Propulsion and Energetics Panel Symposium on Solid Rocket Motor Technology, April 2-5, 1979, Oslo, Norway.

11. Boggs, T. L., Crump, J. E., Kraeutle, K. J., and Zurn, D. E., "Cinephotomicrography and Scanning Eelctron Microscopy as Used to Study Solid Propellant Combustion," Experimental Diagnostics in Combustion of Solids, AIAA Progress in Astronatics and Aeronautics, 1978, Vol. 63, pp. 20-48.

12. Cashdollar, K. L., Lee, C. K., and Singer, J. M., "Three Wavelength Light Transmission Technique to Measure Smoke Particle Size and Concentration," Applied Optics, Vol. 18, No. 11, June 1, 1979.

13. Dobbins, R. A., Crocco, L., and Glassman, I., "Measurement of Mean Particle Sizes of Sprays from Diffractively Scattered Light," AIAA Journal, Vol. 1, No. 8, August 1963, pp. 1882-1886.

14. Nejad, A. S., Schetz, J. A., and Jakubowski, A. K., "Mean Droplet Diameter Resulting From Atomization of a Transverse Liquid Jet in A Supersonic Air Stream," Virginia Polytechnic Institute & State University, College of Engineering, Report No. VPI-Aero-089, AFOSR-TR-79-0004, Nov. 1978.

15. Briones, R. A., and Wuerker, R. F., "Application of Holography to the Combustion Characterization of Solid Rocket Propellants," AFRPL Report AFRPL-TR-77-90, April 1978.

16. Briones, R. A., and Wuerker, R. F., "Holography of Solid Propellant Combustion," Experimental Diagnostics in Combustion of Solids, AIAA, Progress in Astronautics and Aeronautics, 1978, Vol. 63, pp. 251-276.

17. "Close Up Photography and Photomacragraphy," Eastman-Kodak Co., Tech. Publ. N-12, Rochester, N.Y., 1979.

18. Ditore, M. J., Poynter, R., and Schmidt, W., "Zirconium/Aluminum Combustion," Aerojet Solid Propulsion Company, R & D Status Report LBA-MPR-18, April 1980.

INITIAL DISTRIBUTION LIST

		No. Copies
1.	Defense Technical Information Center Cameron Station Alexandria, Virginia 22314	2
2.	Library, Code 0142 Naval Postgraduate School Monterey, California 93940	2
3.	Department Chairman, Code 67 Department of Aeronautics Naval Postgraduate School Monterey, California 93940	1
4.	Assoc. Prof. D. W. Netzer, Code 67Sm Department of Aeronautics Naval Postgraduate School Monterey, California 93940	2
5.	MAJ V. DiLoreto, USMC 1414 West 42 Street Erie, Pennsylvania 16509	2

Thesis
D57635 DiLoreto
c.1
189498
An experimental study of solid propellant deflagration using high speed motion pictures and postfire residue analysis.